

## Radar networks performance analysis and topology optimization

Ivashko, Inna

**DOI**

[10.4233/uuid:1a6dab8e-ebbd-41a1-bd5e-866a9050fc68](https://doi.org/10.4233/uuid:1a6dab8e-ebbd-41a1-bd5e-866a9050fc68)

**Publication date**

2016

**Document Version**

Final published version

**Citation (APA)**

Ivashko, I. (2016). *Radar networks performance analysis and topology optimization*. [Dissertation (TU Delft), Delft University of Technology]. <https://doi.org/10.4233/uuid:1a6dab8e-ebbd-41a1-bd5e-866a9050fc68>

**Important note**

To cite this publication, please use the final published version (if applicable).  
Please check the document version above.

**Copyright**

Other than for strictly personal use, it is not permitted to download, forward or distribute the text or part of it, without the consent of the author(s) and/or copyright holder(s), unless the work is under an open content license such as Creative Commons.

**Takedown policy**

Please contact us and provide details if you believe this document breaches copyrights.  
We will remove access to the work immediately and investigate your claim.

# **RADAR NETWORKS PERFORMANCE ANALYSIS AND TOPOLOGY OPTIMIZATION**



# **RADAR NETWORKS PERFORMANCE ANALYSIS AND TOPOLOGY OPTIMIZATION**

## **Proefschrift**

ter verkrijging van de graad van doctor  
aan de Technische Universiteit Delft,  
op gezag van de Rector Magnificus prof.ir. K. C. A. M. Luyben;  
voorzitter van het College voor Promoties,  
in het openbaar te verdedigen op dinsdag 13 december 2016 om 10:00 uur

door

**Inna IVASHKO**

Master of Science  
National Aviation University, Ukraine  
geboren te Netishyn, Ukraine

Dit proefschrift is goedgekeurd door de

promotor: Prof. DSc. A. G. Yarovoy

copromotor: Dr. O. A. Krasnov

Samenstelling promotiecommissie:

Rector Magnificus,	voorzitter
Prof. DSc. A. G. Yarovoy,	Technische Universiteit Delft, promotor
Dr. O. A. Krasnov,	Technische Universiteit Delft, copromotor
Onafhankelijke leden:	
Prof. dr. P. Lombardo	Sapienza University of Rome, Italy
Prof. DSc. F. I. Yanovsky	National Aviation University, Ukraine
Prof. ir. P. Hoogeboom	Technische Universiteit Delft
Prof. ir. F. le Chevalier	Technische Universiteit Delft
Andere lid:	
Prof. dr. ir. G. J. T. Leus	Technische Universiteit Delft

This research has been carried out at the Delft University of Technology in the MS3 (Microwave Sensing, Signals and Systems) group and supported by the RAEBELL (Feasibility Study of Low-level Airspace Surveillance) project.



*Keywords:* radar networks, convex optimization, greedy optimization, Cramér-Rao lower bound, frame potential

*Printed by:* Ipskamp Drukkers, the Netherlands

Copyright © 2016 by I. Ivashko

ISBN 978-94-6186-751-3

An electronic version of this dissertation is available at

<http://repository.tudelft.nl/>.

*To my family  
and my parents*



# CONTENTS

<b>List of Figures</b>	<b>xi</b>
<b>List of Tables</b>	<b>xiii</b>
<b>List of Acronyms</b>	<b>xv</b>
<b>1 Introduction</b>	<b>1</b>
1.1 Need for a New Sensing Technique . . . . .	2
1.2 Taxonomy of Multistatic Radars . . . . .	2
1.3 Methods of Target Position and Velocity Estimation in Radar Networks . . . . .	6
1.4 Problem Formulation . . . . .	6
1.5 Research Objective and Approaches . . . . .	9
1.6 The Outline of the Thesis . . . . .	9
References . . . . .	10
<b>2 Potential Accuracy of Target Position and Velocity Vector Estimation in Multistatic Radar</b>	<b>15</b>
2.1 System Model . . . . .	16
2.2 The Cramér-Rao Lower Bound . . . . .	17
2.3 Ranging Accuracy of Passive Bistatic Radar with WiFi Transmissions . . . . .	18
2.4 Range and Doppler Frequency Estimation Accuracy in FMCW Radar . . . . .	23
2.5 The Target Localization and Velocity Vector Estimation Accuracy in a Radar Network . . . . .	25
2.6 Incorporation of the Antenna Pattern into the CRLB . . . . .	27
2.7 Conclusion . . . . .	28
References . . . . .	28
<b>3 Estimation Accuracy Analysis in Multistatic Radar</b>	<b>31</b>
3.1 Impact of the Radar Architecture and Cooperation Mode . . . . .	32
3.2 Impact of the Waveform Parameters and the Power Budget . . . . .	34
3.3 Impact of the Measurement Model on Target Localization Accuracy . . . . .	39
3.4 Analysis of Combined Active and WiFi-based Passive Radar Network . . . . .	39
3.5 Conclusion . . . . .	43
References . . . . .	44
<b>4 Accuracy-driven Topology Optimization: Generic Framework</b>	<b>47</b>
4.1 Introduction . . . . .	48
4.1.1 Convexity condition . . . . .	48
4.1.2 Submodularity condition . . . . .	49

4.2	Performance Metrics . . . . .	49
4.2.1	Mean-squared error . . . . .	49
4.2.2	Frame potential . . . . .	50
4.2.3	Log-determinant. . . . .	50
4.2.4	The maximum eigenvalue of the error covariance matrix . . . . .	51
4.3	Multi-modal Parameter Vector . . . . .	52
4.4	Optimization Algorithms . . . . .	52
4.4.1	Convex optimization. . . . .	52
4.4.2	Greedy optimization . . . . .	54
4.5	Bistatic Radar Architecture - Structured Selection. . . . .	54
4.5.1	Convex optimization algorithm . . . . .	56
4.5.2	Greedy optimization . . . . .	58
4.6	Computational Complexity . . . . .	58
4.7	Conclusion . . . . .	58
	References . . . . .	60
<b>5</b>	<b>Accuracy-driven Topology Optimization: Numerical Analysis</b>	<b>63</b>
5.1	Simulation Scenarios . . . . .	64
5.2	Monostatic Radar Network . . . . .	64
5.3	Bistatic Radar Network . . . . .	66
5.3.1	Preselected grids for transmit and receive radar nodes. . . . .	66
5.3.2	Scenario with coincidental transmit and receive radar grids . . . . .	68
5.4	Receivers Topology Selection in Passive Bistatic Radar Network. . . . .	71
5.5	Comparison of the Cost Functions and Optimization Algorithms . . . . .	71
5.6	Topology Optimization Taking into Account Signal Blockage . . . . .	73
5.7	Conclusion . . . . .	73
	References . . . . .	75
<b>6</b>	<b>Conclusions and Future Work</b>	<b>77</b>
6.1	Major Results and Novelties. . . . .	78
6.2	Recommendations for Future Work. . . . .	80
	References . . . . .	81
<b>A</b>	<b>The Evaluation of Frame Potential and Log-Determinant Costs</b>	<b>83</b>
A.1	The Performance of a Single FMCW Radar . . . . .	84
A.1.1	The FP and the LD cost functions for an FMCW radar network. . . . .	84
A.2	The Evaluation of the FP and LD in (A.4) and (A.3) . . . . .	85
<b>B</b>	<b>The Off-Grid Radar Selection</b>	<b>89</b>
B.1	Introduction . . . . .	90
B.1.1	General framework . . . . .	90
B.2	Numerical Results. . . . .	92
B.3	Conclusion . . . . .	93
	References . . . . .	95

---

<b>C Data Association Algorithm for Multiple Targets Localization in the Networks of Monostatic Radars</b>	<b>97</b>
C.1 System Model and Problem Formulation . . . . .	98
C.2 Stage 1 - Target Localization. . . . .	98
C.3 Stage 2 - Analysis of the Target-Network Geometry . . . . .	100
C.4 Stage 3 - Deghosting, Based on the Measurement Tuple Analysis . . . . .	103
C.5 Case Study . . . . .	104
C.6 Conclusion . . . . .	107
References . . . . .	107
<b>Summary</b>	<b>109</b>
<b>Samenvatting</b>	<b>111</b>
<b>List of Publications</b>	<b>113</b>
<b>Acknowledgments</b>	<b>115</b>



# LIST OF FIGURES

1.1 A combined monostatic and bistatic radar network with cooperative transmission-reception mode (indicated with dashed arrows). . . . .	4
1.2 Ghost target phenomena . . . . .	5
1.3 Classification of localization techniques . . . . .	7
1.4 Threshold phenomena of target position estimation with MLE . . . . .	8
2.1 Bistatic radar network with cooperative mode of signal transmission-reception . . . . .	16
2.2 SNR distribution for directional antenna pattern: (a) vertical plane; (b) Y-X plane (target height $h_t = 3000$ m) . . . . .	27
3.1 Error of the target localization versus number of Tx-Rx channels. No restriction on the length of baseline of bistatic radars. . . . .	33
3.2 Error of the target localization versus number of <i>autonomous</i> bistatic channels at different values of baseline. . . . .	34
3.3 Histogram of the target localization error depending on the length of baseline. Values of the target localization error were averaged over 19 numbers of Tx-Rx channels ( $N = 2, 3, \dots, 20$ ) with randomly selected nodes positions in $10^3$ trials. Each bistatic radar operates in autonomous signal reception mode. . . . .	34
3.4 Contour plots of the target localization error ( $\sigma_p, m$ ) in radar networks with autonomous mode of the signal transmission-reception. . . . .	35
3.5 Error of the target localization versus number of monostatic radars (autonomous reception mode) for different values of the signal bandwidth $\Delta f$ . . . . .	36
3.6 Error of the target localization depending on the number of monostatic radars (autonomous reception mode) for different numbers of integrated pulses. . . . .	36
3.7 Error of the target localization versus number of monostatic radars (autonomous reception mode) for different values of effective radiated power (ERP). . . . .	37
3.8 Average error of the target localization for different numbers of monostatic radars and allocated frequency bandwidth . . . . .	38
3.9 Error of the target localization depending on the number of monostatic radars in the first and second measurement models. . . . .	40
3.10 Error of the target localization depending on the number of monostatic radars in the first and third measurement models. . . . .	41
3.11 Principle of passive bistatic radar operation. . . . .	41

3.12	Contour plots of the target localization error ( $\sigma_p, m$ ) . . . . .	42
3.13	Error of the target localization for active FMCW radars versus number of bistatic radars (with one transmit node and varying numbers of receive nodes) for different numbers of active radar nodes. . . . .	43
3.14	Error of the target localization for three active FMCW radars versus number of bistatic radars (with one transmit node and varying numbers of receive nodes) for different signal bandwidths. . . . .	43
5.1	Scenarios of candidate radars positions . . . . .	65
5.2	Contour plots of the target localization error ( $\sigma_p, m$ ) in the network of $L$ monostatic FMCW radars, which have been selected from $N = 161$ candidate positions using convex optimization (Algorithm 1, Chapter 4). . . . .	67
5.3	Selected Tx-Rx channels of bistatic cooperative radar network from preselected Tx/Rx grids ( $L_t = 15, L_r = 20; N_t = 58, N_r = 59$ ). . . . .	68
5.4	Selected Tx-Rx channels in bistatic autonomous radar network from preselected Tx/Rx grids ( $L_t = L_r = 20; N_t = 58, N_r = 59$ ). . . . .	68
5.5	Contour plots of the target localization error ( $\sigma_p, m$ ) in bistatic radar networks, where potential positions of the nodes have been preselected. . . . .	69
5.6	Contour plots of the target localization error ( $\sigma_p, m$ ) in bistatic radar networks with positions, selected from overlapping grids ( $L_t = L_r = 15$ ). . . . .	70
5.7	Target localization error in bistatic radar networks (cooperative mode) with positions, selected by greedy and convex optimization algorithms with LD and $\lambda_{\max}$ cost functions respectively. . . . .	71
5.8	Distribution of the target localization error ( $\sigma_p, m$ ). . . . .	72
5.9	Average error of the target localization for different numbers of optimally placed radars $L$ from the $N = 117$ available ones for the $K = 2$ parameters under estimation and the $M = 171$ grid points for the parameter space. . . . .	73
5.10	Distribution of the error of target localization ( $\sigma_p, m$ ). . . . .	74
B.1	The selected positions of the monostatic radars using discrete (on-grid) and continuous (off-grid) optimization approaches . . . . .	93
B.2	Contour plots of the target localization error ( $\sigma_p, m$ ) in the network of six monostatic radars that explore the autonomous mode of signal transmission-reception . . . . .	94
C.1	Schematic illustration of the target localization . . . . .	101
C.2	Schematic illustration of condition (C.11) . . . . .	103
C.3	Number of ghost targets depending on the radar range resolution for noiseless measurement model (target is located within the volume $1000\text{ m} \times 1000\text{ m} \times 1000\text{ m}$ ). . . . .	106
C.4	Number of ghosts target depending on the radar range resolution $\Delta R$ for $M = 10$ targets . . . . .	106
C.5	Number of ghosts for different noise variances $(\sigma^{(n)})^2$ (number of targets $M = 10$ ; target is located within the volume $1000\text{ m} \times 1000\text{ m} \times 1000\text{ m}$ ) . . . . .	107

# LIST OF TABLES

1.1	Single radar versus radar network . . . . .	4
3.1	Single radar simulation parameters . . . . .	32
3.2	Bandwidth allocation . . . . .	37
4.1	Monostatic versus bistatic radar network topology optimization. . . . .	56
5.1	Single sensor simulation parameters for three scenarios . . . . .	64
5.2	Connection between three considered scenarios of potential radar positions (Fig.5.1), type of the network, and optimization algorithm . . . .	66
C.1	Analysis of the measurements from the first radar . . . . .	104
C.2	Analysis of the measurements from the second radar . . . . .	105
C.3	Additional filtration of potential ghosts . . . . .	105



# LIST OF ACRONYMS

ACF	auto-correlation function
BMI	bilinear matrix inequality
CPU	central processing unit
CRLB	Cramér-Rao lower bound
CSP	continuous sensor placement
DAB	digital audio broadcasting
DBPSK	differential binary phase shift keying
DQPSK	differential quadrature phase shift keying
DSSS	direct sequence spread spectrum
DVB-H	digital video broadcasting - handheld
DVB-T	digital video broadcasting - terrestrial
FIM	Fisher information matrix
FMCW	frequency-modulated continuous wave
FP	frame potential
GDOP	geometric dilution of precision
GMT	ground moving target
GSM	global system for mobile communications
HF	high frequency
LD	log-determinant
LFM	linear frequency modulated
LMI	linear matrix inequality
LSE	least squares estimator
MIMO	multi-input multi-output
MLE	maximum likelihood estimator
MSE	mean squared error
NP	non-deterministic polynomial (time)
OFDM	orthogonal frequency-division multiplexing
OLS	ordinary least squares
PBR	passive bistatic radar
PCL	passive coherent location
QCQP	quadratically constrained quadratic program
RCS	radar cross-section
SDP	semidefinite programming
SNR	signal-to-noise ratio
TDOA	time difference of arrival
UAV	unmanned aerial vehicle
WiFi	wireless fidelity
WLS	weighted least squares



# 1

## INTRODUCTION

*This chapter presents the concept of radar networks and existing unresolved challenges for their efficient exploitation. State-of-the-art methods developed for radar networks performance analysis and topology optimization are reviewed. The research objective and suggested approaches are then formulated. Finally, the structure and a short summary of the thesis chapters are presented.*

### 1.1.1. NEED FOR A NEW SENSING TECHNIQUE

PRESENTLY, conventional standalone radars are widely used in both military and civil domains [1], [2]. Their applications range from small-scale devices for medical imaging to bulky, electronically scanned array radars for space observations [3], [4].

Although a single radar is capable of performing important functions (detection, estimation, classification, and tracking), it can not meet a number of new requirements, posed by modern society. Among such requirements are:

1. 3D (2D) kinematic target data extraction and tracking;
2. coverage of extended areas, including low-level airspace;
3. 24/7 area surveillance with high system robustness.

These challenges have become a triggering force for rediscovery of multistatic systems, which arose in the 1970s [5]. According to [5], **multistatic configuration** consists of many radar units at separate locations, which cooperate with each other. The units may be stationary or moving, although the misleading term "multistatic" is used instead of *multistation* or *multisite*. The replacement of a single complex radar with a network of simple radar units that enclose the observation area enables [6], [7], [8]

1. higher target detection performance;
2. higher estimation accuracy of the target position and velocity vectors;
3. lower minimum detectable velocity;
4. better classification capability.

Moreover, it has been shown that distributed radars play the role of gap filler of the low-level airspace, allowing for detection of an unmanned aerial vehicles (UAV) and hazardous weather phenomena, which occur on altitudes below 3 km [9]. Another benefit of multistatic radar system over a single radar is its feature of *graceful degradation*, which implies only a minor effect on the overall system performance from a single radar node failure [10].

### 1.1.2. TAXONOMY OF MULTISTATIC RADARS

The term "multistatic radar" covers a wide range of systems, which differ from each other by [6], [11], [12]:

1. the radar architecture
  - (a) monostatic, when transmit and receive antennas are collocated;
  - (b) bistatic, when transmit and receive antennas are separated by a distance, comparable to the expected target distance;
2. the type of radar transmitter
  - (a) cooperative (dedicated), which is specially designed for bistatic operation;

- (b) non-cooperative (hitchhiker, when transmitter of opportunity is from a bistatic radar; passive bistatic radar, when transmitter of opportunity is not a radar), which is designed for other purposes;
3. the manner of radar interaction with the target of interest
    - (a) active, when the target, equipped with a radar transponder that replies to signals from the radar interrogator (such as the aircraft target, which cooperates with secondary surveillance radar);
    - (b) passive, when a target does not cooperate with a radar;
  4. the level of autonomy in the signal reception and processing
    - (a) autonomous, when each receiver receives signals only from the dedicated transmitter;
    - (b) cooperative, when each receiver receive signals from all transmitters in the network;
  5. the level of the spatial coherency that is defined as ability to maintain phase stability of the radio frequency signals and interference between separated stations:
    - (a) coherent networks where inter-node phase shifts are known and can be maintained for a long period of time (several hours or days);
    - (b) short term coherent networks where the phase stability is maintained for a short period of time (less than a second);
    - (c) incoherent networks where neither inter-node phase shifts nor their changes with time are not known;
  6. the method of information fusion from individual radar nodes
    - (a) centralized: fusion of radio frequency signals, video signals;
    - (b) decentralized: individual target detections, plots, and tracks.

In this thesis, I focus on radar networks with widely separated antennas, which are also referred to as *statistical multi-input multi-output (MIMO) systems* in scientific literature [7]. According to [7], in statistical MIMO systems, the transmit and receive array elements are broadly spaced, which provides independent scattering responses for each antenna pairing. In contrast to statistical MIMO, coherent MIMO implies close spacing between elements in transmit and receive arrays. It was shown in [13] that statistical MIMO provides higher accuracy of the target parameters estimation compared to *coherent MIMO*. Such superiority in statistical MIMO is achieved due to *diversity gain*, e.g. spatial diversity of the nodes that allows improved measurement performance with the same number of channels.

A diagram of a radar network that consists of both monostatic and bistatic radars with cooperative reception and a passive target in the scene is shown in Fig.1.1. Signals received from cooperative transmitters are indicated with dashed

arrows. The cooperative transmission-reception mode provides an opportunity to increase the number of measurements and thus, to enhance the system performance. A passive target of interest implies a lower signal-to-noise ratio (SNR) of the received signals, compared to active targets, due to the two-way signal propagation (transmitter-target-receiver). From this it follows that network features and parameters of a single radar define system performance [14].

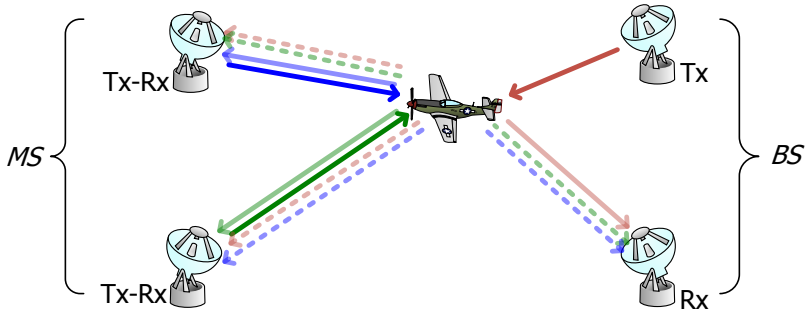


Figure 1.1: A combined monostatic and bistatic radar network with cooperative transmission-reception mode (indicated with dashed arrows).

Although the idea of the simultaneous exploitation of data from multiple radar nodes was already being discussed several decades ago, radar networks have been experimentally studied a great deal over the last few years due to advances in high data rate communication and signal processing capabilities, which made it possible at low cost to synchronize radar nodes and process their outputs simultaneously (and in real time) [15]. When compared to a single radar, data from spatially separated radar nodes enables 3D target localization and tracking (see Table 1.1). This poses additional challenges to the data processing algorithms in the sense that they should provide accurate estimation in scenarios when 1) the number of unknowns is much less than the number of measurements; 2) the measurements are corrupted by noise. Moreover, the price for these advanced functionalities is an additional processing step called *data association* (or *deghosting*).

Table 1.1: Single radar versus radar network

Functionalities	Single radar	Radar network
Detection	lower	higher
Estimation	1D	3D
Tracking	1D	3D

Data association is an inherent part of data processing of 3D targets localization in a radar network. It aims to identify the measurements from the radar nodes to the targets

in the scene. Incorrect identification results in a so-called *ghost phenomena*, that is, estimation of the target's position from a set of measurements that characterize different targets. As a result, the system performance deteriorates due to an increase of the false alarm probability. A geometrical interpretation of this phenomenon is shown in Fig. 1.2.

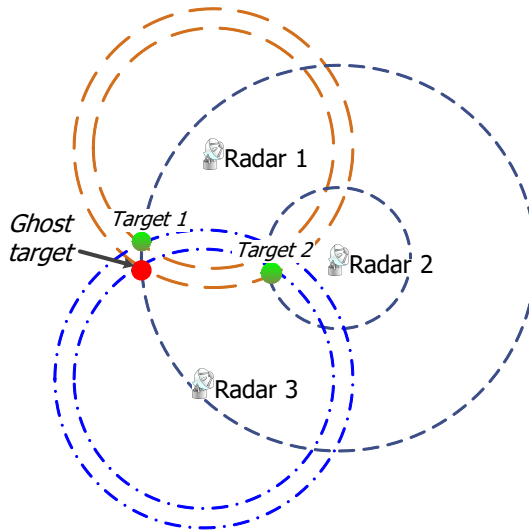


Figure 1.2: Ghost target phenomena

The deghosting problem is often considered in the framework of multiple target tracking. In this case, information of a target's state vector from the previous moment of time is used for data association as well [16]. The availability of such information helps to reduce the number of unresolved ghost targets substantially, compared to the case where there is no available prior knowledge of a target. A number of studies have been dedicated to the development of deghosting algorithms, based only on bearing measurements, both for localization and tracking purposes [17], [18], [19], [20]. Bearing measurements imply a limited observation area of a single radar, which is related to its antenna beamwidth. Despite that a target's range might be unknown, the number of potential ghosts will be lower than in the case of deghosting with range measurements from omnidirectional radars. An algorithm of multiple target coordinate estimation in bistatic MIMO radar, based on estimation of the 3D angles: azimuth transmit, transmit elevation, and receive cone angles is presented in [21].

Operational scenarios can impose limitations on a single radar observation area and thus, will limit the number of potentially detected targets. An example is an automotive radar scenario, where each radar sensor has a limited observation area of about 180 degrees due to its location behind the car's bumper [22]. Doppler measurements can be used for deghosting as well. The ordinary least squares (OLS) approach for target localization, based on the Doppler measurements, was proposed in [23] and modified to the weighted least squares (WLS) approach in [24], where Doppler measurements are further used in data association algorithms.

The type of radar network defines particular features of the deghosting procedure as well. A data association algorithm for MIMO radars that explores signals from transmitters of opportunity was developed in [25]. Since the transmitted signals are not under the user's control, time and/or frequency orthogonality of the signal cannot be provided, thus the authors propose first to perform a measurement-to-transmitter association prior to the measurement-to-object association.

### 1.3. METHODS OF TARGET POSITION AND VELOCITY ESTIMATION IN RADAR NETWORKS

The estimation of a target parameters in a multistatic radar network consists of two steps. The first step is the estimation of the signal parameters, such as time delay, difference in time delay (known in the communication field as time difference of arrival [TDOA]), Doppler shift, signal amplitude, azimuth and elevation angles. Depending on the sensor type, some of these signal parameters are further used for target state vector estimation in the second processing step.

Existing position estimation techniques can be divided into two classes [26]:

- *Deterministic*, which explore geometric relationships between measurements and target position.

Deterministic methods are: lateration, angulation or a combination of both (triangulation). In order to evaluate a three-dimensional target position from range measurements in a monostatic autonomous radar network, the minimum number of radars in the network is three. In this case, the direct target position calculation method can be used for target position estimation, which corresponds to the intersection of three spheres (see Appendix C). In scenarios, when there are more measurements than unknowns or they are corrupted by noise, statistical positioning techniques are used.

- *Statistical* parametric and non-parametric techniques.

Bayesian and maximum likelihood estimators (MLE) are parametric methods that imply some prior statistical knowledge of the parameter vector to be provided.

Non-parametric methods are least squares estimator (LSE), Taylor series estimator and spherical interpolation [27], [28], [29]. These methods do not require any prior statistical knowledge of the parameter vector.

The availability of low-cost, highly accurate Doppler sensors triggered the development of Doppler-based localization techniques. Weighted least squares method and polynomial optimization approach for target localization from Doppler shift measurements in the radar network were proposed in [30] and [24], respectively.

### 1.4. PROBLEM FORMULATION

Both data association and estimation performance of the network is highly affected by the number of radar nodes and their spatial geometry. In the context of data association,

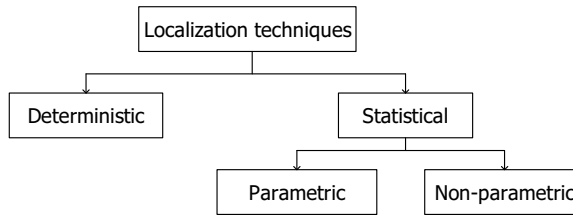


Figure 1.3: Classification of localization techniques

a condensed geometry of radar nodes with respect to surveillance areas leads to a number of incorrect data associations larger than in a geometry with widely separated radars [31]. Therefore, the selection of spatial positions of radar nodes is one of the key tasks in radar network resource allocation. The aim is to achieve optimal system performance with minimum cost. This task can be considered either as a real-time or off-line design task, depending on the particular application. For example, the target localization accuracy of the radar network is determined by ranging errors of each single radar and topology of the nodes [32]. In Global Positioning Systems, this phenomenon is often described with the geometric dilution of precision (GDOP) factor, which is defined as a ratio of the localization error to the ranging error, assumed to be the same for all satellites [33]. In a network of radars, such ranging errors differ from one radar to another due to different target-radar distances and single radar operational characteristics, and therefore, GDOP is not an efficient measure. This effect is captured with Cramér-Rao lower bound (CRLB), which incorporates both a single radar node and system parameters. Moreover, CRLB is a good approximation of the maximum likelihood estimator performance in the high SNR region (asymptotic region). This is not the case for the low SNR region (non-asymptotic region), where the estimator's performance departs from CRLB [34]. These two regions are separated by a threshold SNR as shown in Figure 1.4. Since high system estimation accuracy is the focus of this thesis, we are working with high SNR values from the asymptotic region. Furthermore, a shift of the threshold point (point that separates two regions) to the lower SNR values was observed by increasing the number of transmit and receive antennas [35].

Various techniques for spatial radar (sensor) placement are presented in scientific literature [36], [37], [38], [39], [40]. In general, for a given set of potential radar nodes positions, topology optimization problems are formulated in two ways:

1. Selection of the subset of radar nodes positions with *the minimal cardinality* that meets *fixed requirements to the system performance* in detection, estimation accuracy, classification or tracking quality.
2. Selection of the subset of radar nodes positions that provide *the best possible system performance* with *fixed cardinality*.

Depending on the mission, different performance metrics are used for the system design. Previous studies have mostly focused on the selection of radar network configurations that ensure only accurate target localization. However, a number of radar applications require knowledge of the full target state vector, which includes not

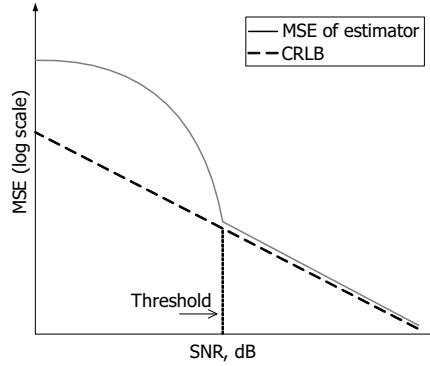


Figure 1.4: Threshold phenomena of target position estimation with MLE

only the location, but also the target velocity at each instant of time [41]. Additionally, the use of the Doppler shift provides a higher detection probability in strong clutter [42]. Topology optimization for the joint position and velocity vector estimation of a ground moving target (GMT) using pulse Doppler radars aboard unmanned aerial vehicles was considered in [43], [41]. The assumption made in [43], is however related to the constant accuracy of the UAV measurements and does not allow for an optimal solution in terms of signal-to-noise ratio. Both approaches from [43] and [41], explore the sensors' mobility, which require real-time optimization.

In this research, I focus on the off-line problem of selecting radar node positions to satisfy prescribed accuracy requirements of the target state vector estimation. The estimation accuracy measures are often chosen to be scalar functions of the error covariance matrix, such as 1) the maximum eigenvalue (E-optimality); 2) the trace (A-optimality); and 3) the log-determinant (D-optimality). Other measures, like mutual information, entropy, and cross-entropy are frequently used as well [44], [45]. The sensor selection problem is combinatorial in nature. Therefore, different optimization techniques are used to solve it in polynomial time. For example, convex optimization methods, which are based on the relaxation of the Boolean constraint  $\{0, 1\}^N$  on the selection coefficients, were shown to perform well in terms of mean squared error (MSE). At the same time, these methods imply a high computational cost. In contrast to convex methods, greedy algorithms have a linear complexity. While the first class of methods requires the cost function to be convex, the second one requires its submodularity. In particular, the log-determinant, the mutual information, and the entropy were shown to be submodular functions. Another submodular function, namely the frame potential (FP), which is a measure for the orthogonality of the rows of the measurement matrix, was introduced in [38] as a proxy for the mean squared error. Together with a low computational complexity, the FP-based greedy algorithm sometimes shows a competitive performance with convex optimization.

## 1.5. RESEARCH OBJECTIVE AND APPROACHES

Since the idea of multistatic radar is to provide a cost-effective solution, low-cost radars with wide-beam omnidirectional antennas are considered to be the most applicable for this purpose. In addition to range estimation, such radars, i.e. frequency-modulated continuous wave (FMCW), can provide Doppler frequency measurements as well. Both types of these measurements or their combination (as will be shown further in this thesis) can be used for target localization. An FMCW radar type with linear frequency modulated (LFM) waveform is considered in this thesis. A major focus of this thesis is a combination of two tasks:

1. development of a radar network performance assessment tool;
2. development of a generic framework for radar network topology optimization.

The first task has been tackled with development of the CRLB-based tool that allows evaluation of the potential accuracy of the target position and velocity vectors estimation in the radar networks. The main idea is to evaluate accuracy of the target range and radial velocity estimation of a single radar (1D). Thereafter, these quantities are used for evaluation of the potential accuracy of 3D target position and velocity vectors estimation, taking into account parameters of the system.

To tackle the second task, I developed two algorithms for radar network topology optimization, which are based on convex and greedy techniques. The optimization problem can be tackled in two ways, i.e. as the selection of the minimum number of radar nodes that meet some prescribed accuracy requirements or the selection of a fixed number of radar nodes that provide maximal estimation accuracy. A generic framework for topology optimization based on non-linear measurement models was developed for this purpose. The maximum eigenvalue, the frame potential and the log-determinant (LD) of the error covariance matrix are used as performance metrics. The LD and FP costs were shown to be submodular, which allows one to use greedy optimization algorithms, ensuring a near-optimal performance and a low computational complexity [38], [46]. The considered costs were redesigned to a specific non-linear model, where the parameter vector can take any value from the known parameter space and can be represented by entries of different modalities (e.g., range and velocity). The developed theoretical framework has been applied for performance assessment as well as for topology optimization of FMCW radar network, dedicated only to the target position estimation or to simultaneous estimation of the target position and velocity. Closed-form expressions of CRLB, FP and LD for an FMCW radar network were derived. As the data association task is very important for radar network operation, I paid some attention to it as well. Appendix C presents the developed data association algorithm for target localization based on time delay measurements in a monostatic radar network. The research, presented in this thesis, was supported by the RAEBELL (Feasibility Study of Low-level Airspace Surveillance) project.

## 1.6. THE OUTLINE OF THE THESIS

The thesis is organized as follows:

**Chapter 2** introduces the developed theory for evaluation of the potential estimation accuracy of target parameters, namely position and velocity vectors, in radar networks. The developed performance estimation framework is based on Cramér-Rao lower bound inequality. The approach for incorporation of the antenna pattern into the CRLB-based model is presented.

**Chapter 3** provides comprehensive analysis of the multistatic radar networks estimation performance. This analysis incorporates investigation of the influence of a single radar node (radar architecture, power budget and waveform parameters) and system (signal reception mode, transmitter type) parameters on the estimation performance. Moreover, the effect of a measurement type on target localization accuracy is studied as well.

**Chapter 4** presents an accuracy-driven topology optimization framework. Three cost functions, namely the minimum eigenvalue, the frame potential, and the log-determinant are developed for a generic, non-linear measurement model. The closed-form expressions for direct evaluation of FP and LD costs for a FMCW radar network are derived. An extension of the framework to the case of multi-modal parameter vector estimation as well as to selection-dependent models is provided.

**Chapter 5** demonstrates a range of applications of the developed framework for radar network topology optimization. Both greedy and convex optimization algorithms have been validated. In parallel, a comparison of the cost functions as well as optimization algorithms is performed.

**Chapter 6** presents the conclusions of the thesis and gives recommendations for future work.

## REFERENCES

- [1] A. Di Lallo, A. Farina, R. Fulcoli, A. Stile, L. Timmoneri, and D. Vigilante, *A real time test bed for 2D and 3D multi-radar tracking and data fusion with application to border control*, in *Radar, 2006. CIE '06. International Conference on* (2006) pp. 1–6.
- [2] F. Folster, H. Rohling, and U. Lubbert, *An automotive radar network based on 77 GHz FMCW sensors*, in *Radar Conference, 2005 IEEE International* (2005) pp. 871–876.
- [3] F. K. Wang, Y. R. Chou, Y. C. Chiu, and T. S. Horng, *Chest-worn health monitor based on a bistatic self-injection-locked radar*, *IEEE Transactions on Biomedical Engineering* **62**, 2931 (2015).
- [4] M. A. Slade, L. A. M. Benner, and A. Silva, *Goldstone solar system radar observatory: Earth-based planetary mission support and unique science results*, *Proceedings of the IEEE* **99**, 757 (2011).
- [5] E. Hanle, *Survey of bistatic and multistatic radar*, *Communications, Radar and Signal Processing, IEE Proceedings F* **133**, 587 (1986).

- [6] V. Chernyak, *Fundamentals of Multisite Radar Systems: Multistatic Radars and Multistatic Radar Systems* (CRC Press/INTECH, 1998).
- [7] J. Li and P. Stoica, *MIMO Radar Signal Processing* (Wiley, 2008).
- [8] J. Verzeilberg, *Coherent multistatic radar imaging*, master thesis, Delft university of technology (2011).
- [9] D. Pepyne, D. McLaughlin, D. Westbrook, E. Lyons, E. Knapp, S. Frasier, and M. Zink, *Dense radar networks for low-flyer surveillance*, in *Technologies for Homeland Security (HST), 2011 IEEE International Conference on* (2011) pp. 413–418.
- [10] H. Griffiths, *Multistatic, MIMO and networked radar: The future of radar sensors?* in *Radar Conference (EuRAD), 2010 European* (2010) pp. 81–84.
- [11] N. Willis and H. Griffiths, *Advances in Bistatic Radar*, Electromagnetics and Radar (Institution of Engineering and Technology, 2007).
- [12] C. Baker, *An introduction to multistatic radar*, in *NATO Research and Technology Organisation Lecture Series RTO-EN-SET-133 (Multistatic Surveillance and Reconnaissance: Sensor, Signals and Data Fusion)* (2009) pp. 1–20.
- [13] A. Haimovich, R. Blum, and L. Cimini, *MIMO radar with widely separated antennas*, *Signal Processing Magazine, IEEE* **25**, 116 (2008).
- [14] I. Ivashko, O. Krasnov, and A. Yarovoy, *Performance analysis of multisite radar systems*, in *Radar Conference (EuRAD), 2013 10th European* (2013).
- [15] F. Robey, S. Coutts, D. Weikle, J. McHarg, and K. Cuomo, *MIMO radar theory and experimental results*, in *Signals, Systems and Computers, 2004. Conference Record of the Thirty-Eighth Asilomar Conference on*, Vol. 1 (2004) pp. 300–304 Vol.1.
- [16] M. Daun, *Deghosting in passive air surveillance systems*, in *Radar Symposium (IRS), 2010 11th International* (2010) pp. 1–8.
- [17] B. Jing, W. Guohong, X. Jianjuan, and W. Xiaobo, *New deghosting method based on generalized triangulation*, *Systems Engineering and Electronics, Journal of* **20**, 504 (2009).
- [18] L. Paradowski, *Qualitative and quantitative characteristics of deghosting in advanced radar systems*, in *Africon Conference in Africa, 2002. IEEE AFRICON. 6th*, Vol. 1 (2002) pp. 19–24 vol.1.
- [19] M. Grabbe, B. Hamschin, and A. Douglas, *A measurement correlation algorithm for line-of-bearing geo-location*, in *Aerospace Conference, 2013 IEEE* (2013) pp. 1–8.
- [20] E. Fishler, A. Haimovich, R. Blum, D. Chizhik, L. Cimini, and R. Valenzuela, *MIMO radar: an idea whose time has come*, in *Radar Conference, 2004. Proceedings of the IEEE* (2004) pp. 71–78.

- [21] J. Li, H. Li, L. Long, G. Liao, and H. Griffiths, *Multiple target three-dimensional coordinate estimation for bistatic MIMO radar with uniform linear receive array*, EURASIP Journal on Advances in Signal Processing **2013**, 1 (2013).
- [22] H. Rabe, E. Denicke, G. Armbrrecht, T. Musch, and I. Rolfes, *Considerations on radar localization in multi-target environments*, Advances in Radio Science **7**, 5 (2009).
- [23] D. Mixon, *Doppler-Only Multistatic Radar* (Biblioscholar, 2012).
- [24] M. Caruso, P. Lombardo, and M. Sedehi, *A weighted least-square approach for multi-target doppler-only localization*, in *IEEE Radar conference, 2013* (2013).
- [25] M. Radmard, S. Karbasi, and M. Nayebi, *Data fusion in MIMO DVB-T-based passive coherent location*, Aerospace and Electronic Systems, IEEE Transactions on **49**, 1725 (2013).
- [26] D. Dardari, M. Luise, and E. Falletti, *Satellite and Terrestrial Radio Positioning Techniques: A Signal Processing Perspective*, Academic Press (Academic Press, 2011).
- [27] A. Sayed, A. Tarighat, and N. Khajehnouri, *Network-based wireless location: challenges faced in developing techniques for accurate wireless location information*, Signal Processing Magazine, IEEE **22**, 24 (2005).
- [28] W. H. Foy, *Position-location solutions by Taylor-series estimation*, IEEE Transactions on Aerospace and Electronic Systems **AES-12**, 187 (1976).
- [29] J. Smith and J. Abel, *The spherical interpolation method of source localization*, IEEE Journal of Oceanic Engineering **12**, 246 (1987).
- [30] I. Shames, A. Bishop, M. Smith, and B. Anderson, *Doppler shift target localization*, Aerospace and Electronic Systems, IEEE Transactions on **49**, 266 (2013).
- [31] A. Samokhin, I. Ivashko, and A. Yarovoy, *Algorithm for multiple targets localization and data association in distributed radar networks*, in *Radar Symposium (IRS), 2014 15th International* (2014) pp. 1–6.
- [32] D. Torrieri, *Statistical theory of passive location systems*, Aerospace and Electronic Systems, IEEE Transactions on **AES-20**, 183 (1984).
- [33] R. Langley, *Dilution of precision*, GPS World , 52 (1999).
- [34] A. Weiss and E. Weinstein, *Fundamental limitations in passive time delay estimation - Part I: Narrow-band systems*, Acoustics, Speech and Signal Processing, IEEE Transactions on **31**, 472 (Apr).
- [35] Q. He, R. Blum, and A. Haimovich, *Non-coherent MIMO radar for target estimation: More antennas means better performance*, in *Information Sciences and Systems, 2009. CISS 2009. 43rd Annual Conference on* (2009) pp. 108–113.
- [36] S. Chepuri and G. Leus, *Sparsity-promoting sensor selection for non-linear measurement models*, Signal Processing, IEEE Transactions on **63**, 684 (2015).

- [37] Q. He, R. Blum, H. Godrich, and A. Haimovich, *Target velocity estimation and antenna placement for MIMO radar with widely separated antennas*, Selected Topics in Signal Processing, IEEE Journal of 4, 79 (2010).
- [38] J. Ranieri, A. Chebira, and M. Vetterli, *Near-optimal sensor placement for linear inverse problems*, Signal Processing, IEEE Transactions on 62, 1135 (2014).
- [39] J. Isaacs, D. Klein, and J. Hespanha, *Optimal sensor placement for time difference of arrival localization*, in *Decision and Control, 2009 held jointly with the 2009 28th Chinese Control Conference. CDC/CCC 2009. Proceedings of the 48th IEEE Conference on (Dec.)* pp. 7878–7884.
- [40] C. Hoyuela, J. Terzuoli, A.J., and R. P. Wasky, *Determining possible receiver locations for passive radar*, Radar, Sonar and Navigation, IEE Proceedings - 152, 206 (2005).
- [41] P. Zhan, D. Casbeer, and A. Swindlehurst, *Adaptive mobile sensor positioning for multi-static target tracking*, Aerospace and Electronic Systems, IEEE Transactions on 46, 120 (2010).
- [42] X. Gong, J. Zhang, and D. Cochran, *When target motion matters: Doppler coverage in radar sensor networks*, in *INFOCOM, 2013 Proceedings IEEE* (2013) pp. 1169–1177.
- [43] G. Gu, P. Chandler, C. Schumacher, A. Sparks, and M. Pachter, *Optimal cooperative sensing using a team of UAVs*, Aerospace and Electronic Systems, IEEE Transactions on 42, 1446 (2006).
- [44] T. Onel, C. Ersoy, and H. Delic, *Information content-based sensor selection and transmission power adjustment for collaborative target tracking*, Mobile Computing, IEEE Transactions on 8, 1103 (2009).
- [45] H. Wang, G. Pottie, K. Yao, and D. Estrin, *Entropy-based sensor selection heuristic for target localization*, in *Information Processing in Sensor Networks, 2004. IPSN 2004. Third International Symposium on* (2004) pp. 36–45.
- [46] M. Shamaiah, S. Banerjee, and H. Vikalo, *Greedy sensor selection: Leveraging submodularity*, in *Decision and Control (CDC), 2010 49th IEEE Conference on* (2010) pp. 2572–2577.



# 2

## POTENTIAL ACCURACY OF TARGET POSITION AND VELOCITY VECTOR ESTIMATION IN MULTISTATIC RADAR

*This chapter aims to provide closed-form expressions for evaluation of the target position and velocity vectors estimation accuracy in radar networks. Two types of signal waveforms, namely WiFi and LFM, will be considered for passive and active radars respectively. First, the lower bounds on target range and Doppler frequency estimation accuracy of a single radar will be derived. Impact of the antenna patterns will be considered for the first time. Finally, these bounds will be used to evaluate potential estimation accuracy of the target position and velocity vector in the network of radars.*

## 2.1. SYSTEM MODEL

Without loss of generality, a bistatic radar network with cooperative signal reception, defined in Chapter 1, is considered in this chapter (Fig. 2.1). The radar networks with monostatic radar architecture and/or an autonomous mode of signal reception are special cases. A general non-linear measurement model for a set of  $N$  possible radar positions is considered

$$\mathbf{y} = \mathbf{f}(\boldsymbol{\alpha}) + \boldsymbol{\xi}, \quad (2.1)$$

where  $\mathbf{y} \in \mathbb{R}^{NQ}$  is the vector of accumulated measurements with  $Q$  being the number of accumulated signal samples per integration time in a single radar,  $\boldsymbol{\alpha} \in \mathbb{R}^K$  is the vector of parameters to be estimated,  $\mathbf{f}$  is the non-linear vector function, and  $\boldsymbol{\xi} \in \mathbb{R}^{NQ}$  is the measurement noise.

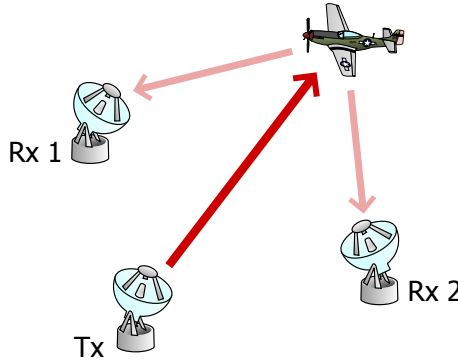


Figure 2.1: Bistatic radar network with cooperative mode of signal transmission-reception

Following the model (2.1), we define the signal reflected from the moving target as

$$\mathbf{y}^{(n)}(t) = \mathbf{f}^{(n)}(t; \boldsymbol{\alpha}) + \boldsymbol{\xi}^{(n)}(t), \quad (2.2)$$

where  $\boldsymbol{\alpha} = [x, y, z, v_x, v_y, v_z]^T$  is the parameter vector to be estimated;  $\boldsymbol{\xi}^{(n)}(t)$  is a zero-mean i.i.d. Gaussian noise with variance  $\sigma^2$  and

$$\mathbf{f}^{(n)}(t; \boldsymbol{\alpha}) = A^{(n)} \exp(-j(t - \tau^{(n)})\omega_d^{(n)}) x^{(n)}(t - \tau^{(n)}) \quad (2.3)$$

with  $x^{(n)}(t - \tau^{(n)})$  as time-delayed transmit signal, reflected from the target;  $A^{(n)} = |A^{(n)}| \exp(j\varphi^{(n)})$  is the non-fluctuating amplitude of the received signal;  $\tau^{(n)}$  is the signal time delay related to bistatic target-radar distance  $R^{(n)}$  as

$$\tau^{(n)} = \frac{R^{(n)}}{c} = \frac{R_t^{(n_t)} + R_r^{(n_r)}}{c}, \quad (2.4)$$

where  $R_t^{(n_t)}$  and  $R_r^{(n_r)}$  are distances from the  $n_t$ th transmitter and  $n_r$ th receiver to the target;  $n_t = 1, \dots, N_t$ , and  $n_r = 1, \dots, N_r$  with  $N_t$  and  $N_r$  being the number of transmitting and receiving radar nodes respectively.

$$R_t^{(n_t)} = \sqrt{(x - x_t^{(n_t)})^2 + (y - y_t^{(n_t)})^2 + (z - z_t^{(n_t)})^2}, \quad (2.5)$$

$$R_r^{(n_r)} = \sqrt{(x - x_r^{(n_r)})^2 + (y - y_r^{(n_r)})^2 + (z - z_r^{(n_r)})^2}, \quad (2.6)$$

$c$  is the speed of light;  $(x, y, z)$ ,  $(x_t^{(n_t)}, y_t^{(n_t)}, z_t^{(n_t)})$ ,  $(x_r^{(n_r)}, y_r^{(n_r)}, z_r^{(n_r)})$  are coordinate vectors of the target,  $n_t$ th Tx and  $n_r$ th Rx nodes. The measured Doppler frequency  $f_d^{(n)} = \omega_d^{(n)}/2\pi$  in the  $n$ th Tx-Rx channel is defined by the radial components of the target velocity towards  $n_t$ th Tx and  $n_r$ th Rx radar nodes

$$f_d^{(n)} = \frac{f_c^{(n_r)}}{c} \left( \frac{\partial R_t^{(n_t)}}{\partial t} + \frac{\partial R_r^{(n_r)}}{\partial t} \right), \quad (2.7)$$

where  $\partial R_t^{(n_t)}/\partial t = (v_x(x - x_t^{(n_t)}) + v_y(y - y_t^{(n_t)}) + v_z(z - z_t^{(n_t)}))/R_t^{(n_t)}$  and  $\partial R_r^{(n_r)}/\partial t = (v_x(x - x_r^{(n_r)}) + v_y(y - y_r^{(n_r)}) + v_z(z - z_r^{(n_r)}))/R_r^{(n_r)}$  with  $v_x, v_y, v_z$  being projections of the target velocity  $\mathbf{v}$  on coordinate axes  $x, y$ , and  $z$ .

Interferences between different radars are excluded, assuming signal orthogonality in frequency or time domain are realized. It is assumed that target detection and consequent signal parameters estimation is performed locally in a single radar node. These estimates are forwarded to the central processing unit afterwards, where the estimation of the target parameters in 3D space takes place. It is assumed that each of  $N_t$  totally available transmitters forms a bistatic sensing pair with each of  $N_r$  available receivers, which results in  $N = N_t N_r$  bistatic pairs.

A single target case is considered throughout the chapter. It is assumed that measurements from multiple targets in the scene are associated by using an appropriate algorithm, like the one presented in Appendix C. Effects of the target rotations are not incorporated in this model. Radar cross-section (RCS) is assumed to be constant during dwell time and follows Swerling I target model. Multipath effects are neglected, assuming that the multipath is suppressed during detection and estimation in a single radar. The signal attenuation that occurs due to the finite target-radar distance is taken into account, following the classic radar equation

$$P_r = \frac{P_t G_t G_r \text{RCS} \lambda^2}{(4\pi)^3 R_t^2 R_r^2 L_{\text{sys}t}} G_{\text{proc}}, \quad (2.8)$$

where  $P_t$  is the transmitted power,  $G_t$  is the Tx antenna gain,  $G_r$  is the Rx antenna gain,  $\lambda$  is the signal wavelength,  $L_{\text{sys}t}$  is the system loss,  $G_{\text{proc}}$  is the processing gain.

## 2.2. THE CRAMÉR-RAO LOWER BOUND

THE Cramér-Rao lower bound defines the lower bound on the variance of any unbiased estimator [3, 4]. For the unbiased estimator  $\hat{\boldsymbol{\alpha}}$  of the parameter vector  $\boldsymbol{\alpha} = [\alpha_1, \alpha_2, \dots, \alpha_K]$  with  $K$  components, the CRLB allows one to evaluate a bound on the variance of each element from the parameter vector  $\boldsymbol{\alpha}$  [4]

$$\text{Var}(\hat{\alpha}_i) \geq [\mathbf{I}^{-1}(\boldsymbol{\alpha})]_{ii}, \quad (2.9)$$

where  $\mathbf{I}$  is the  $K \times K$  Fisher information matrix (FIM) with elements

$$[\mathbf{I}(\boldsymbol{\alpha})]_{ij} = - \left\langle \frac{\partial^2 \ln g(\mathbf{y}; \boldsymbol{\alpha})}{\partial \alpha_i \partial \alpha_j} \right\rangle, \quad (2.10)$$

where  $\mathbf{y}$  is the vector of sampled measurements from (2.1);  $g(\mathbf{y}; \boldsymbol{\alpha})$  is the probability density function parameterized by the unknown parameter  $\boldsymbol{\alpha}$ ; sign  $\langle \cdot \rangle$  means statistical average of the quantity in the brackets;  $i = 1, \dots, K$ ;  $j = 1, \dots, K$ .

The accuracy of the estimation of the target parameters in the radar networks depends on the type of the radar network, topology of the radar nodes, waveform parameters and power budget of each radar. All of these parameters can be incorporated into the CRLB. For example, by analyzing the contour plots of the localization CRLB, impact of different waveform parameters on the overall system performance can be analyzed. Another example is the selection of the most favorable geometry of the radar nodes given the CRLB distribution over the area of interest, like area of potential target location. Therefore, the CRLB can be used as a cost function in the task of radar network resource allocation. It will be shown in Chapter 4, that scalar functions of CRLB can efficiently be used for radar network topology optimization.

### 2.3. RANGING ACCURACY OF PASSIVE BISTATIC RADAR WITH WiFi TRANSMISSIONS

Exploitation of WiFi signals for short-range surveillance applications has demonstrated reasonable performance in terms of the localization accuracy [5]. Moreover, wide accessibility of free WiFi transmitters increases the interest of passive radar network applications. This type of passive surveillance can be used solely or can be integrated with existing surveillance systems in order to increase their performance. The three most commonly used WiFi standards for signal transmission are: 802.11a, 802.11b, and 802.11g. An 802.11 access point periodically transmits a beacon signal, broadcasting its presence and channel information.

The beacon signal consists of two parts, modulated with the direct sequence spread spectrum (DSSS) modulation. One part uses differential binary phase shift keying (DBPSK), and the other exploits quadrature phase shift keying (DQPSK). The 11-chip Barker code is used

$$\mathbf{c} = [1, -1, 1, 1, -1, 1, 1, 1, -1, -1, -1]. \quad (2.11)$$

The DSSS signal is

$$s_{DSSS}(t) = \sum_{n=0}^{N-1} d_n b(t - nT_s), \quad (2.12)$$

where  $d_n$  is the  $n$ th complex symbol in the modulation scheme (BPSK, QPSK);  $T_s = 1 \mu s$  is the symbol duration;  $b(t)$  is the pulse shape function

$$b(t) = \sum_{k=0}^{10} c[k] w(t - kT_c), \quad (2.13)$$

where  $c[k]$  is the  $k$ th element in the Barker code;  $w(t)$  is the chip time-window;  $T_c = T_s/11 = 0.0909 \mu s$  is the chip duration. The chip time-window is assumed such that

$$w(t) = \begin{cases} \exp(i\omega_c t), & t \in [0, T_c] \\ 0, & \text{otherwise} \end{cases} \quad (2.14)$$

with the carrier frequency of the transmitted signal  $f_c$ . The received radar signal, reflected from the target, is represented with the measurement model for a single radar given by (2.1) with  $N = 1$ :

$$y(t) = A s_{DSSS}(t + \tau) + \xi(t) = f(t; \boldsymbol{\alpha}) + \xi(t), \quad (2.15)$$

where  $\boldsymbol{\alpha} = [x, y, z]$  is the target position parameter vector. According to [6], elements of the FIM can be derived from the ambiguity function  $\chi(\tau, \omega_d)$  as well:

$$I_{\alpha_i \alpha_j} = -\frac{|A|^2}{N_0} \frac{\partial^2 |\chi(\tau, \omega_d)|^2}{\partial \alpha_i \partial \alpha_j}. \quad (2.16)$$

For zero Doppler shift, the ambiguity function is reduced to the auto-correlation function (ACF):

$$\chi(\tau) = \frac{\int_{-\infty}^{+\infty} s_{DSSS}(t) s_{DSSS}^*(t + \tau) dt}{\int_{-\infty}^{+\infty} s_{DSSS}(t) s_{DSSS}^*(t) dt}. \quad (2.17)$$

Function  $w(t - nT_s - kT_c)$  is defined as

$$w(t - nT_s - kT_c) = \begin{cases} \exp(i w_c(t - nT_s - kT_c)), & t \in [nT_s + kT_c, nT_s + (k+1)T_c] \\ 0, & \text{otherwise} \end{cases}$$

Similarly,

$$w^*(t - nT_s - qT_c) = \begin{cases} \exp(-i w_c(t - nT_s - qT_c)), & t \in [nT_s + qT_c, nT_s + (q+1)T_c] \\ 0, & \text{otherwise} \end{cases}$$

Then the denominator will be simplified to

$$\begin{aligned} \int_0^{NT_s} s_{DSSS}(t) s_{DSSS}^*(t) dt &= \sum_{n=0}^{N-1} |d_n|^2 \int_0^{NT_s} |b(t - nT_s)|^2 dt = \\ &= \sum_{n=0}^{N-1} |d_n|^2 \sum_{k=0}^{N-1} c^2[k] \int_{nT_s + kT_c}^{nT_s + (k+1)T_c} 1 dt = 11NT_c = NT_s. \end{aligned} \quad (2.18)$$

The numerator is

$$\int_0^{NT_s} s_{DSSS}(t) s_{DSSS}^*(t + \tau) dt = \sum_{n=0}^{N-1} d_n \sum_{m=0}^{N-1} d_m^* \int_0^{NT_s} b(t - nT_s) b^*(t + \tau - mT_s) dt. \quad (2.19)$$

Functions  $b(t - nT_s)$  and  $b^*(t + \tau - mT_s)$  overlap at  $n = m$  and  $n = m - 1$ . Let us consider these two cases separately.

1.  $n = m = 0$

$$\int_0^{NT_s} b(t)b^*(t+\tau)dt = \sum_{q=0}^{10} c[q] \sum_{k=0}^{10} c[k] \int_0^{NT_s} w(t-qT_c)w^*(t+\tau-kT_c)dt; \quad (2.20)$$

Functions  $w(t-qT_c)$  and  $w^*(t+\tau-kT_c)$  overlap at  $k = q = 0$  and  $k = q + 1$ . These two cases will be considered separately.

(a)  $k = q = 0$

$$\int_0^{NT_s} w(t-qT_c)w^*(t+\tau-kT_c)dt = \int_0^{NT_s} w(t)w^*(t+\tau)dt. \quad (2.21)$$

The domain of function  $w(t)$  has been defined in (2.14). Similarly, for function  $w^*(t+\tau)$

$$w^*(t+\tau) = \begin{cases} \exp(-iw_c(t+\tau)), & t \in [-\tau, \tau + T_c] \\ 0, & \text{otherwise} \end{cases}$$

Consequently, the overlapping interval of these two functions is  $t \in [0, T_c - \tau]$ . The integral (2.21) will be

$$\int_0^{NT_s} w(t)w^*(t+\tau)dt = \int_0^{T_c-\tau} e^{iw_c t} e^{-iw_c(t+\tau)} = e^{-iw_c \tau} [T_c - \tau]. \quad (2.22)$$

(b)  $k = q + 1$  ( $q = 0, k = 1$ )

$$\int_0^{NT_s} w(t-qT_c)w^*(t+\tau-kT_c)dt = \int_0^{NT_s} w(t)w^*(t+\tau-T_c)dt \quad (2.23)$$

Again, function  $w(t)$  is non-zero on the interval  $t \in [0, T_c]$ ; and function  $w^*(t+\tau-T_c)$  is defined as

$$w^*(t+\tau-T_c) = \begin{cases} \exp(-iw_c(t+\tau-T_c)), & t \in [T_c-\tau, 2T_c-\tau] \\ 0, & \text{otherwise} \end{cases}$$

The overlapping interval of these two functions is  $t \in [T_c - \tau, T_c]$ . Then integral (2.23) becomes

$$\int_0^{NT_s} w(t)w^*(t+\tau-T_c)dt = e^{-iw_c(\tau-T_c)}\tau. \quad (2.24)$$

Let us introduce the following notation:

$$B_{q,k} = \int_0^{NT_s} w(t - qT_c) w^*(t + \tau - kT_c) dt.$$

Consequently,  $B_{q,q} = (T_c - \tau) e^{-i\omega_c \tau}$ ,  $B_{q,q+1} = \tau e^{-i\omega_c(\tau - T_c)}$  and we will get

$$\begin{aligned} \sum_{q=0}^{10} c[q] \sum_{k=0}^{10} c[k] B_{q,k} &= \sum_{q=0}^{10} c^2[q] B_{q,q} + \sum_{q=0}^9 c[q] c[q+1] B_{q,q+1} = \\ &= 11 [T_c - \tau] e^{-i\omega_c \tau}. \end{aligned} \quad (2.25)$$

Finally, for  $n = m$

$$\int_0^{NT_s} b(t - nT_s) b^*(t + \tau - mT_s) dt = 11 [T_c - \tau] e^{-i\omega_c \tau}; \quad (2.26)$$

2.  $n = m - 1$  ( $n = 0, m = 1$ )

$$\begin{aligned} \int_0^{NT_s} b(t) b^*(t + \tau - T_s) dt &= \\ &= \sum_{q=0}^{10} c[q] \sum_{k=0}^{10} c[k] \int_0^{NT_s} w(t - qT_c) w^*(t + \tau - kT_c - T_s) dt; \end{aligned} \quad (2.27)$$

Functions  $w(t - qT_c)$  and  $w^*(t + \tau - kT_c - T_s)$  will overlap only at  $k = q - 10$ .

(a)  $k = q - 10$  ( $k = 0, q = 10$ )

$$\int_0^{NT_s} w(t - qT_c) w^*(t + \tau - kT_c - T_s) dt = \int_0^{NT_s} w(t - 10T_c) w^*(t + \tau - T_s) dt \quad (2.28)$$

Function  $w(t - 10T_c)$  is defined such that

$$w(t - 10T_c) = \begin{cases} \exp(i\omega_c(t - 10T_c)), & t \in [10T_c, 11T_c] \\ 0, & \text{otherwise} \end{cases}.$$

And function  $w^*(t + \tau - T_s)$  is defined as

$$w^*(t + \tau - T_s) = \begin{cases} \exp(-i\omega_c(t + \tau - T_s)), & t \in [T_s - \tau, T_s + T_c - \tau] \\ 0, & \text{otherwise} \end{cases}.$$

These two functions overlap on the interval  $t \in [T_s - \tau, T_s]$ . Consequently, (2.28) is simplified to

$$\int_0^{NT_s} w(t - 10T_c)w^*(t + \tau - T_s)dt = \tau e^{-iw_c(\tau - T_c)}. \quad (2.29)$$

Let us introduce a new notation:

$$C_{q,k} = \int_0^{NT_s} w(t - qT_c)w^*(t + \tau - kT_c - T_s)dt.$$

Consequently,  $C_{q,q} = 0$ ,  $C_{q,q-10} = e^{-iw_c(\tau - T_c)}\tau$  and we will get

$$\sum_{q=0}^{10} c[q] \sum_{k=0}^{10} c[k] C_{q,k} = \sum_{q=10}^{10} c[q] c[q-10] C_{q,q-10} = -\tau e^{-iw_c(\tau - T_c)}. \quad (2.30)$$

Finally, at  $n = m - 1$ :

$$\int_0^{NT_s} b(t - nT_s)b^*(t + \tau - mT_s)dt = -\tau e^{-iw_c(\tau - T_c)}. \quad (2.31)$$

In order to find a closed-form expression of the numerator (2.19), let us introduce the following notation:  $G_{n,m} = \int_0^{NT_s} b(t - nT_s)b^*(t + \tau - mT_s)dt$ . Then, we will get  $G_{n,n} = 11[T_c - \tau]e^{-iw_c\tau}$ ,  $G_{n,n-1} = -\tau e^{-iw_c(\tau - T_c)}$ . The numerator is simplified to

$$\begin{aligned} \int_0^{NT_s} s_{DSSS}(t)s_{DSSS}^*(t + \tau)dt &= \sum_{n=0}^{N-1} d_n \sum_{m=0}^{N-1} d_m^* G_{n,m} = \sum_{n=0}^{N-1} |d_n|^2 G_{n,n} + \sum_{n=1}^{N-1} d_n d_{n-1}^* G_{n,n-1} = \\ &= 11N[T_c - \tau]e^{-iw_c\tau} + (-\tau)e^{-iw_c(\tau - T_c)} \sum_{n=1}^{N-1} d_n d_{n-1}^*. \end{aligned} \quad (2.32)$$

The auto-correlation function is then given by

$$\chi(\tau) = \frac{1}{NT_s} e^{-iw_c\tau} \left[ 11N[T_c - \tau] + (-\tau)e^{iw_c T_c} \left[ \sum_{n=1}^{N-1} d_n d_{n-1}^* \right] \right]. \quad (2.33)$$

Substituting (2.33) into (2.16), we get

$$(I^{-1})_{\tau\tau} = \frac{T_c^2}{2\text{SNR}}. \quad (2.34)$$

## 2.4. RANGE AND DOPPLER FREQUENCY ESTIMATION ACCURACY IN FMCW RADAR

Each FMCW radar transmits a burst of linear frequency-modulated pulses that can be represented by

$$x^{(n)}(t) = A_0 \exp\left(jt \left[\omega_c + \text{frac}\left(\frac{t}{T_s}\right)\Delta\omega\right]\right), \quad (2.35)$$

where  $A_0 = |A_0| \exp(j\varphi_0)$  is the transmit signal amplitude,  $\omega_c = 2\pi f_c$  with  $f_c$  the signal centre frequency,  $\Delta\omega = 2\pi\Delta f$  with  $\Delta f$  the signal bandwidth,  $n = 1, \dots, N$ , and  $T_s$  is the sweep time;  $0 < t < DT_s$  with  $D$  integrated number of pulses. The received radar signal, shifted in time and Doppler, is given by (2.1) with  $N = 1$ .

Except for the time delay and Doppler frequency, the complex signal amplitude  $A^{(n)}$  of the received signal is estimated as well. Consequently, the parameter vector in this stage of the signal parameters estimation is equal to four  $K = 4$ :  $\boldsymbol{\psi} = [\tau, \omega_d, |A|, \varphi]$ . Neither absolute value  $|A|$  nor phase  $\varphi$  is used to estimate target position and velocity. Therefore, complex signal amplitude plays the role of nuisance parameter in the considered model.

Since the measured signal samples are complex parameters, equation (2.10) can be rewritten as [4]

$$I_{ij} = \frac{1}{\sigma^2} \text{Re} \sum_{q=1}^Q \left( \frac{\partial f_q^*}{\partial \alpha_i} \right) \left( \frac{\partial f_q}{\partial \alpha_j} \right), \quad Q \gg K \quad (2.36)$$

The received noiseless signal resulting from the reflection of one target is shifted in time and frequency and is given by (2.3).

As was discussed before, the complex signal amplitude is one of the parameters in the estimation. The FIM is

$$\mathbf{I} = \begin{pmatrix} I_{\tau\tau} & I_{\tau\omega_d} & I_{\tau\varphi} & I_{\tau|A|} \\ I_{\omega_d\tau} & I_{\omega_d\omega_d} & I_{\omega_d\varphi} & I_{\omega_d|A|} \\ I_{\varphi\tau} & I_{\varphi\omega_d} & I_{\varphi\varphi} & I_{\varphi|A|} \\ I_{|A|\tau} & I_{|A|\omega_d} & I_{|A|\varphi} & I_{|A||A|} \end{pmatrix}. \quad (2.37)$$

From equation (2.36), the elements of the FIM are

$$I_{\tau\tau} = \frac{|A|^2}{\sigma^2 Q^2} \sum_{q=1}^Q \left[ \omega_c + \text{frac}\left(\frac{t_q - \tau}{T_s}\right)\Delta\omega - \omega_d \right]^2;$$

$$I_{\omega_d\omega_d} = \frac{|A|^2}{\sigma^2 Q^2} \sum_{q=1}^Q (t_q - \tau)^2;$$

$$I_{|A||A|} = \frac{1}{\sigma^2 Q};$$

$$I_{\varphi\varphi} = \frac{|A|^2}{\sigma^2 Q};$$

$$I_{\tau\omega_d} = \frac{|A|^2}{\sigma^2 Q^2} \sum_{q=1}^Q (t_q - \tau) [\omega_c + \text{frac}\left(\frac{t_q - \tau}{T_s}\right) \Delta\omega - \omega_d];$$

$$I_{\tau|A|} = 0;$$

$$I_{\tau\varphi} = -\frac{|A|^2}{\sigma^2 Q^2} \sum_{q=1}^Q [\omega_c + \text{frac}\left(\frac{t_q - \tau}{T_s}\right) \Delta\omega - \omega_d];$$

$$I_{\omega_d|A|} = 0;$$

$$I_{\omega_d\varphi} = -\frac{|A|^2}{\sigma^2 Q^2} \sum_{q=1}^Q (t_q - \tau);$$

$$I_{\varphi|A|} = 0;$$

Consequently, the FIM becomes a block matrix

$$\mathbf{I} = \begin{pmatrix} \mathbf{G} & \mathbf{0} \\ \mathbf{0} & I_{|A||A|} \end{pmatrix}; \quad (2.38)$$

where the matrix  $\mathbf{G}$  is

$$\mathbf{G} = \begin{pmatrix} I_{\tau\tau} & I_{\tau\omega_d} & I_{\tau\varphi} \\ I_{\omega_d\tau} & I_{\omega_d\omega_d} & I_{\omega_d\varphi} \\ I_{\varphi\tau} & I_{\varphi\omega_d} & I_{\varphi\varphi} \end{pmatrix}. \quad (2.39)$$

The inverted FIM is

$$\mathbf{I}^{-1} = \begin{pmatrix} \mathbf{G}^{-1} & \mathbf{0} \\ \mathbf{0} & I_{|A||A|}^{-1} \end{pmatrix}, \quad (2.40)$$

that follows from

$$\mathbf{\Pi}^{-1} = \begin{pmatrix} \mathbf{G}\mathbf{G}^{-1} & \mathbf{0} \\ \mathbf{0} & I_{|A||A|} I_{|A||A|}^{-1} \end{pmatrix} = \begin{pmatrix} \mathbf{1} & \mathbf{0} \\ \mathbf{0} & \mathbf{1} \end{pmatrix} \quad (2.41)$$

The variances of the time delay and Doppler frequency measurement errors are

$$\sigma_{\tau\tau}^2 = [\mathbf{I}^{-1}]_{\tau\tau} = [\mathbf{G}^{-1}]_{\tau\tau} = \frac{1}{\det(\mathbf{G})} [I_{\omega_d\omega_d} I_{\varphi\varphi} - I_{\varphi\omega_d}^2]; \quad (2.42)$$

$$\sigma_{\omega_d\omega_d}^2 = [\mathbf{I}^{-1}]_{\omega_d\omega_d} = [\mathbf{G}^{-1}]_{\omega_d\omega_d} = \frac{1}{\det(\mathbf{G})} [I_{\tau\tau} I_{\varphi\varphi} - I_{\varphi\tau}^2]. \quad (2.43)$$

Using the Taylor series expansion, the closed-form expressions of the error variances of estimation of the time delay and Doppler frequency are

$$\sigma_{\tau\tau}^2 \approx \frac{3}{2} \frac{1}{\Delta\omega^2 SNR} \quad (2.44)$$

$$\sigma_{\omega_d\omega_d}^2 \approx \frac{6}{T_s^2 D^2 SNR} \quad (2.45)$$

Here  $SNR$  is defined as  $SNR = \frac{|A|^2}{2\sigma^2}$ .

## 2.5. THE TARGET LOCALIZATION AND VELOCITY VECTOR ESTIMATION ACCURACY IN A RADAR NETWORK

The accuracy of the target data estimation based on target range and radial velocity, estimated locally in a single radar, will be analyzed in subsequent chapters. Three major measurement models are analyzed: 1) target localization, based on time delays; 2) target position and/or velocity vector estimation, based on Doppler frequency shifts; 3) target position and/or velocity vector estimation, based on time delays and Doppler frequency shifts (Doppler shifts are used both for target localization and velocity estimation). All three models imply a two-step estimation procedure. The first step is the estimation of the target range and/or radial velocity in a single radar. The second step is the estimation of the target position and/or velocity vectors. Consequently, we use the chain rule for evaluation of the FIM on the target position and velocity vectors [4]

$$\mathbf{I}(\boldsymbol{\alpha}) = \mathbf{H}^T \mathbf{I}(\boldsymbol{\psi}) \mathbf{H}, \quad (2.46)$$

where

$$\mathbf{H} = \frac{\partial \boldsymbol{\psi}(\boldsymbol{\alpha})}{\partial \boldsymbol{\alpha}} \quad (2.47)$$

is  $N \times K$  Jacobian matrix with  $K$  being the number of estimation parameters. In particular, for three measurement models we will have:

1.  $\boldsymbol{\alpha} = [x, y, z]$ ,  $\boldsymbol{\psi} = \tau$ , and

$$\mathbf{H} = \begin{bmatrix} \frac{\partial \tau^{(1)}}{\partial x} & \frac{\partial \tau^{(1)}}{\partial y} & \frac{\partial \tau^{(1)}}{\partial z} \\ \vdots & \vdots & \vdots \\ \frac{\partial \tau^{(n)}}{\partial x} & \frac{\partial \tau^{(n)}}{\partial y} & \frac{\partial \tau^{(n)}}{\partial z} \end{bmatrix}; \quad (2.48)$$

2.  $\boldsymbol{\alpha} = [x, y, z, v_x, v_y, v_z]$ ,  $\boldsymbol{\psi} = \omega_d$ , and

$$\mathbf{H} = \begin{bmatrix} \frac{\partial \omega_d^{(1)}}{\partial x} & \frac{\partial \omega_d^{(1)}}{\partial y} & \frac{\partial \omega_d^{(1)}}{\partial z} & \frac{\partial \omega_d^{(1)}}{\partial v_x} & \frac{\partial \omega_d^{(1)}}{\partial v_y} & \frac{\partial \omega_d^{(1)}}{\partial v_z} \\ \vdots & \vdots & \vdots & \vdots & \vdots & \vdots \\ \frac{\partial \omega_d^{(n)}}{\partial x} & \frac{\partial \omega_d^{(n)}}{\partial y} & \frac{\partial \omega_d^{(n)}}{\partial z} & \frac{\partial \omega_d^{(n)}}{\partial v_x} & \frac{\partial \omega_d^{(n)}}{\partial v_y} & \frac{\partial \omega_d^{(n)}}{\partial v_z} \end{bmatrix}; \quad (2.49)$$

3.  $\boldsymbol{\alpha} = [x, y, z, v_x, v_y, v_z]$ ,  $\boldsymbol{\psi} = [\tau, \omega_d]$ , and

$$\mathbf{H} = \begin{bmatrix} \frac{\partial \tau^{(1)}}{\partial x} & \frac{\partial \tau^{(1)}}{\partial y} & \frac{\partial \tau^{(1)}}{\partial z} & \frac{\partial \tau^{(1)}}{\partial v_x} & \frac{\partial \tau^{(1)}}{\partial v_y} & \frac{\partial \tau^{(1)}}{\partial v_z} \\ \vdots & \vdots & \vdots & \vdots & \vdots & \vdots \\ \frac{\partial \tau^{(n)}}{\partial x} & \frac{\partial \tau^{(n)}}{\partial y} & \frac{\partial \tau^{(n)}}{\partial z} & \frac{\partial \tau^{(n)}}{\partial v_x} & \frac{\partial \tau^{(n)}}{\partial v_y} & \frac{\partial \tau^{(n)}}{\partial v_z} \\ \frac{\partial \omega_d^{(1)}}{\partial x} & \frac{\partial \omega_d^{(1)}}{\partial y} & \frac{\partial \omega_d^{(1)}}{\partial z} & \frac{\partial \omega_d^{(1)}}{\partial v_x} & \frac{\partial \omega_d^{(1)}}{\partial v_y} & \frac{\partial \omega_d^{(1)}}{\partial v_z} \\ \vdots & \vdots & \vdots & \vdots & \vdots & \vdots \\ \frac{\partial \omega_d^{(n)}}{\partial x} & \frac{\partial \omega_d^{(n)}}{\partial y} & \frac{\partial \omega_d^{(n)}}{\partial z} & \frac{\partial \omega_d^{(n)}}{\partial v_x} & \frac{\partial \omega_d^{(n)}}{\partial v_y} & \frac{\partial \omega_d^{(n)}}{\partial v_z} \end{bmatrix}; \quad (2.50)$$

The derivatives of the time delay and Doppler frequency with respect to the target coordinates and velocities are:

$$\begin{aligned}
 \frac{\partial \tau^{(n)}}{\partial x} &= \frac{1}{c} \left( \frac{(x - x_t^{(n_t)})}{R_t^{(n_t)}} + \frac{(x - x_r^{(n_r)})}{R_r^{(n_r)}} \right); & \frac{\partial \tau^{(n)}}{\partial v_x} &= 0; \\
 \frac{\partial \tau^{(n)}}{\partial y} &= \frac{1}{c} \left( \frac{(y - y_t^{(n_t)})}{R_t^{(n_t)}} + \frac{(y - y_r^{(n_r)})}{R_r^{(n_r)}} \right); & \frac{\partial \tau^{(n)}}{\partial v_y} &= 0; \\
 \frac{\partial \tau^{(n)}}{\partial z} &= \frac{1}{c} \left( \frac{(z - z_t^{(n_t)})}{R_t^{(n_t)}} + \frac{(z - z_r^{(n_r)})}{R_r^{(n_r)}} \right); & \frac{\partial \tau^{(n)}}{\partial v_z} &= 0.
 \end{aligned} \tag{2.51}$$

$$\begin{aligned}
 \frac{\partial \omega_d^{(n)}}{\partial x} &= \frac{\omega_c}{c} \left( \frac{(R_t^{(n_t)})^2 v_x - b_t^{(n_t)}(x - x_t^{(n_t)})}{(R_t^{(n_t)})^3} + \frac{(R_r^{(n_r)})^2 v_x - b_r^{(n_r)}(x - x_r^{(n_r)})}{(R_r^{(n_r)})^3} \right); \\
 \frac{\partial \omega_d^{(n)}}{\partial y} &= \frac{\omega_c}{c} \left( \frac{(R_t^{(n_t)})^2 v_y - b_t^{(n_t)}(y - y_t^{(n_t)})}{(R_t^{(n_t)})^3} + \frac{(R_r^{(n_r)})^2 v_y - b_r^{(n_r)}(y - y_r^{(n_r)})}{(R_r^{(n_r)})^3} \right); \\
 \frac{\partial \omega_d^{(n)}}{\partial z} &= \frac{\omega_c}{c} \left( \frac{(R_t^{(n_t)})^2 v_z - b_t^{(n_t)}(z - z_t^{(n_t)})}{(R_t^{(n_t)})^3} + \frac{(R_r^{(n_r)})^2 v_z - b_r^{(n_r)}(z - z_r^{(n_r)})}{(R_r^{(n_r)})^3} \right); \\
 \frac{\partial \omega_d^{(n)}}{\partial v_x} &= \frac{\omega_c}{c} \left( \frac{(x - x_t^{(n_t)})}{R_t^{(n_t)}} + \frac{(x - x_r^{(n_r)})}{R_r^{(n_r)}} \right); \\
 \frac{\partial \omega_d^{(n)}}{\partial v_y} &= \frac{\omega_c}{c} \left( \frac{(y - y_t^{(n_t)})}{R_t^{(n_t)}} + \frac{(y - y_r^{(n_r)})}{R_r^{(n_r)}} \right); \\
 \frac{\partial \omega_d^{(n)}}{\partial v_z} &= \frac{\omega_c}{c} \left( \frac{(z - z_t^{(n_t)})}{R_t^{(n_t)}} + \frac{(z - z_r^{(n_r)})}{R_r^{(n_r)}} \right);
 \end{aligned} \tag{2.52}$$

where

$$b_t^{(n_t)} = v_x(x - x_t^{(n_t)}) + v_y(y - y_t^{(n_t)}) + v_z(z - z_t^{(n_t)}).$$

The lower bounds on target position and velocity estimation can be used to evaluate potential accuracy of the radar network depending on its type and the measurement model. For example, the use of time delay and Doppler frequency (the third measurement model) for target localization will provide higher accuracy than the use of only Doppler frequency (the second measurement model) due to two times higher number of measurements. This can be seen from construction of the Jacobian matrix ((2.49) and (2.50)). Consequently, in order to reach the same localization accuracy with two measurement models, the number of (Doppler) sensors in the second measurement model should be higher than the number of sensors in the third model. The impact of the measurement model on the target localization accuracy for different number of the radar nodes will be analyzed in the next chapter. For further convenience, two new notations are introduced:

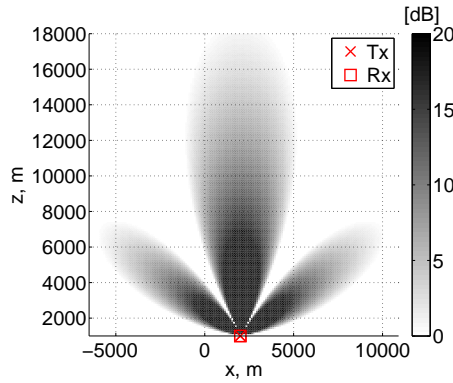
$$\sigma_p = \sqrt{\sigma_x^2 + \sigma_y^2 + \sigma_z^2}, \tag{2.53}$$

$$\sigma_v = \sqrt{\sigma_{v_x}^2 + \sigma_{v_y}^2 + \sigma_{v_z}^2}, \quad (2.54)$$

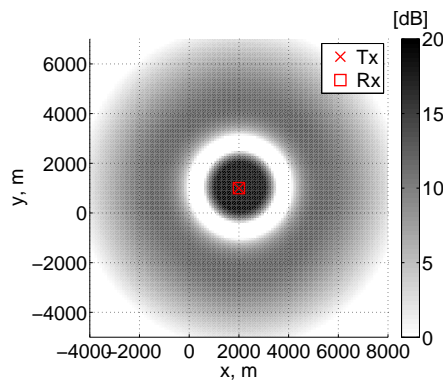
where  $(\sigma_x^2, \sigma_y^2, \sigma_z^2)$  and  $(\sigma_{v_x}^2, \sigma_{v_y}^2, \sigma_{v_z}^2)$  are variances of the target position and velocity vectors estimation, evaluated from CRLB. In subsequent chapters, parameters  $\sigma_p$  and  $\sigma_v$  are used as measures of the target position and velocity vectors estimation accuracy in multistatic radars.

## 2.6. INCORPORATION OF THE ANTENNA PATTERN INTO THE CRLB

The antenna pattern determines the spatial distribution of the radiated power and thus the signal-to-noise ratio of the signals received from different directions [7], as shown in Figure 2.2. The antenna pattern is incorporated into the CRLB as a spatial dependence of the signal-to-noise ratio upon the target range  $R$ , elevation  $\alpha$  and azimuth  $\phi$ .



(a)



(b)

Figure 2.2: SNR distribution for directional antenna pattern: (a) vertical plane; (b) Y-X plane (target height  $h_t = 3000$  m)

We rewrite equation (2.8) as

$$SNR(\alpha, \phi, R) = \frac{P_t G^2(\alpha, \phi) RCS \lambda^2}{(4\pi)^3 R^4 L_{sys} N_{rec}} G_{proc}, \quad (2.55)$$

where  $N_{rec}$  is the receiver noise power. The antenna radiation pattern is represented as the dependence of the SNR upon the target coordinates  $(R, \alpha, \phi)$  in the equations (2.42) and (2.43) for variance of time delay and radial velocity estimation:  $\sigma_{\tau\tau}^2 = \sigma_{\tau\tau}^2(\alpha, \phi, R)$ ;  $\sigma_{\omega_d \omega_d}^2 = \sigma_{\omega_d \omega_d}^2(\alpha, \phi, R)$ . Spherical coordinates can be transformed into the Cartesian coordinates as:  $x = R \sin \alpha \sin \phi$ ;  $y = R \sin \alpha \cos \phi$ ;  $z = R \cos \alpha$ .

## 2.7. CONCLUSION

Theoretical bounds on the target localization and velocity estimation accuracy in a multistatic radar network were derived. Since these bounds depend on a single radar estimation performance, closed-form expressions for direct evaluation of the target range and radial velocity estimation accuracy for WiFi and LFM signals have been provided. The ranging accuracy of the single radar is shown to be inversely proportional to the signal bandwidth, while the radial velocity estimation accuracy is inversely proportional to the integration time. The developed framework allows for radar network localization accuracy evaluation for three types of measurements: time delay, Doppler frequency shift and a combination of both. Moreover, an approach for incorporating antenna pattern into the CRLB has been proposed for the first time. This allows for explicit representation of the error distribution across the area of potential target location, depending on the antenna pattern of each radar. Additionally, the scalar functions of the covariance matrix can be used for selection of the radar network geometry that provides minimum error of the target parameters estimation. This will be shown in Chapter 4.

## REFERENCES

- [1] I. Ivashko, O. Krasnov, and A. Yarovoy, *Topology optimization of monostatic radar networks with wide-beam antennas*, in *European Microwave Conference (EuMC), 2015 12th* (2015).
- [2] I. M. Ivashko, O. A. Krasnov, and A. G. Yarovoy, *Sparsity-based optimization of the sensors positions in radar networks with separated transmit and receive nodes*, *Int. J. Distrib. Sen. Netw.* **2016** (2016), 10.1155/2016/9437602.
- [3] H. Van Trees, *Detection, Estimation, and Modulation Theory*, *Detection, Estimation, and Modulation Theory No. Part 1* (Wiley, 2004).
- [4] S. Kay, *Fundamentals of Statistical Signal Processing: Estimation Theory*, Prentice Hall Signal Processing Series No. Volume 1 (Prentice Hall, 1993).
- [5] F. Colone, P. Falcone, C. Bongioanni, and P. Lombardo, *Wifi-based passive bistatic radar: Data processing schemes and experimental results*, *Aerospace and Electronic Systems*, *IEEE Transactions on* **48**, 1061 (2012).

- 
- [6] F. Chevalier, *Principles of Radar and Sonar Signal Processing*, Artech House Radar Library (Artech House, 2002).
- [7] C. Balanis, *Antenna Theory: Analysis and Design* (Wiley, 2012).



# 3

## ESTIMATION ACCURACY ANALYSIS IN MULTISTATIC RADAR

*In this chapter the potential estimation accuracy of the target kinematic parameters in multisite radar networks will be analyzed using Cramér-Rao lower bound, developed in Chapter 2. The system performance depending on a single radar architecture and signal processing mode will be analyzed in Section 3.1. Impact of the waveform parameters and power budget on the system performance will be investigated in Section 3.2. The impact of the types of measurements on the target localization accuracy will be investigated in Section 3.3. The possibility of improving system estimation performance by using signals from the Tx of opportunity will be discussed in Section 3.4. Concluding remarks will be given in Section 3.5.*

---

Parts of this chapter have been published in [1], [2], [3].

### 3.1. IMPACT OF THE RADAR ARCHITECTURE AND COOPERATION MODE

PERFORMANCE of multistatic radar network is determined by the unique features of the system (such as radar node architecture, signal reception mode, type of measurements used for target localization) and highly affected by the number of radar nodes and their topology. Therefore, potential accuracy of target localization in different systems is compared using statistical averaging of localization error,  $\sigma_p$ , over  $10^3$  randomly simulated topologies of radar nodes for nineteen numbers of transmit-receive channels  $N = 2, \dots, 20$ . In this chapter, scenarios with short-range FMCW/WiFi radar networks are considered. Parameters of the single radar node are given in Table 3.1. Different numbers of radar nodes positions and 300 target positions are randomly simulated over the area of  $500 \text{ m} \times 500 \text{ m}$  from a uniform distribution.

Table 3.1: Single radar simulation parameters

Parameter	WiFi radar	FMCW radar
Transmitted power, $P_t$	20 dBm (EIRP)	10 dBm (EIRP)
Antenna gain, $G$	8 dB	10 dB
Carrier frequency, $f_c$	2.4 GHz	25 GHz
Waveform bandwidth, $\Delta f$	11 MHz	300 MHz
Noise figure, $F_n$	10 dB	8 dB
System losses, $F_{\text{sys}t}$	4 dB	15 dB
Pulse/symbol duration, $T_s$	$1 \mu\text{s}$	$0.8 \mu\text{s}$
No. of integrated pulses	512	512

Fig. 3.1 presents the dependence of the averaged error of target localization ( $\sigma_p$ ) on the number of monostatic and bistatic radars for two modes of the signal transmission-reception: autonomous and cooperative. The target localization error has been evaluated assuming target position estimation based on time delay measurements, using theory developed in Chapter 2. The results demonstrate the following. First, the estimation performance of the monostatic and bistatic radar networks can be further enhanced by using the cooperative mode of signal transmission-reception. The reason is that cooperative mode allows for larger number of measurements, leading to higher SNR and thus, higher estimation accuracy. Second, in the networks with autonomous reception mode, spatial separation of Tx and Rx nodes does not lead to better estimation accuracy, compared to the collocated Tx-Rx radar architecture. This is explained by the fact that an overly long or overly short baseline, compared to expected target distance, disrupts contours of constant SNR or leads to quasi-monostatic architecture. This effect can be illustrated with Cassini ovals [4]. Third, bistatic and monostatic radar networks show equivalent estimation accuracy, when cooperative mode of the signal reception is used. To summarize, the length of the baseline, the transmitter-target-receiver distance, and the transmitter-target-receiver angle form basic geometrical characteristics of bistatic radars that have to be selected properly for their efficient exploitation.

Next, target localization accuracy in bistatic radar networks with different lengths of baseline  $l = 0, 10, 20, \dots, 100$  m will be evaluated. Both Tx and Rx nodes positions have been simulated randomly. Once location of Tx node has been selected, location of the dedicated Rx node is selected as such that lies on the circle with radius  $l$  and center in Tx position. Fig. 3.2 shows histogram of the averaged target localization error in bistatic radar network with autonomous signal transmission-reception and different baseline values. As one can see, localization accuracy of bistatic radar networks with different baselines does not differ significantly from one to another. Moreover, these results are equivalent to the results of estimation accuracy of monostatic radar network ( $l = 0$  m). The results, presented in Fig. 3.2 have been averaged over nineteen numbers of Tx-Rx channels (from two to twenty) for different values of baselines and presented in the form of histogram in Fig. 3.3. The estimation accuracy of netted bistatic radars with zero baselines, which correspond to a quasi-bistatic radar architecture, is equivalent to the performance of bistatic radars with baselines of 10 m, 50 m, and 70 m. Fig. 3.4 shows the distribution of a target localization error for three types of networks, depending on a single radar node architecture: bistatic radars with arbitrary selected length of baseline, bistatic radars with baseline of 50 m, and monostatic radars. Large separation of transmit and receive radar nodes, i.e. with baselines in the order of 200 m (Fig.3.4a), plays a destructive role leading to poor system performance in the area of interest. At the same time, separation of the bistatic nodes by a 50m baseline provides slightly better estimation performance. To summarize, the spatial diversity of Tx and Rx nodes in the systems with autonomous transmission-reception does not lead to enhancement of the overall system performance.

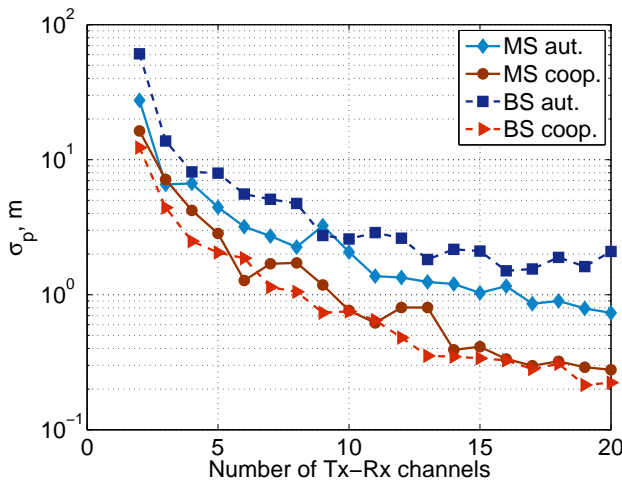


Figure 3.1: Error of the target localization versus number of Tx-Rx channels. No restriction on the length of baseline of bistatic radars.

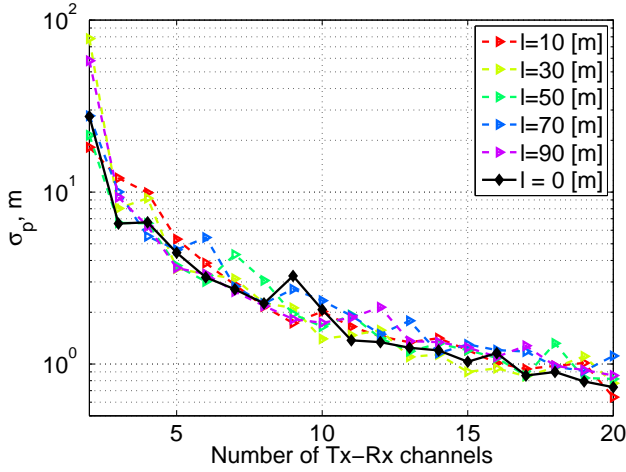


Figure 3.2: Error of the target localization versus number of *autonomous* bistatic channels at different values of baseline.

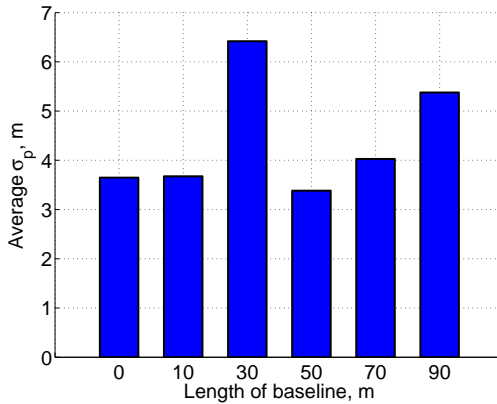


Figure 3.3: Histogram of the target localization error depending on the length of baseline. Values of the target localization error were averaged over 19 numbers of Tx-Rx channels ( $N = 2, 3, \dots, 20$ ) with randomly selected nodes positions in  $10^3$  trials. Each bistatic radar operates in autonomous signal reception mode.

### 3.2. IMPACT OF THE WAVEFORM PARAMETERS AND THE POWER BUDGET

In the previous section, it has been shown that the radar network system performance depends on the number of radar nodes, their positions, architecture, and cooperation. In general, the more nodes constituting the network, the better the estimation accuracy of the whole system. However, the lower and upper limits of the achievable system performance are determined by the parameters of a single radar node, such as power

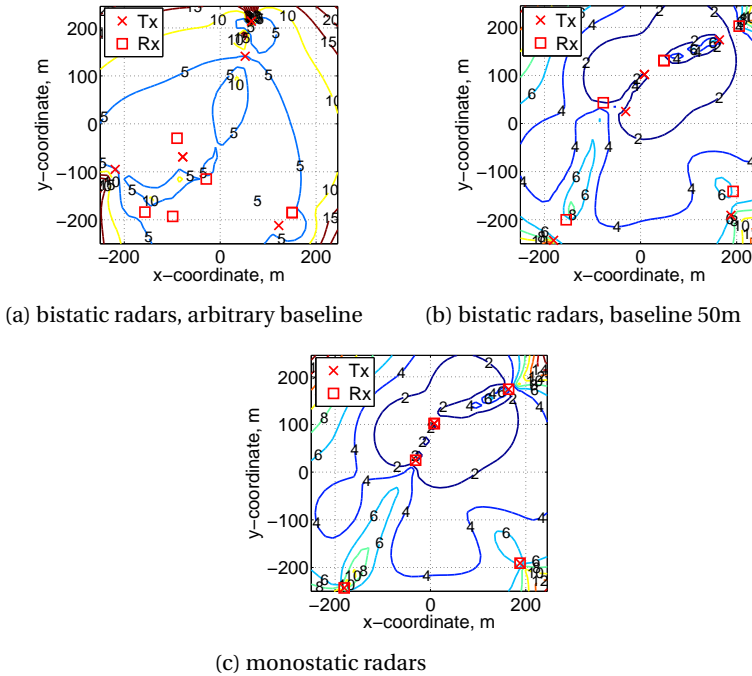


Figure 3.4: Contour plots of the target localization error ( $\sigma_p$ , m) in radar networks with autonomous mode of the signal transmission-reception.

budget and waveform characteristics [1]. The analysis of this dependence of the radar network estimation performance upon the parameters of a single radar forms the focus of this section.

The monostatic radar network with autonomous signal transmission-reception and parameters of the single radar from Table 3.1 has been taken as a benchmark. Results of the target localization accuracy for this type of the network and networks with waveform bandwidth of  $\Delta f = [200, 400, 500]$  MHz are shown in Fig. 3.5. One can see that an equivalent estimation accuracy to the radar network with ten nodes having 300 MHz bandwidth can be achieved in the radar network with five nodes that use 500 MHz bandwidth. The reason is that in both cases, total bandwidth of the network is approximately the same, 3 GHz and 2.5 GHz. Despite the fact that a single radar ranging accuracy is determined by operational signal bandwidth, the estimation accuracy of the system is directly proportional to the product of Tx-Rx channels number and signal bandwidth, as will be demonstrated. Similarly, the higher estimation accuracy of the system can be achieved with longer integration time, leading to a smaller number of radars being required to satisfy the same accuracy constraint (Fig.3.6). This is due to SNR enhancement, achieved with averaging a larger number of measurements. However, for moving target observation, an overly long integration time will deteriorate ranging accuracy, causing a range migration effect.

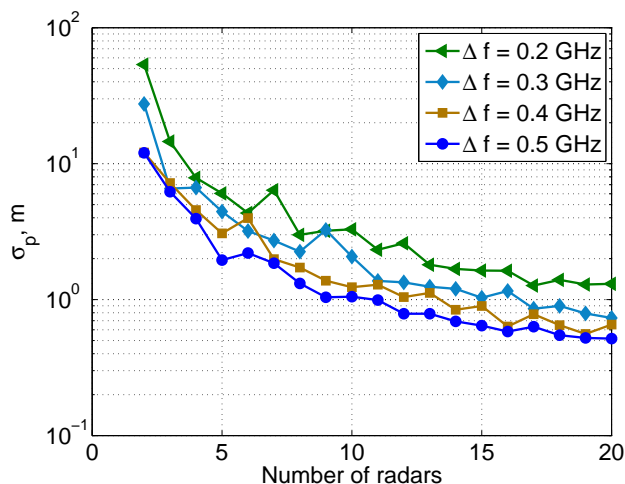


Figure 3.5: Error of the target localization versus number of monostatic radars (autonomous reception mode) for different values of the signal bandwidth  $\Delta f$ .

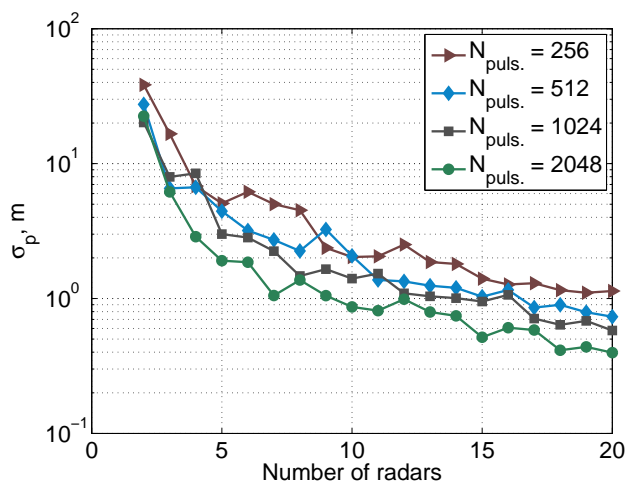


Figure 3.6: Error of the target localization depending on the number of monostatic radars (autonomous reception mode) for different numbers of integrated pulses.

Increasing the transmit power of a single radar results in fewer radar nodes being required to achieve high system localization accuracy (less than 1 m) as shown in Fig. 3.7. This is an intuitive result, since higher transmit power is inversely proportional to the estimation error of the received signal parameters.

In the preceding results of the numerical analysis, an assumption with respect to the signals' orthogonality has been made. The three most common ways to obtain

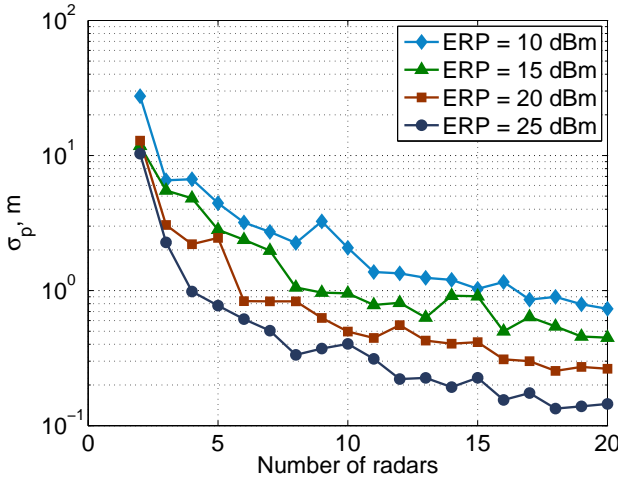


Figure 3.7: Error of the target localization versus number of monostatic radars (autonomous reception mode) for different values of effective radiated power (ERP).

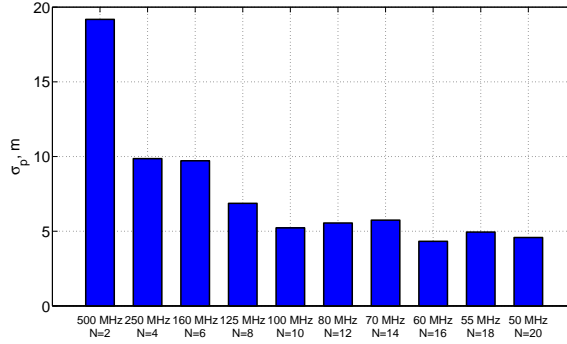
orthogonal waveforms are [5]: 1) time division; 2) frequency division; 3) code division. Some implementations of the signals' orthogonality for FMCW MIMO are proposed in [6], [7]. Since frequency orthogonality requires no overlap in frequencies of the transmit signal, the widening of the frequency band of a large number of transmitters as in Fig. 3.5 does not allow for implementation of this type of signal separation. However, frequency division is an attractive technique due to its simplicity in realization. Thus, in the subsequent analysis the radar network system performance is analyzed versus the number of radar nodes and the occupied bandwidth. The entire bandwidth of the network is 1 GHz. The signal bandwidth of a single radar transmitter depends on the number of nodes and is set according to Table 3.2.

Table 3.2: Bandwidth allocation

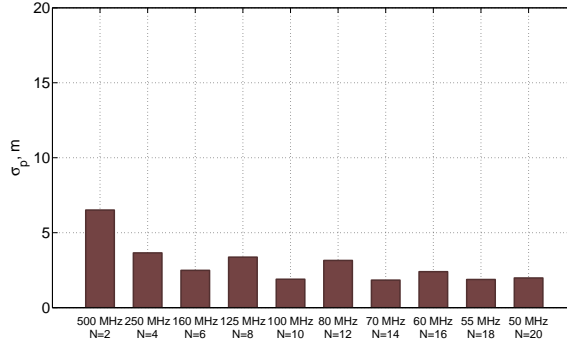
No. of Tx	2	4	6	8	10	12	14	16	18	20
$\Delta f$ , MHz	500	250	160	125	100	80	70	60	55	50

Fig. 3.8 shows an averaged error of the target localization for different numbers of monostatic radars and allocated frequency bandwidth. As one can see, the impact of these two parameters on the system estimation performance is different for two reception modes. First, increasing signal bandwidth by two times requires half as many radar nodes to achieve the same estimation accuracy. For radar network with cooperative mode this relation holds for pairs of radar nodes numbers  $N = 4$  and  $N = 8$ ;  $N = 10$  and  $N = 20$ . For radar network with autonomous mode this relation holds only for  $N = 10$  and  $N = 20$  number of nodes. Second, in a network with cooperative reception, target localization error is approximately the same starting from  $N = 4$  radars with  $\Delta f = 250$  MHz bandwidth, which means that allocation of wider bandwidth to a

smaller number of radars can significantly reduce this number. Third, in a network with autonomous reception, variations of the values of average target localization error are negligible starting from  $N = 10$  radars with  $\Delta f = 100$  MHz bandwidth.



(a) autonomous mode



(b) cooperative mode

Figure 3.8: Average error of the target localization for different numbers of monostatic radars and allocated frequency bandwidth

To summarize, proper selection of parameters of a single radar node enhances system estimation accuracy and thus can reduce the number of radar nodes and overall system costs. For example, to achieve estimation accuracy in the order of 1 m with five radars, signal bandwidth should be increased to 500 MHz or ERP should be 5 dBm higher. The latter is preferable as frequency orthogonality might be required for signal separation. Another option is to increase integration time, which is not preferable for maneuvering targets, as has been discussed previously. For a limited number of radars,  $N = 5$  for example, a system estimation accuracy that is equivalent to the estimation accuracy of the network with  $N = 10$  radars (that provide a two times lower estimation error) can be achieved by increasing the signal bandwidth to 400 MHz or by increasing the effective radiated power to 20 dBm. The noise figure reduction is another way to improve measurement accuracy of a single radar.

### 3.3. IMPACT OF THE MEASUREMENT MODEL ON TARGET LOCALIZATION ACCURACY

Although an FMCW radar provides measurements of Doppler frequency shifts, target localization based on range measurements has so far been assumed. This section focuses on investigation of the impact of the measurement model on target localization accuracy in the network of radars. In particular, three measurement models that are used for target localization are compared: 1) only time delay estimation of the received signal; 2) only Doppler shift estimation; 3) time delay and Doppler shift estimation of the received signal. For considered parameters of a single radar node (Table 3.1), range and velocity resolutions are 0.5 m and 0.03 m/s.

The curves of the average error of the target localization versus the number of monostatic radars for the first and third measurement models are shown in Fig. 3.10. As apparent from the results, although the estimation accuracy of the second model increases with increase of the target speed, the range-based localization outperforms the (radial) velocity-based localization for networks with high- or low-resolution radars. Since the system performance degrades with decrease of the radar resolution (Figs. 3.5 and 3.9), competitive performance with Doppler measurements can be achieved in localization of fast-moving targets with narrow band radars, i.e. with range resolution less than or equal to 50 MHz. Even so, the achieved estimation error is in the order of  $10^2$  m, which is very high for short-range applications. An average error of the target localization versus number of monostatic radars for the first and second measurement models is shown in Fig. 3.9. The effect of the target velocity in the third measurement model (time delay together with Doppler shift measurements) is not so evident as in the second one (only Doppler) as illustrated in Fig. 3.10. Moreover, the usefulness of the Doppler information is ambiguous and depends on the radar range resolution: for low-resolution radars the use of the Doppler measurements along with the range measurements leads to better estimation accuracy of the system, which is equivalent to the performance of high-resolution radars. At the same time, use of the Doppler measurements in wide band radars does not enhance the localization performance of the system and thus is not practical.

To summarize, Doppler measurements and range measurements lead to an equivalent localization accuracy of fast moving targets in narrow band radars. Provided accuracy, in general, is not high. However, use of Doppler measurements along with range measurements in such narrow band radars provides significant improvement in system estimation accuracy.

### 3.4. ANALYSIS OF COMBINED ACTIVE AND WIFI-BASED PASSIVE RADAR NETWORK

The distributed active radar system performance can be further enhanced by using the signals from transmitters of opportunity that form bistatic pairs with widely distributed Rx nodes of the existing active radar networks. In particular, the exploitation of transmissions from WiFi access points is assumed.

Passive listening of the signals from Tx of opportunity, reflected from the targets of

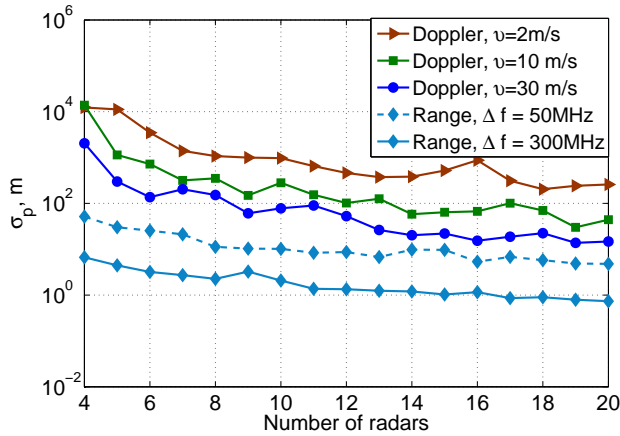


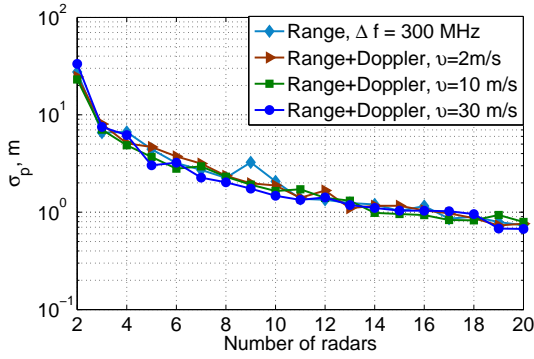
Figure 3.9: Error of the target localization depending on the number of monostatic radars in the first and second measurement models.

interest forms the concept of passive coherent location (PCL). Fig. 3.11 demonstrates the basic principle of the passive bistatic radar (PBR). Two antennas are used for target parameters estimation. The *reference* antenna is pointed in the direction of the transmitter of opportunity. The signal, reflected from the target, is received in the *surveillance* antenna. This signal is matched with the signal from the *reference* antenna in the processing unit.

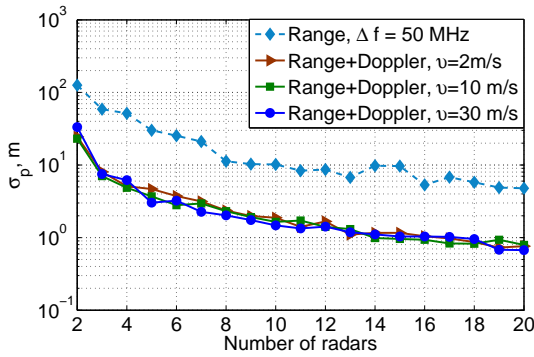
There are three types of PBR depending on their operational range: 1) PBR for long range surveillance (Tx of opportunity: HF broadcast emitters, FM broadcast emitter, DAB broadcast emitter, TV analogue waveform, DVB-T OFDM digital waveform, DVB-H OFDM digital waveform, GSM) [8], [9], [10]; 2) medium-short range PBR (WiMAX-based transmissions) [11]; 3) short range/indoor PBR (WiFi access points serve as transmitters of opportunity) [12].

Fig. 3.12a shows distribution of the localization error at three FMCW radars of the network depicted in Fig. 3.4c. The estimation performance with three radar nodes is substantially worse, compared to the one with five radars. Enhancement of the estimation accuracy and increase of the coverage area can be achieved with use of the signals from Tx of opportunity, as shown in Fig. 3.12b, where WiFi bistatic radar is integrated into the existing FMCW network. The observed improvement is a decrease of the estimation error of about 20% in the areas around the bistatic WiFi radar.

Averaged errors of the target localization for one, two, and three active FMCW radars versus number of integrated bistatic radars (with one transmit node and varying receive nodes) are plotted in Fig. 3.13. The position of each radar node was generated randomly over the area of 500 m × 500 m. The target localization error is averaged over 10<sup>3</sup> MC trials for each different number of the receiving nodes of WiFi signal. The third receiver added to the network leads to a significant decrease of the estimation error, especially with the system with using one active FMCW radar. An addition of bistatic radars leads to a decrease of the target localization error, but after adding the ninth PBR, further



(a) bandwidth of a single radar  $\Delta f = 300$  MHz



(b) bandwidth of a single radar  $\Delta f = 50$  MHz

Figure 3.10: Error of the target localization depending on the number of monostatic radars in the first and third measurement models.

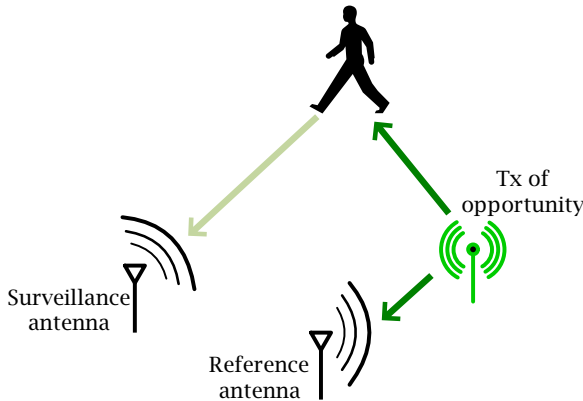
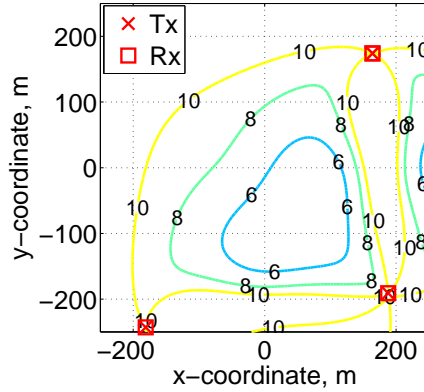
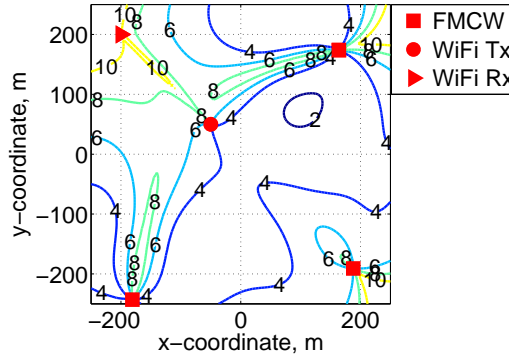


Figure 3.11: Principle of passive bistatic radar operation.



(a) FMCW radars



(b) FMCW and WiFi-based radars

Figure 3.12: Contour plots of the target localization error ( $\sigma_p$ , m).

improvement of the estimation accuracy is not observed.

The same effect from adding the ninth WiFi receiver is observed for different values of the signal bandwidth in active radars. As shown in Fig. 3.14, the effect of signal bandwidth of the active radars on the overall system performance is meaningful up until the ninth bistatic channel is added into the system: until that point, the wider the bandwidth, the better the system estimation accuracy. This is demonstrated in Fig. 3.5 as well, where regardless of the number of nodes, a clear relation between a single radar bandwidth and the system accuracy is observed.

To summarize, the use of signals from Tx of opportunity is another alternative for extending the coverage area and enhancing performance of the radar network. Moreover, the number of bistatic receivers will not be significantly large and, as was shown for the considered scenario, and can be in the range of six to nine nodes, depending on the number of active radars and their range resolution.

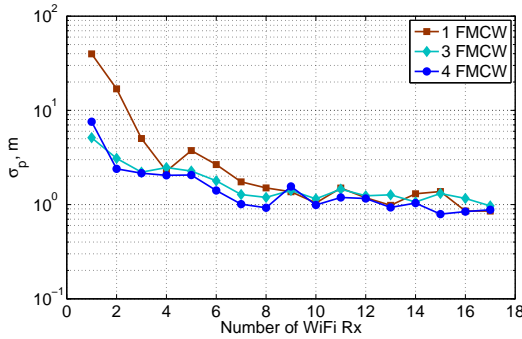


Figure 3.13: Error of the target localization for active FMCW radars versus number of bistatic radars (with one transmit node and varying numbers of receive nodes) for different numbers of active radar nodes.

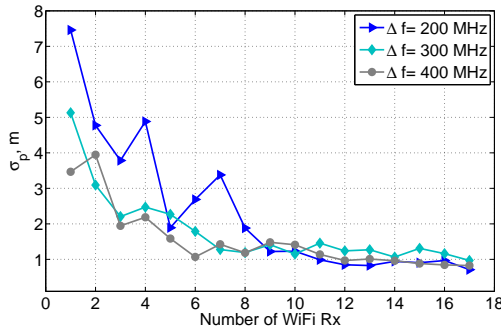


Figure 3.14: Error of the target localization for three active FMCW radars versus number of bistatic radars (with one transmit node and varying numbers of receive nodes) for different signal bandwidths.

### 3.5. CONCLUSION

In this chapter the potential estimation accuracy of the target kinematic parameters in multisite radar networks for different radar node parameters and system operational modes has been analyzed using the Cramér-Rao lower bound. Specifically, impact of the following parameters on the system estimation accuracy has been investigated: 1) radar architecture: monostatic and bistatic; 2) signal reception mode: autonomous and cooperative; 3) waveform parameters (bandwidth and integration time) and power budget; 4) type of the measurements for target localization: time delay, Doppler shift, time delay together with Doppler shift; 5) use of signals from transmitters of opportunity.

The analysis has shown that the cooperative mode of signal reception allows for an increase of the estimation accuracy by up to 40% as compared to the autonomous mode. It has been found that a monostatic radar networks and a bistatic radar networks with cooperative mode of signal reception provide an equivalent target localization accuracy. This means that for given parameters of the system, there is no need for the spatial separation of transmit and receive radar nodes that reduces the system complexity as well as acquisition and maintenance costs. The waveform bandwidth, integration

time, and transmit power are additional resources that can be used for improvement of the system estimation accuracy. Thus, if waveform and power budget parameters can be considered as variables in the radar network topology optimization algorithm, the limitations in one resource (number of nodes, for example) can be compensated for by use of another (integration time, for instance).

It has been shown that use of only Doppler shift measurements for target localization provides a lower estimation accuracy than both high and low resolution range measurements. An equivalent performance with Doppler measurements can be achieved with a larger number of nodes that allows increase of the total time on target, without increasing the integration time of a single radar. At the same time, use of the Doppler shift measurements in addition to the range measurements (the third measurement model) in narrow-band radars yields a significant improvement in the system estimation accuracy. This is not the case for wide-band radars, where the use of the target velocity does not provide any further improvement.

The possibility of extending the coverage of the active radar network by exploiting the signals from transmitters of opportunity was investigated. It has been shown that addition of the measurements from passive radars results in higher system estimation accuracy, especially in the areas not covered with active radars. However, for parameters of active and passive radars, used in this chapter, addition of more than seven bistatic radars into the network does not lead to a further decrease of the localization error, which does not go below 1 m.

## REFERENCES

- [1] I. Ivashko, O. Krasnov, and A. Yarovoy, *Performance analysis of multisite radar systems*, in *Radar Conference (EuRAD), 2013 10th European* (2013).
- [2] I. Ivashko, O. Krasnov, and A. Yarovoy, *Receivers topology optimization of the combined active and WiFi-based passive radar network*, in *European Microwave Conference (EuMC), 2014 11th* (2014) pp. 1820–1823.
- [3] I. Ivashko, O. Krasnov, and A. Yarovoy, *Topology optimization of monostatic radar networks with wide-beam antennas*, in *European Microwave Conference (EuMC), 2015 12th* (2015).
- [4] T. Johnsen and K. Olsen, *Bi- and multistatic radar*, in *NATO Research and Technology Organisation Lecture Series RTO-EN-SET-086bis (Advanced radar systems, signal and data processing)* (2007) pp. 4–1 – 4–34.
- [5] V. Chernyak, *Fundamentals of Multisite Radar Systems: Multistatic Radars and Multistatic Radar Systems* (CRC Press/INC, 1998).
- [6] J. J. M. de Wit, W. L. van Rossum, and A. J. de Jong, *Orthogonal waveforms for FMCW MIMO radar*, in *2011 IEEE RadarCon (RADAR)* (2011) pp. 686–691.
- [7] G. Babur, O. A. Krasnov, A. Yarovoy, and P. Aubry, *Nearly orthogonal waveforms for MIMO FMCW radar*, *IEEE Transactions on Aerospace and Electronic Systems* **49**, 1426 (2013).

- [8] P. E. Howland, D. Maksimiuk, and G. Reitsma, *FM radio based bistatic radar*, IEE Proceedings - Radar, Sonar and Navigation **152**, 107 (2005).
- [9] C. Y. Pui and M. Trinkle, *GPS bistatic radar using phased-array technique for aircraft detection*, in *2013 International Conference on Radar* (2013) pp. 274–279.
- [10] D. K. P. Tan, H. Sun, Y. Lu, M. Lesturgie, and H. L. Chan, *Passive radar using global system for mobile communication signal: theory, implementation and measurements*, IEE Proceedings - Radar, Sonar and Navigation **152**, 116 (2005).
- [11] T. Higgins, T. Webster, and E. L. Mokole, *Passive multistatic radar experiment using WiMAX signals of opportunity. Part 1: Signal processing*, IET Radar, Sonar Navigation **10**, 238 (2016).
- [12] P. Falcone, F. Colone, A. Macera, and P. Lombardo, *Two-dimensional location of moving targets within local areas using wifi-based multistatic passive radar*, IET Radar, Sonar Navigation **8**, 123 (2014).



# 4

## ACCURACY-DRIVEN TOPOLOGY OPTIMIZATION: GENERIC FRAMEWORK

*In this chapter, a generic framework for radar network topology selection will be developed and presented. The developed theory relies on a non-linear measurement model. Performance metrics of the system estimation accuracy will be presented in Section 4.2. Section 4.3 will provide an extension to multi-modal parameter vector estimation. Convex and greedy optimization algorithms, with an extension to selection-dependent models, will be presented in Section 4.4. Finally, Section 4.5 will conclude this chapter.*

## 4.1. INTRODUCTION

WHILE power budget and waveform parameters determine performance of a single radar node [3], network parameters (radar architecture, coherency, transmitter type), the number of radar nodes and their spatial locations determine the overall performance of radar networks [4]. Along with the single radar node characteristics, network parameters define the total coverage area in terms of predefined detection and accuracy of the target parameter estimates, as well as the overall robustness of the system. Therefore, an efficient exploitation of the radar network requires optimal node allocation. The latter can be considered either as a real-time or off-line design task, depending on the particular application. The selection of spatial positions of radar nodes is one of the key tasks in radar network resource allocation. It aims to achieve optimal performance with the minimum system cost. As has been mentioned in Chapter 1, topology optimization problems can be formulated in two ways:

$$\begin{array}{l} \min |\mathcal{I}| \\ \text{s.t. } f(\mathcal{I}) \geq \lambda_g; \end{array} \quad (4.1)$$

$$\begin{array}{l} \min f(\mathcal{I}); \\ \text{s.t. } |\mathcal{I}| = L; \end{array} \quad (4.2)$$

where  $\mathcal{N}$  ( $|\mathcal{N}| = N$ ) is a set of potential radar node positions and  $\mathcal{L} = \{i_1, \dots, i_L\}$  ( $|\mathcal{L}| = L$ ) is the set of the most informative radar node positions, such that  $\mathcal{L} \subseteq \mathcal{N}$  and thus  $L \leq N$ ,  $\mathcal{I}$ ; is a set of selected positions of radars and  $\lambda_g$  is a threshold value on the cost function.

In this chapter, the focus is on the problem of radar sensor selection for accurate estimation of the target state vector. The measures of the estimation accuracy are often chosen to be scalar functions of the error covariance matrix, such as 1) the maximum eigenvalue (E-optimality); 2) the trace (A-optimality); and 3) the log-determinant (D-optimality). Other measures, like mutual information, entropy, and cross-entropy are frequently used as well [5], [6]. The sensor selection problem is combinatorial in nature. Therefore, different optimization techniques are used to solve it in polynomial time. For example, convex optimization methods, which are based on the relaxation of the Boolean constraint  $\{0, 1\}^N$  on the selection coefficients, were shown to perform well in terms of mean squared error.

### 4.1.1. CONVEXITY CONDITION

If  $\mathbf{X}$  is a convex set in a real vector space and  $f(\cdot)$  is a function  $\mathbf{X} \rightarrow \mathbf{R}$ .  $f(\cdot)$  is convex if

$$f(tx_1 + (1-t)x_2) \leq tf(x_1) + (1-t)f(x_2), \quad \forall x_1, x_2 \in \mathbf{X}, 0 \leq t \leq 1. \quad (4.3)$$

Examples of convex functions include norms, geometric mean, and log-determinant (concave) [7]. The convex optimization methods imply a high computational cost, i.e. cubic in the size of the problem. On the other hand, greedy algorithms have a linear complexity. While convex methods require the cost function to be convex, greedy algorithms require it to be submodular.

### 4.1.2. SUBMODULARITY CONDITION

The submodularity of the function is related to the concept of diminishing returns in economics and means the following: for two sets  $\mathcal{X}$  and  $\mathcal{Y}$  such that  $\mathcal{X} \subset \mathcal{Y} \subset \mathcal{N}$  and element  $j \in \mathcal{N} \setminus \mathcal{Y}$ , the function  $f(\cdot)$  is submodular if

$$f(\mathcal{X} + j) - f(\mathcal{X}) \geq f(\mathcal{Y} + j) - f(\mathcal{Y}). \quad (4.4)$$

This property allows one to reach a near-optimal solution with greedy algorithms [8]. Moreover, greedy algorithms have a linear complexity in the size of the problem and, therefore, are of particular interest for large-scale problems. In particular, the log-determinant, the mutual information, and the entropy were shown to be submodular functions. Another submodular function, namely the frame potential (FP), which is a measure for the orthogonality of the rows of the measurement matrix, was introduced in [9] as a proxy for the mean squared error. Together with a low computational complexity, the FP-based greedy algorithm sometimes shows a competitive performance compared to convex optimization [9].

## 4.2. PERFORMANCE METRICS

The general non-linear measurement model defined in (2.1) is considered here. Since the error covariance matrix for a non-linear measurement model depends on the parameter vector  $\boldsymbol{\alpha}$ , the covariance-based cost functions depend on  $\boldsymbol{\alpha}$  as well [1]. Therefore, we grid the parameter space and perform the optimization considering the complete set of  $M$  grid points  $\{\boldsymbol{\alpha}_1, \boldsymbol{\alpha}_2, \dots, \boldsymbol{\alpha}_M\}$ . Furthermore, we linearize the model (2.1) around every grid point  $\boldsymbol{\alpha}_m$  applying a first-order Taylor series expansion,

$$\mathbf{y} \approx \mathbf{f}(\boldsymbol{\alpha}_m) + \mathbf{G}_m^{(\mathcal{N})}(\boldsymbol{\alpha} - \boldsymbol{\alpha}_m) + \boldsymbol{\xi}, \quad (4.5)$$

where the entries of the matrix  $\mathbf{G}_m^{(\mathcal{N})} \in \mathbb{R}^{NQ \times K}$  are  $[\mathbf{G}_m^{(\mathcal{N})}]_{(n-1)Q+k, k} = \left. \frac{\partial f_{(n-1)Q+k}(\boldsymbol{\alpha})}{\partial \alpha_k} \right|_{\boldsymbol{\alpha}=\boldsymbol{\alpha}_m}$ ;  $q = 1, \dots, Q$ ;  $n = 1, \dots, N$ ;  $k = 1, \dots, K$ ; and  $m = 1, \dots, M$ .

### 4.2.1. MEAN-SQUARED ERROR

In the presence of zero-mean i.i.d. Gaussian noise with variance  $\sigma^2$ , the mean squared error, which is equal to the Cramér-Rao lower bound, of the estimate of  $\boldsymbol{\alpha}_m$  based on a set  $\mathcal{L}$  of selected radars is given by:

$$\text{MSE} = \text{E}(\|\boldsymbol{\alpha}_m - \hat{\boldsymbol{\alpha}}_m\|_2^2) = \sigma^2 \sum_{k=1}^K \frac{1}{\lambda_{m,k}}, \quad (4.6)$$

where  $\lambda_{m,k}$  is the  $k$ th eigenvalue of the matrix  $\mathbf{T}_m^{(\mathcal{L})} = \mathbf{G}_m^{\dagger(\mathcal{L})} \mathbf{G}_m^{(\mathcal{L})} \in \mathbb{R}^{K \times K}$ , with matrix  $\mathbf{G}_m^{(\mathcal{L})} \in \mathbb{R}^{LQ \times K}$  such that  $[\mathbf{G}_m^{(\mathcal{L})}]_{(l-1)Q+k, k} = [\mathbf{G}_m^{(\mathcal{N})}]_{(il-1)Q+k, k}$ .

The MSE has many local minima in the optimal selection vector and, therefore, is rarely used in practice. Alternative cost functions to the MSE are the maximum eigenvalue and the log-determinant of the error covariance matrix, as well as the frame potential. Moreover, FP and LD costs were shown to be monotonic and submodular functions that gives possibility to optimize them using greedy algorithms [9], [10].

### 4.2.2. FRAME POTENTIAL

In frame theory, frame is defined as a generalization of a basis of a vector space to sets that may be linearly dependent. Frame potential is a scalar property of the frame that measures orthogonality between vectors. According to [9], FP for linear measurement model is given by:

$$\text{FP}(\mathcal{L}) = \sum_{i,j \in \mathcal{L}} |\boldsymbol{\psi}_i \cdot \boldsymbol{\psi}_j|^2, \quad (4.7)$$

where  $\boldsymbol{\psi}_j$  is the  $j$ th row of matrix  $\boldsymbol{\Psi} \in \mathbb{R}^{L \times K}$  that represents known linear model. We modify this definition to the non-linear model with  $Q$  measurements accumulated per integration time in each of the radars from the set  $\mathcal{L}$ :

$$\text{FP}_m(\mathcal{L}) = \sum_{i,j \in \mathcal{L}} \left| \text{tr}\{\mathbf{G}_m^{(i)} \mathbf{G}_m^{(j)\dagger}\} \right|^2, \quad (4.8)$$

where  $\mathbf{G}_m^{(i)} \in \mathbb{R}^{Q \times K}$  is the submatrix of  $\mathbf{G}_m^{(\mathcal{N})}$  given by  $[\mathbf{G}_m^{(i)}]_{q,k} = [\mathbf{G}_m^{(\mathcal{N})}]_{(i-1)Q+q,k}$ . The minimization of the FP is equivalent to the minimization of the mean squared error. While the MSE function has many local minima, the use of the FP allows for a near optimal solution in terms of the minimum MSE. Since  $\text{FP}_m$  from (4.8) will be different for every grid point  $\boldsymbol{\alpha}_m$  from the parameter space, minimization of the joint (weighted) frame potential is considered:

$$\text{FP}(\mathcal{L}) = \sum_{m=1}^M p_m \text{FP}_m(\mathcal{L}), \quad (4.9)$$

where  $p_m > 0$  is the weight that represents the probability that the true  $\boldsymbol{\alpha}$  lies on the grid point  $\boldsymbol{\alpha}_m$ ;  $\sum_{m=1}^M p_m = 1$ . If target parameters are uniformly distributed in the space, then  $p_m = 1/M$ . Higher weights, assigned to specific  $\text{FP}_m$ , will bias the network topology selection towards better estimates of corresponding  $\boldsymbol{\alpha}_m$ . An example scenario is parameter space that represents an area of potential target location and higher weights are assigned to the grid points that lie on the border of this area. A straightforward application of such scenario is a radar network topology optimization for border control.

Related to the weighted FP, the following monotonic submodular cost function is maximized

$$F(\mathcal{S}) = \text{FP}(\mathcal{N}) - \text{FP}(\mathcal{N} \setminus \mathcal{S}), \quad (4.10)$$

where  $\mathcal{S} = \mathcal{N} \setminus \mathcal{L}$ .

### 4.2.3. LOG-DETERMINANT

The log-determinant of the error covariance matrix, which indicates the log-volume of the confidence ellipsoid is given by

$$\text{LD}_m(\mathcal{L}) = \log \det \left[ \sum_{i \in \mathcal{L}} \text{tr}\{\mathbf{G}_m^{(i)} \mathbf{G}_m^{(i)\dagger}\} \right]^{-1}. \quad (4.11)$$

Similar to the weighted FP, the weighted log-determinant over the set of grid points from the parameter space is given by

$$\text{LD}(\mathcal{L}) = \sum_{m=1}^M p_m \log \det \left[ \sum_{i \in \mathcal{L}} \text{tr}\{\mathbf{G}_m^{(i)} \mathbf{G}_m^{(i)\dagger}\} \right]^{-1}. \quad (4.12)$$

In order to apply greedy optimization, the LD-based cost has to be monotonic and submodular and is given by [11]

$$F(\mathcal{L}) = - \sum_{m=1}^M p_m \left( \log \det \left[ \sum_{i \in \mathcal{L}} \text{tr} \{ \mathbf{G}_m^{(i)} \mathbf{G}_m^{(i)\dagger} \} + \epsilon \mathbf{I}_K \right]^{-1} + K \log \epsilon \right), \quad (4.13)$$

where  $\epsilon > 0$  is a small positive number,  $\mathbf{I}_K$  is the unit matrix of size  $K$ , and the term  $(K \log \epsilon)$  ensures that the function (4.13) is zero for an empty set  $\mathcal{L}$ .

#### 4.2.4. THE MAXIMUM EIGENVALUE OF THE ERROR COVARIANCE MATRIX

The maximum eigenvalue of the error covariance matrix corresponds to the minimum eigenvalue of the information matrix  $\lambda_{\min}(\text{FIM})$ , which indicates the length of the major semi-axis of the error ellipsoid and is a function of the maximum estimation error. The detailed derivation of the FIM can be found in Chapter 2.

In the convex optimization algorithm, we use the minimum eigenvalue of the FIM  $\lambda_{\min}(\text{FIM})$  as a performance measure and constraint it with the threshold  $\lambda_g$ . In this way we constrain the maximum value of the estimation (localization error) error  $\boldsymbol{\sigma}_{pos} = \tilde{\boldsymbol{\theta}} - \boldsymbol{\theta}$ , which has to be within an origin-centered ellipsoid (in case of a parameter vector with three components, e.g. 3D target localization) with the longest axis  $R_e$  and probability higher than  $P_e$ :  $\Pr(\|\boldsymbol{\sigma}_{pos}\|_2 \leq R_e) \geq P_e$  [12].

The probability  $P_e$  is given by [13]:

$$P_e(q) = \frac{K}{2^{K/2} \Gamma(K/2 + 1)} \int_0^{\sqrt{q}} \rho^{K-1} \exp\left(-\frac{\rho^2}{2}\right) d\rho, \quad (4.14)$$

where  $K$  is the number of parameters under estimation;  $\Gamma(\cdot)$  is the Gamma function;  $q$  is the constant that defines the size of the  $K$ -dimensional region enclosed by the surface (in two dimensions, the surface is an ellipse; in three dimensions, it is an ellipsoid; in the general case of  $K$  dimensions it may be considered a hyperellipsoid).

For 3D target position and velocity estimation  $K = 6$ , for 2D:  $K = 4$ ; for 3D and 2D target positioning only  $K = 3$  and  $K = 2$ . The simplified terms of corresponding integrals are:

$$P_e(q) = 1 - \exp(-q/2), \quad K = 2 \quad (4.15)$$

$$P_e(q) = \text{erf}(\sqrt{q}/2) - \frac{\sqrt{2q}}{\pi} \exp(-q/2), \quad K = 3 \quad (4.16)$$

$$P_e(q) = 1 - \exp(-q/2) \left( \frac{q}{2} + 1 \right), \quad K = 4 \quad (4.17)$$

$$P_e(q) = 1 - \exp(-q/2) \left( \frac{q^2}{8} + \frac{q}{2} + 1 \right), \quad K = 6 \quad (4.18)$$

where the error function is:

$$\text{erf}(x) = \frac{2}{\sqrt{\pi}} \int_0^x \exp(-t^2) dt. \quad (4.19)$$

The minimum eigenvalue  $\lambda_{\min}(\text{FIM})$  is related to the semi-major axis as  $R_e^2 = q \lambda_{\min}(\text{FIM})$ .

### 4.3. MULTI-MODAL PARAMETER VECTOR

Without loss of generality, let us consider a model where the parameter vector consists of multi-modal parameters. Examples of such a model are combinations of the simultaneous estimation of target range, radial velocity, and bearing in a single radar. Basically, the parameter vector for each grid point from the parameter space is a combination of two vectors with different measurement units  $\boldsymbol{\alpha}_m = [\boldsymbol{\alpha}_{m,1}, \boldsymbol{\alpha}_{m,2}]^T$ , where  $\boldsymbol{\alpha}_{m,1} \in \mathbb{R}^{K_1}$  and  $\boldsymbol{\alpha}_{m,2} \in \mathbb{R}^{K_2}$ , with the total number of parameters under estimation given by  $K = K_1 + K_2$ . This also results in splitting of the system matrix  $\mathbf{G}_m^{(\mathcal{N})}$  as  $\mathbf{G}_m^{(\mathcal{N})} = [\mathbf{G}_{m,1}^{(\mathcal{N})}, \mathbf{G}_{m,2}^{(\mathcal{N})}]$  with  $\mathbf{G}_{m,1}^{(\mathcal{N})} \in \mathbb{R}^{QN \times K_1}$  and  $\mathbf{G}_{m,2}^{(\mathcal{N})} \in \mathbb{R}^{QN \times K_2}$ .

The MSE is then expressed as:

$$\text{MSE} = E(\|\boldsymbol{\alpha}_{m,1} - \hat{\boldsymbol{\alpha}}_{m,1}\|_2^2) + E(\|\boldsymbol{\alpha}_{m,2} - \hat{\boldsymbol{\alpha}}_{m,2}\|_2^2). \quad (4.20)$$

However, since  $\boldsymbol{\alpha}_{m,1}$  and  $\boldsymbol{\alpha}_{m,2}$  represent different modalities, their errors should be treated differently. Therefore, we would like to introduce the weighting coefficients  $w_{m,1}$  and  $w_{m,2}$  in the MSE, which allow us to put a different emphasis on each term:

$$\text{MSE} = w_{m,1}E(\|\boldsymbol{\alpha}_{m,1} - \hat{\boldsymbol{\alpha}}_{m,1}\|_2^2) + w_{m,2}E(\|\boldsymbol{\alpha}_{m,2} - \hat{\boldsymbol{\alpha}}_{m,2}\|_2^2). \quad (4.21)$$

This can be implicitly realized by rewriting the model in (4.5) as

$$\mathbf{y} \approx \mathbf{f}(\boldsymbol{\alpha}_m) + \tilde{\mathbf{G}}_m^{(\mathcal{N})}(\tilde{\boldsymbol{\alpha}} - \tilde{\boldsymbol{\alpha}}_m) + \boldsymbol{\xi}, \quad (4.22)$$

where  $\tilde{\mathbf{G}}_m^{(\mathcal{N})}$  is the modified weighted matrix:

$$\tilde{\mathbf{G}}_m^{(\mathcal{N})} = \left[ \frac{1}{\sqrt{w_{m,1}}} \mathbf{G}_{m,1}^{(\mathcal{N})}, \quad \frac{1}{\sqrt{w_{m,2}}} \mathbf{G}_{m,2}^{(\mathcal{N})} \right], \quad (4.23)$$

and where  $\tilde{\boldsymbol{\alpha}}_m = [\sqrt{w_{m,1}}\boldsymbol{\alpha}_{m,1}, \sqrt{w_{m,2}}\boldsymbol{\alpha}_{m,2}]^T$  is the weighted parameter vector. Using the model (4.22) in the submodular costs (4.10) and (4.13) will implicitly relate these costs to the weighted MSE (4.21). The possibility to operate with the weights  $p_m$ ,  $w_{m,1}$ , and  $w_{m,2}$ , expands the set of application scenarios for topology optimization of radar networks. For example, the radar network topology for parameter vector estimation can be optimized for scenarios, in which some grid points are uni-modal, while others are multi-modal.

### 4.4. OPTIMIZATION ALGORITHMS

For the sake of simplicity, we assume that all radars in the network have the same operating parameters, although this assumption can easily be relaxed.

#### 4.4.1. CONVEX OPTIMIZATION

The convex optimization problem of radar network topology selection is formulated as the selection of the *minimum* number of the most informative radar positions from the  $N$  available ones, such that prescribed estimation accuracy of the parameter vector will be satisfied for each  $\boldsymbol{\alpha}_m$ ,  $m = 1, \dots, M$ . This forms the first type of the optimization

problem defined in (4.1). The minimum eigenvalue of the FIM,  $\lambda_{\min}$ , is used as a performance metric.

The cardinality minimization problem (4.1) can be represented as the minimization of the  $l_1$ -norm of the selection vector  $\mathbf{w} \in \mathbb{R}^N$  with entries  $0 \leq w^{(n)} \leq 1$  that is a relaxed Boolean constraint  $\{0, 1\}$ , which represents when the  $n$ th radar position is selected or not. As has been shown in Chapter 2, the FIM on the estimation accuracy of the  $2D/3D$  target parameters in the radar network is a function of the estimation accuracy of the target radar signal parameters in a single radar  $\boldsymbol{\psi}_m^{(n)} = [\tau_m^{(n)}, \omega_{d_m}^{(n)}, |A_m^{(n)}|, \varphi_m^{(n)}]$ . Moreover it has an additive character and can be given as

$$\mathbf{I}(\boldsymbol{\alpha}_m) = \sum_{n=1}^N \mathbf{I}^{(n)}(\boldsymbol{\alpha}_m), \quad (4.24)$$

where  $\mathbf{I}^{(n)}(\boldsymbol{\alpha}_m)$  is the FIM evaluated from the measurements of the  $n$ th radar. Consequently, the contribution of each single radar to the overall system estimation accuracy can be interpreted as the exploitation of the measurements from that specific radar for the parameter vector estimation and can be given as

$$\mathbf{I}(\boldsymbol{\alpha}) = \sum_{n=1}^N w_n \mathbf{I}^{(n)}(\boldsymbol{\alpha}), \quad (4.25)$$

where each  $w^{(n)}$  specifies whenever  $n$ th position of the radar is selected or not, that is whenever the measurements from this radar are used or not for target radar signal parameters estimation. Additionally, in order to provide the sparse solution, we introduce another (re-)weighting vector  $\mathbf{u} = [u^{(1)}, \dots, u^{(N)}]^T$  and explore *re-weighted*  $l_1$ -norm minimization [14]. Consequently, we can re-write the generic optimization problem of the first type (4.1) as

$$\begin{aligned} & \mathbf{w}_k = \operatorname{argmin}(\mathbf{u}_k^T \mathbf{w}), \quad \mathbf{w} \in R^N \\ & \text{s.t. } \sum_{n=1}^N w^{(n)} \mathbf{I}^{(n)}(\boldsymbol{\alpha}_m) - \lambda_g \mathbb{1}_3 \geq 0, \quad m = 1, \dots, M; \\ & \begin{bmatrix} \mathbf{W} & \mathbf{w} \\ \mathbf{w}^T & 1 \end{bmatrix} \succeq 0; \\ & \operatorname{diag}(\mathbf{W}) = \mathbf{w}; \end{aligned} \quad (4.26)$$

where  $\mathbf{W} = \mathbf{w}\mathbf{w}^T$ ; the constraint  $\begin{bmatrix} \mathbf{W} & \mathbf{w} \\ \mathbf{w}^T & 1 \end{bmatrix} \succeq 0$  is equivalent to  $\mathbf{W} \succeq \mathbf{w}\mathbf{w}^T$  and it is called the semidefinite programming (SDP) relaxation of the original non-convex quadratically constrained quadratic programs (QCQP), which in our case is represented by equality constraint  $\mathbf{W} = \mathbf{w}\mathbf{w}^T$ . The pseudocode of the convex optimization is presented in Algorithm 1 with  $\epsilon$  being a small number that prevents division by zero.

The randomization technique can be further used in order to compute good approximate solutions [15]. The main idea behind this technique is the following: to model the vector of the weighting coefficients  $\mathbf{w}$  as a Gaussian variable with  $\mathbf{w} \sim \mathcal{N}(\mathbf{w}, \mathbf{W} - \mathbf{w}\mathbf{w}^T)$ , solve a problem (4.26) for sufficient number of sampled  $\mathbf{w}$  from this

**Algorithm 1:** Convex optimization algorithm

**Input** :  $M$  matrices  $\mathbf{G}_m^{(\mathcal{N})}$ , the set of available radar positions  $\mathcal{N}$ , performance metric function, e.g.  $\lambda_{\min}(\mathbf{I}(\boldsymbol{\alpha}_m))$ , and the constant on the estimation error  $\lambda_g$ .

**Output** : Coordinates of the minimum number of selected radar positions.

**Initialize:** The iteration counter  $k = 0$  and the (re-)weight vector  $\mathbf{u} = \mathbb{1}_N$ .

**Repeat** : Until  $k$  attains a specified maximum number of iterations  $k_{max}$ .

Solve the weighted  $l_1$ -norm minimization problem (4.26) for the optimum  $\mathbf{W}$  in the  $k$ th iteration.

Update the weight vector  $u_k^{(n)} = 1 / [\epsilon + w_k^{(n)}]$  for each  $n = 1, \dots, N$ .

4

distribution and keep the best feasible point. This procedure guarantees that the feasible point will be at most  $2/\pi \approx 64\%$  suboptimal [15].

**4.4.2. GREEDY OPTIMIZATION**

We formulate the topology optimization problem, based on greedy optimization, as the selection of the  $L$  most informative radar positions from the  $N$  available ones, where  $L$  is known a priori. This is the second type of optimization problem defined in (4.2). Both (submodular) functions, namely the frame potential and the log-determinant are used as performance metrics.

The maximization of the function  $F(\cdot)$  from (4.10) corresponds to removing rows from the matrix  $\mathbf{G}_m^{(\mathcal{N})}$ , while the maximization of  $F(\cdot)$  from (4.13) corresponds to accumulating rows in order to form the matrix  $\mathbf{G}_m^{(\mathcal{L})}$ . The pseudocode for the maximization of these two cost functions is given in Algorithm 2.

**4.5. BISTATIC RADAR ARCHITECTURE - STRUCTURED SELECTION**

To represent the measurement model of bistatic radar network, we use the model (4.5)

$$\mathbf{y} \approx \mathbf{f}(\boldsymbol{\alpha}_m) + \mathbf{G}_m^{(\mathcal{N})}(\boldsymbol{\alpha} - \boldsymbol{\alpha}_m) + \boldsymbol{\xi}, \quad (4.27)$$

where  $\mathcal{N}$  is the set of all available radar node positions  $\mathcal{N} = \mathcal{N}_t \cup \mathcal{N}_r$  with the set of available positions for transmit nodes  $\mathcal{N}_t$  and the set of available positions for receive nodes  $\mathcal{N}_r$ ;  $N$  is the number of Tx-Rx channels defined as  $N = N_t N_r$ . The sets of the most informative Tx and Rx node positions are  $\mathcal{L}_t = \{s_1, \dots, s_{L_t}\}$  and  $\mathcal{L}_r = \{j_1, \dots, j_{L_r}\}$  with  $L = L_t L_r$ , the most informative measurements from corresponding Tx-Rx channels, where  $L_t$  and  $L_r$  are the number of selected Tx and Rx nodes.

Bistatic radar architecture poses the following challenges for radar networks topology optimization:

1. *Selection-dependent optimization*, that imposes a structured selection of measurements from the measurement matrix in contrast to monostatic radar networks (Table 4.1).

---

**Algorithm 2:** Greedy algorithm for monostatic radar network topology optimization

---

**Input** :  $M$  matrices  $\mathbf{G}_m^{(\mathcal{N})}$ , the set of available radar positions  $\mathcal{N}$ , the number of radar positions to be selected  $L$ , and function  $F(\cdot)$  (from (4.10) or (4.13)).

**Output** : Positions of  $L$  radars.

**Initialize:** The radar set,  $\mathcal{I}$ .

1. For (weighted) FP cost function:

$$\mathcal{I} = \arg \min_{i,j \in \mathcal{N}} \sum_{m=1}^M p_m \left| \text{tr} \{ \mathbf{G}_m^{(i)} \mathbf{G}_m^{(j)\dagger} \} \right|^2.$$

2. For (weighted) LD cost function:

$$\mathcal{I} = \arg \max_{i \in \mathcal{N}} F(\mathbf{G}_m^{(i)}).$$

**Repeat** : Until  $L$  positions are found

1. Find the radar  $i = \arg \max_{i \notin \mathcal{I}} F(\mathcal{I} \cup i)$ .

2. Update  $\mathcal{I}$ :  $\mathcal{I} = \mathcal{I} \cup i$ .

3. For (weighted) FP cost function:

(a) If  $|\mathcal{I}| = N - L$ , stop.

(b) Assign the set of selected positions  $\mathcal{L} = \mathcal{N} \setminus \mathcal{I}$ .

4. For (weighted) LD cost function:

(a) If  $|\mathcal{I}| = L$ , stop.

(b) Assign the set of selected positions  $\mathcal{L} = \mathcal{I}$ .

---

2. The selection of Tx and Rx node positions from one set of available locations, i.e.  $\mathcal{N}_t = \mathcal{N}_r = \mathcal{N}$ . This raises the problem of a trade-off of dedicating available locations either to transmission or reception, avoiding selection of collocated radar architecture. The measurement matrix has size  $\mathbf{G} \in \mathbb{R}^{(N^2 - N) \times K}$ . Further in this thesis, we refer to this problem as model with overlapping Tx and Rx grids.

The topology optimization problem of bistatic radar network can be treated as a design of the sparse sampling matrix  $\mathbf{W} \in \mathbb{R}^{N_t \times N_r}$  with specific structure, which is defined by the cooperation mode between transmitters and receivers (cooperative or autonomous). Matrix  $\mathbf{W}$  is defined as

$$\mathbf{W} = \mathbf{w}_t \mathbf{w}_r^T, \quad (4.28)$$

where  $\mathbf{w}_t \in \mathbb{R}^{N_t}$  and  $\mathbf{w}_r \in \mathbb{R}^{N_r}$  are the selection vectors for Tx and Rx radar nodes, which indicate when the available positions for Tx and Rx radar nodes are selected (1) or not (0).

Table 4.1: Monostatic versus bistatic radar network topology optimization.

Radar architecture	Measurement matrix	Remark
MS	$\mathbf{G} \in \mathbb{R}^{N \times K}$	Measurements from cooperative pairs can not be selected separately.
BS	$\mathbf{G} \in \mathbb{R}^{(N_t \cdot N_r) \times K}$	Selection process involves measurements from <i>cooperative</i> pairs that have to be incorporated into the cost function evaluation (only cooperative mode) and excluded from the measurement matrix (both cooperative and autonomous modes).

4

Then we can rewrite the measurement model (4.5) as

$$\mathbf{y} \approx \mathbf{f}(\boldsymbol{\alpha}_m) + \text{diag}(\mathbf{W}) \mathbf{G}_m^{(N)} (\boldsymbol{\alpha} - \boldsymbol{\alpha}_m) + \boldsymbol{\xi} \quad (4.29)$$

We can formulate general optimization problem as

$$\begin{aligned} & \max_{\mathbf{w} \in \{0,1\}^{N_t \times N_r}} f(\mathcal{I}) \\ & \text{s.t. } \mathbf{W} = \mathbf{w}_t \mathbf{w}_r^T \\ & \quad \|\mathbf{w}_t\|_0 = L_t \\ & \quad \|\mathbf{w}_r\|_0 = L_r \end{aligned} \quad (4.30)$$

#### 4.5.1. CONVEX OPTIMIZATION ALGORITHM

In this section, we consider a bistatic radar network with a cooperative mode of signal transmission-reception, i.e. signals scattered from the target due to illumination by all of the transmit radar nodes are received in all of the receiving radar nodes. Then the Fisher information matrix that characterizes the system performance can be represented as

$$\mathbf{I}(\mathbf{w}_t, \mathbf{w}_r, \boldsymbol{\alpha}_m) = \sum_{n=1}^{N_t} \sum_{s=1}^{N_r} w_t^{(n)} w_r^{(s)} \mathbf{I}(\boldsymbol{\alpha}_m)^{(ns)}. \quad (4.31)$$

In order to choose the favorable geometry of bistatic radars, the positions of transmitting  $N_t$  and receiving nodes  $N_r$  has to be optimized simultaneously. The minimization function is then a sum of two (re-weighted)  $l_1$ -norms, and the problem

of the multistatic radar network geometry optimization is formulated as

$$\begin{aligned}
 & \min_{\mathbf{w}_t \in R^{N_t}, \mathbf{w}_r \in R^{N_r}} \left( \mathbf{u}_t^T \mathbf{w}_t + \mathbf{u}_r^T \mathbf{w}_r \right) \\
 & \text{s.t.} \sum_{n=1}^{N_t} \sum_{s=1}^{N_r} w_t^{(n)} w_r^{(s)} \mathbf{I}(\boldsymbol{\alpha}_m)^{(nm)} - \lambda_g \mathbb{1}_3 \geq 0, \quad m = 1, \dots, M \\
 & w_t^{(n)} \in \{0, 1\}, \quad n = 1, \dots, N_t \\
 & w_r^{(s)} \in \{0, 1\}, \quad s = 1, \dots, N_r
 \end{aligned} \tag{4.32}$$

where  $\mathbf{u}_t$ ,  $\mathbf{u}_r$  are weight vectors for the number of Tx and Rx radar units with the elements  $[u_t^{(n)}]_k = \frac{1}{\epsilon + [w_t^{(n)}]_k}$  and  $[u_r^{(s)}]_k = \frac{1}{\epsilon + [w_r^{(s)}]_k}$  respectively. The notation  $\mathbf{I} \geq \mathbb{1}$  means that matrix  $(\mathbf{I} - \mathbb{1})$  is semi-positive definite ( $\mathbf{I}$  and  $\mathbb{1}$  are symmetrical matrices).

Constraint in (4.32) implies the *bilinear matrix inequality* (BMI) problem. BMI problems are NP-hard and include all quadratic problems. There are local and global methods for the solution of BMI optimization problems. The local method implies an alternate optimization over the parameters  $\mathbf{w}_t$  and  $\mathbf{w}_r$ . In the global method (branch-and-bound type) the solution can be found by relaxing the BMI problem to the linear matrix inequality (LMI) problem. We apply semidefinite relaxation to solve the problem of the geometry optimization of multistatic radar networks.

#### SEMIDEFINITE RELAXATION IN BMI PROBLEM OF MULTISTATIC RADAR NETWORK GEOMETRY OPTIMIZATION

First, we substitute the bilinear terms  $w_t^{(n)}$ ,  $w_r^{(s)}$  in (4.32) with new variable  $\boldsymbol{\gamma} = [w_t^{(1)}, \dots, w_t^{(N_t)}, w_r^{(1)}, \dots, w_r^{(N_r)}]^T$  and introduce the bound on the  $\gamma_j$  [16]. Consequently, the optimization problem (4.32) will be

$$\begin{aligned}
 & \min_{\mathbf{w}_t \in R^{N_t}, \mathbf{w}_r \in R^{N_r}} \left( \mathbf{u}_t^T \mathbf{w}_t + \mathbf{u}_r^T \mathbf{w}_r \right) \\
 & \text{s.t.} \sum_{n=1}^{N_t} \sum_{s=1}^{N_r} g_{nm} \mathbf{I}(\boldsymbol{\alpha}_m)^{(ns)} - \lambda \mathbb{1}_2 \geq 0, \quad m = 1, \dots, M \\
 & g^{(ns)} = w_t^{(n)} w_r^{(s)}, \quad n = 1, \dots, N_t; \quad s = 1, \dots, N_r
 \end{aligned} \tag{4.33}$$

Then we relax the constraint on  $g^{(ns)}$  as LMI

$$\begin{aligned}
 & \min_{\mathbf{w}_t \in R^{N_t}, \mathbf{w}_r \in R^{N_r}} \left( \mathbf{u}_t^T \mathbf{w}_t + \mathbf{u}_r^T \mathbf{w}_r \right) \\
 & \text{s.t.} \sum_{n=1}^{N_t} \sum_{s=1}^{N_r} g^{(ns)} \mathbf{I}(\boldsymbol{\alpha}_m)^{(ns)} - \lambda_g \mathbb{1}_3 \geq 0, \quad m = 1, \dots, M \\
 & \begin{bmatrix} \mathbf{Y} & \boldsymbol{\gamma} \\ \boldsymbol{\gamma}^T & 1 \end{bmatrix} \geq 0
 \end{aligned} \tag{4.34}$$

where  $\mathbf{Y} = \boldsymbol{\gamma} \boldsymbol{\gamma}^T$ .

The problem (4.34) is a semidefinite programming (SDP) problem in the variables  $\mathbf{G}$  and  $\boldsymbol{\gamma}$ . Similar to the monostatic radar network optimization, the algorithm for the selection of the multistatic radar network topology is

1. *Initialize* the iteration counter  $k = 0$  and the weight vectors  $\mathbf{u}_t = \mathbf{1}_{N_t}$ ,  $\mathbf{u}_r = \mathbf{1}_{N_r}$ .
2. *Solve* the weighted  $l_1$ -norm minimization problem (4.34) for the optimum  $\boldsymbol{\gamma}_k$  in the  $k$ -th iteration.
3. *Update* the weight vectors:  $[u_t^{(n)}]_k = \frac{1}{\epsilon + [w_t^{(n)}]_k}$  and  $[u_r^{(s)}]_k = \frac{1}{\epsilon + [w_r^{(s)}]_k}$  for each  $n = 1, \dots, N_t$  and  $s = 1, \dots, N_r$ .
4. *Stop* on convergence or when  $k$  attains a specified maximum number of iterations  $k_{max}$ , otherwise, increment  $k$  and go to step 2.

4

#### 4.5.2. GREEDY OPTIMIZATION

Pseudocode of the greedy optimization algorithm is presented in Algorithm 3. This algorithm takes into account the scenario when two sets for potential Tx and Rx radar node positions do overlap, iteratively excluding positions of the nodes, collocated to the optimal ones.

#### 4.6. COMPUTATIONAL COMPLEXITY

Both the FP and the LD cost functions explore the greedy Algorithm 2. The complexity of the greedy Algorithm 2 for the weighted log-det cost function is linear with respect to the number of potential radar nodes positions  $N$ ,  $O(N)$ , since  $N$  matrices are evaluated in Algorithm 2. For the weighted frame potential the complexity of the same algorithm is cubic with respect to  $N$ ,  $O(N^3)$ . This is related to the fact that for each of the  $N - L$  steps, there are  $(N - S)^2$  terms ( $S = 3, \dots, (N - L)$ ). The complexity of the algorithm can be further reduced to  $O(N^2)$  by exploiting the recursive property of the FP function. Based on this, for large-scale problems with  $L \ll N$  and  $K \ll N$ , the LD cost function allows for a lower computational complexity, compared to the FP cost. At the same time, Algorithm 2 for the LD cost is cubic in number of parameters under estimation  $K$ ,  $O(K^3)$ , while for the FP it is linear in  $K$ ,  $O(K)$ . Therefore, exploiting the LD cost for problems where  $K$  is in the order of  $N$  would entail a higher complexity, compared to the FP.

#### 4.7. CONCLUSION

In this chapter, a generic framework of radar network topology optimization, based on convex and greedy algorithms, has been proposed. Three cost functions were analyzed: the frame potential, the log-determinant and the minimum eigenvalue, with the last two being scalar functions of the error covariance matrix. The theory is developed based on the non-linear measurement model with an extension to the case of multi-modal parameter vector estimation. Moreover, a so-called problem of structural selection has been tackled. Such a structural selection is presented in the radar networks with a cooperative mode of signal reception. The formulation of the cost function, which allows off-grid radar selection, has been presented as well. The developed approach is

---

**Algorithm 3:** Greedy algorithm for bistatic radar network topology optimization
 

---

**Input** : Matrix  $\mathbf{G}$ , two sets of potential radar nodes positions  $\mathcal{N}_t$  and  $\mathcal{N}_r$ , the number of Tx nodes  $L_t$  and Rx nodes  $L_r$  positions to be selected.

**Output** : Positions of  $L_t$  Tx nodes and  $L_r$  Rx nodes.

**Initialize:** The radar Tx and Rx sets,  $\mathcal{S}$  and  $\mathcal{J}$ .

$\mathcal{S} \cup \mathcal{J} = \arg \max_{s \in \mathcal{S}, j \in \mathcal{J}} F(\mathbf{g}^{(s,j)})$ .

The sets of cooperative Tx/Rx nodes:  $\mathcal{A}_t = \{\} (|\mathcal{A}_t| = 0)$  and  $\mathcal{A}_r = \{\} (|\mathcal{A}_r| = 0)$ .

**For** :  $t = 1$  to  $L_t$

**For** :  $r = 1$  to  $L_r$

1. Find the optimal measurement from corresponding Tx-Rx channel

(a) for *cooperative* reception mode:

$$\{s, j\} = \arg \max_{s \in \mathcal{S}, j \in \mathcal{J}} F(\mathcal{S} \cup s, \mathcal{J} \cup j, \mathcal{A}_t \cup j, \mathcal{A}_r \cup s);$$

(b) for *autonomous* reception mode:  $\{s, j\} = \arg \max_{s \in \mathcal{S}, j \in \mathcal{J}} F(\mathcal{S} \cup s, \mathcal{J} \cup j)$ .

2. Update

$$\mathcal{S}: \mathcal{S} = \mathcal{S} \cup s;$$

$$\mathcal{J}: \mathcal{J} = \mathcal{J} \cup j;$$

$$\mathcal{A}_t: \mathcal{A}_t = \mathcal{A}_t \cup j;$$

$$\mathcal{A}_r: \mathcal{A}_r = \mathcal{A}_r \cup s;$$

(a) for *overlapping* Tx and Rx radar nodes grids  $\mathcal{N}_t = \mathcal{N}_r = \mathcal{N}$ :

$$\mathcal{N}_t: \mathcal{N}_t = \mathcal{N}_t \setminus \{s \cup j\};$$

$$\mathcal{N}_r: \mathcal{N}_r = \mathcal{N}_r \setminus \{s \cup j\}.$$

(b) for *different* Tx and Rx radar nodes grids  $\mathcal{N}_t \neq \mathcal{N}_r$ :

$$\mathcal{N}_t: \mathcal{N}_t = \mathcal{N}_t \setminus s;$$

$$\mathcal{N}_r: \mathcal{N}_r = \mathcal{N}_r \setminus j.$$


---

not limited to the spatial selection of the radar nodes and can be applied for scenarios of temporal (the selection of the most informative measurements in a single radar) as well as spatio-temporal (the selection of the most informative measurements within a network of radars, with centralized data processing, i.e. on the level of sampled measurements) data selection.

## REFERENCES

- [1] I. M. Ivashko, O. A. Krasnov, and A. G. Yarovoy, *Sparsity-based optimization of the sensors positions in radar networks with separated transmit and receive nodes*, *Int. J. Distrib. Sen. Netw.* **2016** (2016), 10.1155/2016/9437602.
- [2] I. Ivashko, G. Leus, and A. Yarovoy, *Radar network topology optimization for joint target position and velocity estimation*, *Signal Processing* **130**, 279 (2017).
- [3] M. Skolnik, *Radar Handbook, Third Edition*, Electronics electrical engineering (McGraw-Hill Companies, Incorporated, 2008).
- [4] J. Li and P. Stoica, *MIMO Radar Signal Processing* (Wiley, 2008).
- [5] T. Onel, C. Ersoy, and H. Delic, *Information content-based sensor selection and transmission power adjustment for collaborative target tracking*, *Mobile Computing, IEEE Transactions on* **8**, 1103 (2009).
- [6] H. Wang, G. Pottie, K. Yao, and D. Estrin, *Entropy-based sensor selection heuristic for target localization*, in *Information Processing in Sensor Networks, 2004. IPSN 2004. Third International Symposium on* (2004) pp. 36–45.
- [7] S. Boyd and L. Vandenberghe, *Convex Optimization* (Cambridge University Press, 2004).
- [8] M. Fisher, G. Nemhauser, and L. Wolsey, *An analysis of approximations for maximizing submodular set functions—ii*, in *Polyhedral Combinatorics, Mathematical Programming Studies*, Vol. 8, edited by M. Balinski and A. Hoffman (Springer Berlin Heidelberg, 1978) pp. 73–87.
- [9] J. Ranieri, A. Chebira, and M. Vetterli, *Near-optimal sensor placement for linear inverse problems*, *Signal Processing, IEEE Transactions on* **62**, 1135 (2014).
- [10] M. Shamaiah, S. Banerjee, and H. Vikalo, *Greedy sensor selection: Leveraging submodularity*, in *Decision and Control (CDC), 2010 49th IEEE Conference on* (2010) pp. 2572–2577.
- [11] S. Rao, S. Chepuri, and G. Leus, *Greedy sensor selection for non-linear models*, in *Signal Processing Conference (EUSIPCO), 2016 Proceedings of the 24th European* (2016).
- [12] F. Gustafsson and F. Gunnarsson, *Mobile positioning using wireless networks: possibilities and fundamental limitations based on available wireless network measurements*, *Signal Processing Magazine, IEEE* **22**, 41 (2005).

- [13] D. Torrieri, *Statistical theory of passive location systems*, Aerospace and Electronic Systems, IEEE Transactions on **AES-20**, 183 (1984).
- [14] E. Candès, M. Wakin, and S. Boyd, *Enhancing sparsity by reweighted  $l_1$  minimization*, Journal of Fourier Analysis and Applications **14**, 877 (2008).
- [15] A. d'Aspremont and S. Boyd, *Relaxations and randomized methods for nonconvex QCQPs*, EE392o Class Notes (2003).
- [16] S. Boyd and L. Vandenberghe, *Semidefinite programming relaxations of non-convex problems in control and combinatorial optimization*, (1997).



# 5

## ACCURACY-DRIVEN TOPOLOGY OPTIMIZATION: NUMERICAL ANALYSIS

*In this chapter, the developed optimization framework will be applied for the best radar network topology selection in different scenarios within three case studies. The goal of this chapter is to demonstrate the versatility of the developed tool as well as to compare optimization algorithms and cost functions. In particular, the optimization algorithm will be applied for short- and middle-range radar networks that consist of monostatic (Section 5.2) and bistatic (Section 5.3) radars or a combination of both (Section 5.4). Different signal reception modes will be considered as well. Finally, three cost functions, LD, FP, and maximum eigenvalue of the covariance matrix, will be compared in Section 5.5.*

---

Parts of this chapter have been published in [1], [2], [3].

## 5.1. SIMULATION SCENARIOS

IN this chapter, three case studies will be considered:

1. low airspace observation in the city of The Hague, represented by 161 candidate positions of medium-range FMCW radars that correspond to 7 locations of C2000 and 154 locations of existing GSM masts coordinates and which can be found in [4];
2. the area of the TU Delft university campus, represented by 117 non-uniformly distributed candidate positions of short-range FMCW radars;
3. passenger surveillance in the airport terminal area with low airspace surveillance in 42 candidate positions of short-range FMCW radars.

Parameters of a single radar node for three scenarios are listed in Table 5.1. For simplicity, throughout this chapter, we refer to these scenarios as The Hague, TU Delft, and airport area. Table 5.2 gives an overview of the scenarios of potential radar positions, type of the network, and optimization algorithms used for radar network topology selection in corresponding scenarios. It is assumed that target position is estimated from range measurements, unless otherwise stated.

Table 5.1: Single sensor simulation parameters for three scenarios

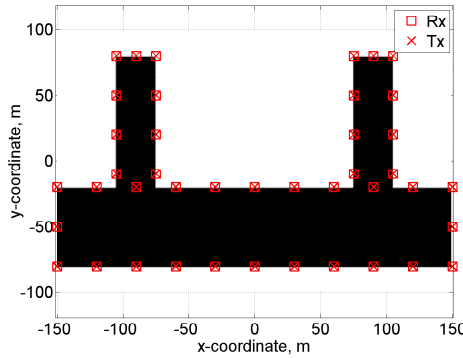
Parameter	WiFi radar	FMCW radar (short-range)	FMCW radar (medium-range)
Transmitted power, $P_t$	20dBm (EIRP)	10dBm (EIRP)	25 W
Antenna gain, $G$	8 dB	10 dB	3.8 dB
Carrier frequency, $f_c$	2.4 GHz	25 GHz	1.36 GHz
Sweep time, $T_s$	1 $\mu$ s	0.8 $\mu$ s	0.5 ms
Number of integrated pulses, $N_{\text{puls}}$	512	512	512
Waveform bandwidth, $\Delta f$	11 MHz	300 MHz	5 MHz
Noise figure, $F_n$	10 dB	8 dB	10 dB
System losses $F_{\text{sys}t}$	4 dB	15 dB	6 dB

## 5.2. MONOSTATIC RADAR NETWORK

In this simulation, the first scenario of potential radar nodes positions depicted in Fig. 5.1a is considered. As has been demonstrated with Fig. 3.1 and Fig. 3.8 in Chapter 3, the radar network with cooperative mode of signal transmission-reception provides higher system estimation accuracy than the radar network with autonomous mode. These two cooperation modes have been integrated into the radar network topology optimization algorithm as well. Fig. 5.2 shows contour plots of the target localization error for selected topologies of two types of the radar networks: one with autonomous and another



(a) City of The Hague with 161 candidate radar positions: coordinates of C200 and GSM masts. The area dimension is approx. 10 km × 12 km. (b) The TU Delft campus with 117 candidate radar positions. The area dimension is approx. 800 m × 800 m.



(c) The airport terminal area with 42 candidate radar positions. The area dimension is approx. 300 m × 150 m.

Figure 5.1: Scenarios of candidate radars positions

one with cooperative reception modes. The results were obtained by selection of the minimum number of radar nodes required to satisfy the constraint on the maximum value of the localization error  $R_e = 3\text{ m}$  (with probability  $P_e = 95\%$ ), which is expressed in the form of a constraint on the maximum eigenvalue of the Fisher information matrix, using convex Algorithm 1, provided in Chapter 4. As apparent from the results, the number of radar nodes is three times smaller in the system with cooperative mode ( $L = 5$ ) than in one with autonomous mode ( $L = 15$ ). At the same time, as a result of cooperative reception, the number of Tx-Rx channels is higher by ten (almost two times higher) than with autonomous reception. Nevertheless, the contour line on localization error that

Table 5.2: Connection between three considered scenarios of potential radar positions (Fig.5.1), type of the network, and optimization algorithm

Radar architecture and cooperation mode	Convex (minimum eigenvalue of covariance matrix)	Greedy (log-determinant of covariance matrix)	Section	Remarks
MS aut.	TU Delft	TU Delft	5.5	FP cost minimization is performed as well signal blockage is accounted for
	The Hague Airport area		5.2 5.6	
MS coop.	The Hague		5.2	
BS aut.		TU Delft	5.3	
BS coop.	TU Delft	TU Delft	5.3, 5.5	
BPR	Airport area		5.4	

encloses the target area in a cooperative network corresponds to higher localization error (Fig. 5.2b) than the one in an autonomous network (Fig. 5.2a). The reason is the lower spatial diversity gain, achieved with five sensing locations.

### 5.3. BISTATIC RADAR NETWORK

In this analysis, the scenario around the area of the TU Delft campus with 117 potential radar nodes locations is considered (Fig. 5.1b). The greedy algorithm with LD cost minimization is used for optimal topology selection of bistatic radar nodes.

#### 5.3.1. PRESELECTED GRIDS FOR TRANSMIT AND RECEIVE RADAR NODES

Candidate positions for Tx and Rx radar nodes have been randomly preselected from available  $N = 117$  locations, such that 58 positions have been selected on transmit and 59 on receipt (see Fig. 5.5, where locations of potential Tx and Rx radar node positions are marked together with the optimal ones). Indexes of the selected and selected together with cooperative Tx-Rx pairs in the network with cooperative mode for  $L_t = 15$  and  $L_r = 20$  are shown in Figs. 5.3a and 5.3b, respectively. As one can see, 15 Tx-Rx channels are selected such that each transmitter has a dedicated receiver. This is an expected behavior of the algorithm, which aims to select the maximal number of so-called independent Tx-Rx channels, such that the maximal number of total (cooperative) channels will be provided. Note that an additional (cooperative) five Rx nodes are selected only in pairs with the first optimal receiver. This is due to the system cooperative mode, which means that selected Rx nodes form cooperative pairs with other selected transmitters as well. Indexes of the  $N = 20$  selected Tx-Rx channels

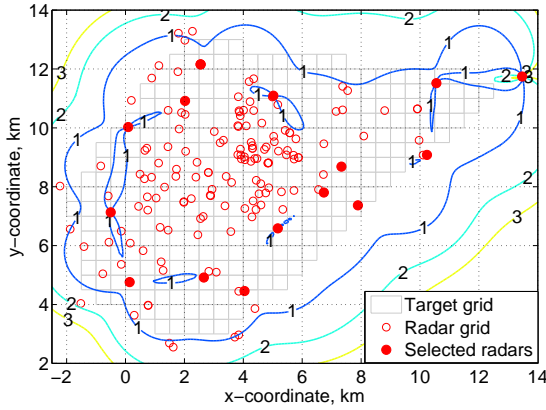
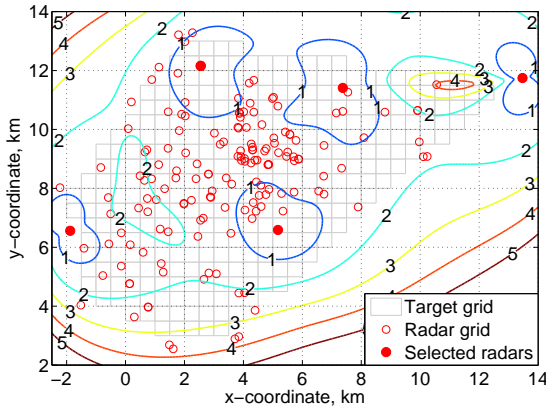
(a)  $L = 15$  autonomous radars(b)  $L = 5$  cooperative radars

Figure 5.2: Contour plots of the target localization error ( $\sigma_p$ , m) in the network of  $L$  monostatic FMCW radars, which have been selected from  $N = 161$  candidate positions using convex optimization (Algorithm 1, Chapter 4).

in the radar network with autonomous transmission-reception mode are shown in Fig. 5.4. As one can observe, the indexes of selected pairs differ considerably from the ones in the system with cooperative mode (Fig. 5.3a), although two topologies may look similar at first glance, which is shown in Fig. 5.5 (the selected cooperative and autonomous Tx-Rx pairs have the same color code). Although the total number of Tx and Rx nodes is higher in the network with autonomous mode (amounting to 40), than in the network with cooperative mode (amounting to 35), the estimation accuracy of the latter is about three times higher.

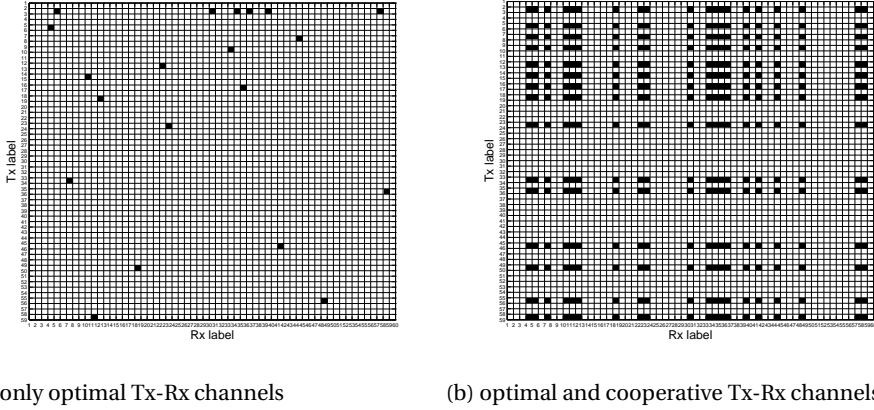


Figure 5.3: Selected Tx-Rx channels of bistatic cooperative radar network from preselected Tx/Rx grids ( $L_t = 15$ ,  $L_r = 20$ ;  $N_t = 58$ ,  $N_r = 59$ ).

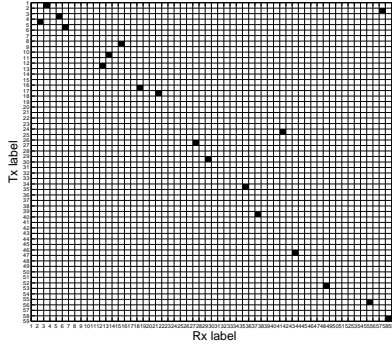
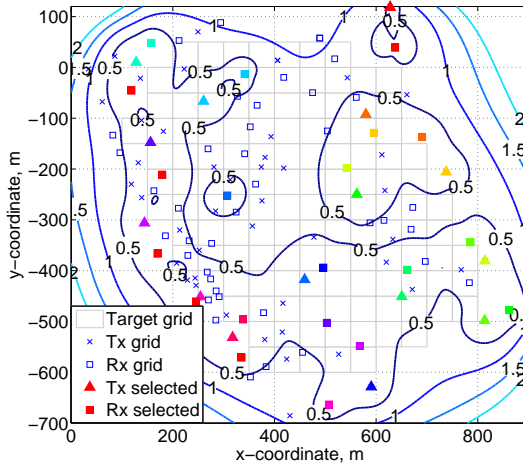


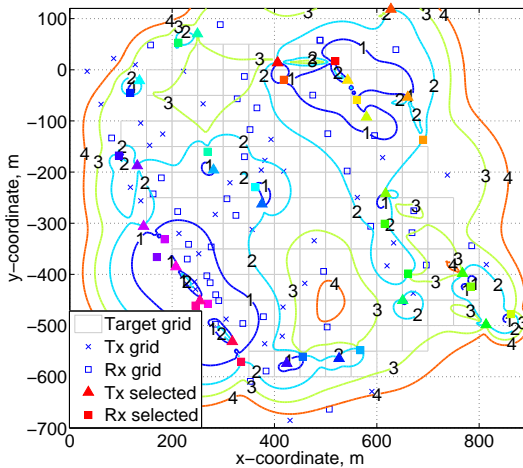
Figure 5.4: Selected Tx-Rx channels in bistatic autonomous radar network from preselected Tx/Rx grids ( $L_t = L_r = 20$ ;  $N_t = 58$ ,  $N_r = 59$ ).

### 5.3.2. SCENARIO WITH COINCIDENTAL TRANSMIT AND RECEIVE RADAR GRIDS

In the previous scenario with preselected Tx-Rx grids, sets  $\mathcal{N}_t$  and  $\mathcal{N}_r$  of the potential radar node positions have been defined such that they are not equal to each other. This simplifies the selection task, because the trade-off of devoting a particular position either to transmission or reception does not have to be made. However, in some scenarios, the decision to devote a particular location either to transmission or reception has to be made, avoiding selection of monostatic radar architecture. In this scenario, we have  $\mathcal{N}_t = \mathcal{N}_r = \mathcal{N}$  and  $|\mathcal{N}_t| = |\mathcal{N}_r| = |\mathcal{N}| = 117$  (Fig. 5.1b). Although both convex and greedy optimization algorithms can be used for bistatic radar network topology optimization, the convex algorithm does not provide a desired topology selection, resulting in a collocated radar architecture as shown in Fig. 5.6a, where 15 collocated radars are



(a) cooperative mode,  $L_t = 15$  and  $L_r = 20$ .



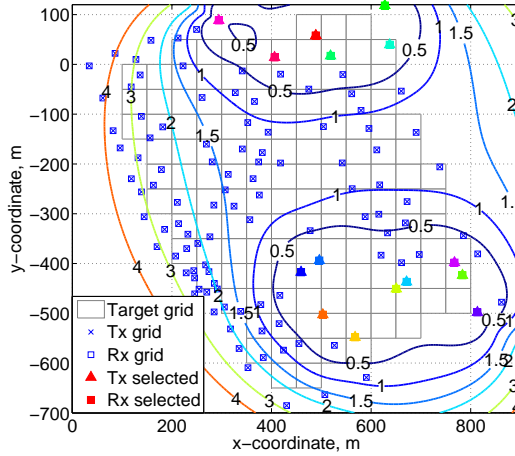
(b) autonomous mode,  $L_t = L_r = 20$

Figure 5.5: Contour plots of the target localization error ( $\sigma_p$ , m) in bistatic radar networks, where potential positions of the nodes have been preselected.

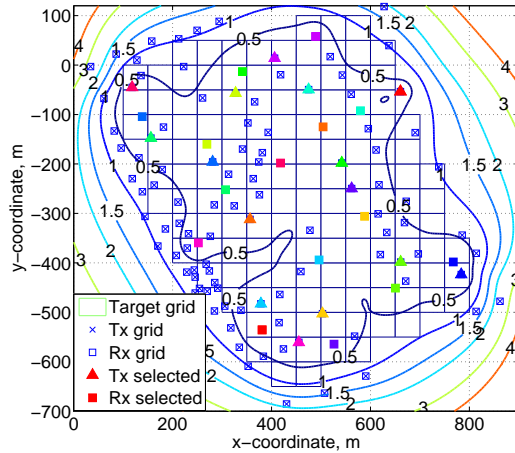
selected.

In contrast to the convex algorithm, the greedy algorithm allows for bistatic radar selection with widely separated transmit and receive radar nodes from the same sets of Tx/Rx grids (Fig. 5.6b). This is realized by iterative removal of corresponding measurements from the measurement matrix. As was shown in Chapter 3, such a network with widely separated Tx and Rx radar nodes results in higher system estimation

accuracy than the network with collocated radars, like the one selected with the convex algorithm. For the considered scenario, this is demonstrated as well in Fig. 5.6.



(a) convex minimization of  $\lambda_{\max}$  (cooperative mode)



(b) greedy minimization of LD (cooperative mode)

Figure 5.6: Contour plots of the target localization error ( $\sigma_p$ , m) in bistatic radar networks with positions, selected from overlapping grids ( $L_t = L_r = 15$ ).

Next, we compare performance of convex and greedy topology optimization algorithms for a bistatic radar network at a different number of Tx-Rx channels. Performance of these algorithms are compared for coincidental transmit and receive radar grids, which are shown in Fig. 5.1b. Both convex and greedy optimization algorithms for bistatic radar network topology optimization can be found in Chapter 4.

Averaged error of target localization over  $M = 171$  points of potential target locations for topology of bistatic radar networks selected with two algorithms is shown in Fig. 5.7. As one can see, the greedy optimization algorithm outperforms the convex one, resulting in lower localization error.

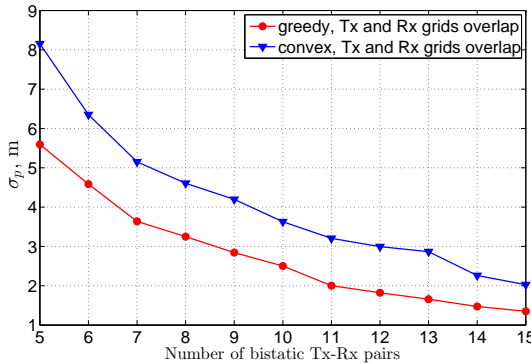


Figure 5.7: Target localization error in bistatic radar networks (cooperative mode) with positions, selected by greedy and convex optimization algorithms with LD and  $\lambda_{\max}$  cost functions respectively.

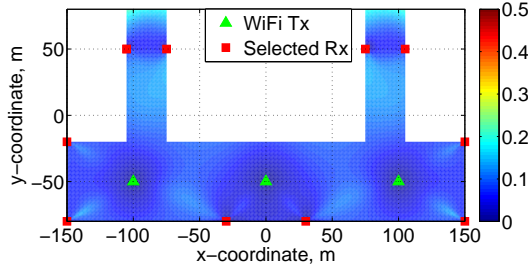
## 5.4. RECEIVERS TOPOLOGY SELECTION IN PASSIVE BISTATIC RADAR NETWORK

As has been demonstrated in Chapter 2, the use of the signals from transmitters of opportunity (by integrating dedicated receivers) leads to higher estimation accuracy of the system without increasing the number of active radars. In this section, the applicability of optimization algorithm for receiver topology optimization in a passive bistatic and a passive combined with active radar network is demonstrated. The scenario of the airport terminal area with 42 candidate radar node positions is considered in this section (5.1c). *Note:* signal blockage in the considered indoor scenario is not considered in this model.

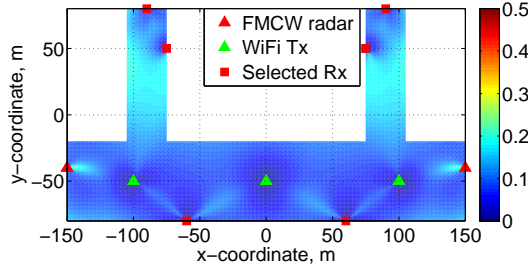
The distribution of position estimation error for two types of networks with fixed positions of WiFi transmitters, FMCW radars and selected positions of WiFi receivers is shown in Fig. 5.8. An optimization was performed with the convex algorithm based on  $\lambda_{\max}$  minimization. When comparing two plots, Fig. 5.8a and Fig. 5.8b, one can see that four additional receiving nodes are enough to achieve the same accuracy as with two active radars in the system.

## 5.5. COMPARISON OF THE COST FUNCTIONS AND OPTIMIZATION ALGORITHMS

In this section, we compare convex and greedy optimization algorithms in terms of error of target localization. The scenario of the TU Delft campus, represented by a non-uniform radar grid with  $N = 117$  potential positions of the radar nodes, is



(a) WiFi-based bistatic radars



(b) WiFi-based bistatic and FMCW monostatic radars

Figure 5.8: Distribution of the target localization error ( $\sigma_p$ , m).

considered here (Fig. 5.1b). Equal values of the weights on the grid points from the parameter space, i.e.,  $p_m = 1/M$ , are used here.

Three performance metrics are compared: the frame potential, the log-determinant, and the maximum eigenvalue of the error covariance matrix ( $\lambda_{\max}$ ). While the first two costs are optimized using a greedy approach, the third one,  $\lambda_{\max}$ , is exploited in the convex optimization algorithm. The dependence of the average target localization error on the number of selected radars  $L$  for the three costs is shown in Fig. 5.9. The LD cost function leads to more favorable radar network geometries in terms of average target localization error, compared to the FP. Moreover, it allows for better or equivalent estimation accuracy, compared to the  $\lambda_{\max}$ -driven optimization. Additionally, the linear complexity of the greedy algorithms in terms of  $N$  signifies the advantage of the LD over other cost functions. The overlap of the curves for a large  $L$  is caused by the high density of the radar grid relative to the size of the target area.

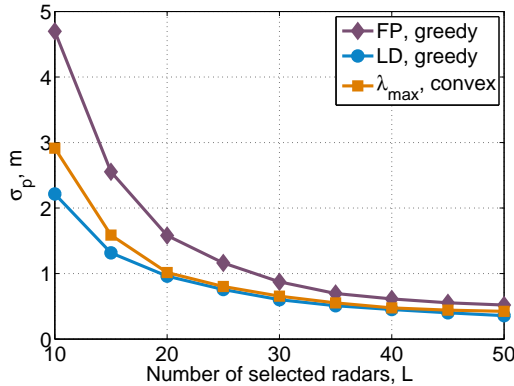


Figure 5.9: Average error of the target localization for different numbers of optimally placed radars  $L$  from the  $N = 117$  available ones for the  $K = 2$  parameters under estimation and the  $M = 171$  grid points for the parameter space.

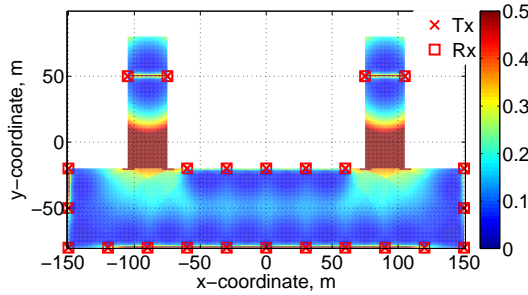
## 5.6. TOPOLOGY OPTIMIZATION TAKING INTO ACCOUNT SIGNAL BLOCKAGE

In this section, we consider the scenario of the indoor target localization in the airport terminal area with 42 potential positions of radar nodes (Fig. 5.1c). Antenna radiation patterns of the radars are assumed to be omnidirectional. The optimal radar node positions were selected by convex minimization of  $\lambda_{\max}$  cost with and without taking into account signal blockage in the indoor scenario. In order to take into account signal blockage, the same approach that has been proposed in Chapter 2 for antenna pattern incorporation, was used here. Optimization has been performed for the maximum value of the localization error  $R_e = 0,5$  m with probability  $P_e = 95\%$ . The distribution of the error of target localization is shown in Fig. 5.10. Apparently, when signal blockage is not taken into account in the optimization procedure, the selected radar network geometry would not provide full coverage of the area of interest as shown in Fig. 5.10a. In contrast to this, optimization taking into account signal blockage naturally results in the radar network geometry that provides full coverage of the target areas in indoor scenarios (Fig. 5.10b).

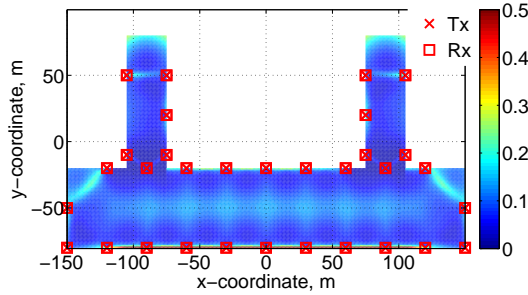
## 5.7. CONCLUSION

In this chapter, the developed optimization framework has been applied for the best radar network topology selection in different scenarios. The scenarios mainly differ in radar operational range, architecture, reception mode and model of candidate radar positions. In particular, it has been shown that taking into account the cooperative mode of signal transmission-reception allows a smaller number of nodes to be selected in order to satisfy the same accuracy constraints.

It was shown that taking into account signal blockage in the indoor scenario results in a network topology that provides full coverage of the surveillance area in terms of



(a) positions of the radar nodes were selected without taking into account signal blockage



(b) positions of the radar nodes were selected taking into account signal blockage

Figure 5.10: Distribution of the error of target localization ( $\sigma_p, m$ ).

required system estimation accuracy. And vice versa, without taking signal blockage into account, the selected radar network geometry will not fully cover the target area due to signal blockage effects inherent to indoor scenarios. It has been demonstrated that greedy optimization outperforms the convex one in the bistatic radar topology selection with coinciding grids. This is reflected in the fact that convex optimization results in a monostatic (quasi-bistatic) radar architecture, instead of a bistatic one. This leads to the lower estimation accuracy, compared to the bistatic radar network topology selected with the greedy algorithm. Moreover, the greedy algorithm with log-determinant minimization provides the network topology that results in the lowest estimation error, compared to the greedy minimization of frame potential and convex minimization of maximum eigenvalue of the covariance matrix. Taking into account that

greedy algorithms scale linearly in the dimension of the problem, it is recommended to use them for topology optimization, considering the advantages mentioned above.

## REFERENCES

- [1] I. Ivashko, O. Krasnov, and A. Yarovoy, *Receivers topology optimization of the combined active and WiFi-based passive radar network*, in *European Microwave Conference (EuMC), 2014 11th* (2014) pp. 1820–1823.
- [2] I. Ivashko, O. Krasnov, and A. Yarovoy, *Topology optimization of monostatic radar networks with wide-beam antennas*, in *European Microwave Conference (EuMC), 2015 12th* (2015).
- [3] I. Ivashko, G. Leus, and A. Yarovoy, *Radar network topology optimization for joint target position and velocity estimation*, *Signal Processing* **130**, 279 (2017).
- [4] *Waar staan de GSM en UMTS masten in Nederland?* <http://www.gsmmasten.nl>, accessed: 2015-03-19.



# 6

## CONCLUSIONS AND FUTURE WORK

*This chapter summarizes the main results and novelties of the thesis followed by recommendations for future work.*

## 6.1. MAJOR RESULTS AND NOVELTIES

RECENT experimental and theoretical results justify a wide spectrum of applications, where data from widely separated radar nodes are used in order to provide reliable and cost-effective surveillance solutions over extended areas. Regardless of the type of the radar network, its performance is drastically affected by the number of nodes and their topology. Standard and intuitive solutions that imply symmetrical and balanced topology of the nodes often cannot be applied to real operational environments, which are encumbered with objects of different origin. Thus, the development of a generic resource allocation tool that provide a user-oriented solutions in the system design stage became the goal of this thesis.

The major focus of this thesis covers two mutually connected areas:

1. the development of the tool for assessment of potential accuracy of target parameters estimation in radar networks;
2. the development of the generic framework for accuracy-driven radar network topology optimization.

In addition, the question of data association in radar networks has been studied. The following results have been achieved within the framework of this thesis:

1. *Lower bounds on the target position and velocity estimation accuracy in radar networks.* Closed-form expressions of the errors of target position and velocity estimation in active (LFM waveform) and passive (WiFi waveform) radars were derived using Cramér-Rao lower bound. Beside waveform parameters, a power budget, including antenna radiation patterns of a single radar, was incorporated into the CRLB. The ranging accuracy of the single radar was shown to be inversely proportional to the signal bandwidth, while the radial velocity estimation accuracy is inversely proportional to the integration time. The radar antenna pattern has been incorporated into the CRLB analysis for the first time. It has been shown that areas of high and low estimation accuracy are mainly determined by the antenna pattern of each radar node. It has been demonstrated that a similar approach can be used effectively for taking into account effects of radar beam blockage and consequently can be used for radar management during the deployment and run-time phases. Incorporation of the antenna pattern significantly improve qualitative analysis of the potential estimation accuracy that can be achieved in radar network, allowing for representation of the areas of (common) illumination as well as non-illuminated areas. Moreover, possibility to incorporate type of a single radar architecture, its waveform and power budget parameters, as well as mode of the signal reception forms versatile analysis tool that can be further upgraded.
2. *Analysis of the estimation accuracy of kinematic target data in radar networks of different types.* CRLB-based analysis of the radar networks versus a single radar node (waveform, power budget, architecture) and network parameters (transmitter type, cooperation mode, measurement model) was done. It has been shown that the cooperative mode of signal reception increases the estimation

accuracy by up to 40% compared to the autonomous mode. It has been found that both bistatic and monostatic radar networks with an autonomous mode of signal reception provide equivalent accuracy of the target parameters estimation. Comparison of the target localization accuracy achieved with different types of measurements has been made for the first time. It was shown that given the same number of radars, target localization accuracy achieved with range measurements (both high and low resolution) is higher than with Doppler shift measurements. At the same time, usage of Doppler information together with range information, in narrow band radars (with waveform bandwidth in the order of 50 MHz), allows for 20–25% improvement in the localization accuracy. Presented results of numerical analysis show impact of different parameters of radar network on its estimation accuracy. The results demonstrate possibility to enhance estimation accuracy of the network with fixed number of nodes by exploiting resources of a single radar node or by using another type of measurements.

3. *Methodology for radar network topology optimization.* Novel convex and greedy algorithms were developed for radar network topology optimization. Three cost functions were derived: the frame potential, the log-determinant and the minimum eigenvalue, with the last two being scalar functions of the error covariance matrix. The developed theoretical framework incorporates single radar parameters and network type. In particular, a solution for the structural selection problem that arises in bistatic radar networks has been developed. It has been shown that greedy minimization of LD cost allows for better performance than the convex minimization of  $\lambda_{\max}$  in terms of error of target parameters estimation. Moreover, greedy optimization outperforms the convex one for the task of bistatic radar topology selection, allowing selection of bistatic radar architecture. This is not the case for convex optimization that results in a monostatic radar architecture. The developed tools can be used for large-scale radar network topology optimization during the deployment phase, including selecting the number of radar nodes required to achieve the required operational performance. This potential has been illustrated in three case studies: low airspace surveillance in The Hague, low airspace surveillance at the TU Delft campus, and passenger surveillance in an airport terminal.
4. *Data association algorithm.* A novel data association algorithm for multiple target localization, based on range measurements in a single moment of time was developed. The algorithm performance has been tested for different topologies of the radar networks, different values of a single radar node resolution, number of targets, and their locations with respect to the radars. For scenarios when targets are located far away from each other, the number of incorrect associations is approximately 40% less, compared to the scenarios when targets are located closely together. It has been shown that system performance can be improved by increasing a single radar node resolution: a two times higher resolution leads to 50% fewer ghosts. Thus, the results obtained provide extra information in the form of potential constraints for the radar network topology selection.

## 6.2. RECOMMENDATIONS FOR FUTURE WORK

The research presented in this thesis triggers new research questions and identifies directions for further investigation. The detailed recommendations for future work as a continuation of this study are as follows:

1. *Localization accuracy enhancement by adding more measurements.* In Chapter 3, it has been demonstrated that use of the Doppler shift measurements together with time delay measurements in the network of narrow band radars provides higher localization accuracy than each type of measurement alone. An interesting direction for further investigation would be to analyze radar network localization performance by adding other types of measurements, like angle of arrival or time integration (integration of several measurements obtained from the target at different times), if available. It was shown that addition of these types of measurements to the standard time difference of arrival measurements improves localization accuracy of mode S distributed sensor networks [1].
2. *Radar network topology optimization using other cost functions.* The developed optimization framework in Chapter 4, aims to select radar network topology that ensures prescribed estimation accuracy requirements. Other system performance measures like probability of detection, ambiguity function, and accurate target tracking can be considered as well [2], [3], [4].
3. *Waveform bandwidth constraint in the optimization algorithm.* In Chapter 3, it has been discussed that in order to filter out or separate signals from (non) cooperative transmitters, frequency orthogonality can be applied. Therefore, it would be useful to introduce constraint on the signal bandwidth of a single radar node that depends on the number of selected radars.
4. *Data association algorithm with target detection probability.* The developed data association algorithm for multiple targets localization, presented in Appendix B, assumes that all targets in the scene are detected in each of the radar nodes. The incorporation of the target detection probability will affect the performance of the data association algorithm and may lead to a twofold outcome and therefore, would be interesting to investigate. On one hand, the number of measurements from one target will decrease, which may deteriorate the algorithm performance as has been demonstrated for different numbers of the radar nodes. On the other hand, computational complexity of the algorithm may decrease due to a smaller number of measurement combinations.
5. *Data association algorithm for wide-beam directional radar antennas.* The efficiency of the the developed data association algorithm has been demonstrated for networks of radars that employ omnidirectional antennas. This assumption implies more misleading data associations, i.e. ghost targets, due to multiple intersection points of the ranging spheres. The incorporation of the radar antenna directivity will lead to a smaller number of intersection points, and thus to a smaller number of unresolved measurements. At the same time, some targets

might not be covered by all the radars of the network, which will deteriorate the algorithm performance.

## REFERENCES

- [1] G. Galati, M. Leonardi, I. Mantilla-Gaviria, and M. Tosti, *Lower bounds of accuracy for enhanced mode-S distributed sensor networks*, Radar, Sonar Navigation, IET **6**, 190 (2012).
- [2] A. K. Gostar, R. Hoseinnezhad, and A. Bab-Hadiashar, *Robust multi-bernoulli sensor selection for multi-target tracking in sensor networks*, IEEE Signal Processing Letters **20**, 1167 (2013).
- [3] W. Wang, Y. Liang, E. P. Xing, and L. Shen, *Nonparametric decentralized detection and sparse sensor selection via weighted kernel*, IEEE Transactions on Signal Processing **64**, 306 (2016).
- [4] F. Arlery, R. Kassab, U. Tan, and F. Lehmann, *Efficient optimization of the ambiguity functions of multi-static radar waveforms*, in *17th International Radar Symposium 2016 (IRS 2016)* (2016) pp. 1–5.



# A

## THE EVALUATION OF FRAME POTENTIAL AND LOG-DETERMINANT COSTS

*In this appendix, the closed-form expressions for the evaluation of frame potential and log-determinant cost functions are provided. First, the estimation performance of the target range and radial velocity of a single FMCW radar is evaluated. Next, the guidelines for FP and LD evaluation based on a single radar performance is provided.*

### A.1. THE PERFORMANCE OF A SINGLE FMCW RADAR

ASSUMING a fixed sampling frequency that results in  $Q$  accumulated signal samples per integration time  $DT_s$  in each radar, the measurement model for a single radar is then given by (2.1) for  $N = 1$  ( $\mathcal{N} = \{1\}$ ). We linearize the noiseless signal  $\mathbf{f}(\boldsymbol{\alpha}_m)$  around the parameter vector  $\boldsymbol{\beta}_m = [\beta_{m,1}, \beta_{m,2}]^T$  with  $J = 2$  components,  $\beta_{m,1} = \tau_m$  and  $\beta_{m,2} = \omega_{d_m}$ . The matrix  $\mathbf{G}_m^{(1)} \in \mathbb{R}^{Q \times J}$  is then given by  $[\mathbf{G}_m^{(1)}]_{q,j} = \frac{\partial f_q(\boldsymbol{\alpha}_m)}{\partial \beta_{m,j}} \frac{1}{\sqrt{w_{m,j}}}$  ( $j = 1, \dots, J$ ) with

$$\begin{aligned} \frac{\partial f_q(\boldsymbol{\alpha}_m)}{\partial \beta_{m,1}} &= -j|A_m^{(1)}| \left[ \omega_c + 2\text{frac}\left(\frac{t_q - \tau_m^{(1)}}{T_s}\right) \Delta\omega - \omega_{d_m}^{(1)} \right] \\ &\quad \times e^{j(t_q - \tau_m^{(1)})} \left[ \omega_c + \text{frac}\left(\frac{t_q - \tau_m^{(1)}}{T_s}\right) \Delta\omega - \omega_{d_m}^{(1)} \right] + j\varphi_m^{(1)}; \\ \frac{\partial f_q(\boldsymbol{\alpha}_m)}{\partial \beta_{m,2}} &= -j|A_m^{(1)}| \left( t_q - \tau_m^{(1)} \right) e^{j(t_q - \tau_m^{(1)})} \left[ \omega_c + \text{frac}\left(\frac{t_q - \tau_m^{(1)}}{T_s}\right) \Delta\omega - \omega_{d_m}^{(1)} \right] + j\varphi_m^{(1)}. \end{aligned}$$

We define the performance of a single radar that characterizes the estimation accuracy of the time delay and Doppler frequency of the signal, reflected from the target represented by the  $m$ th grid point from the parameter space, as

$$P_m^{(1)} = \text{tr}\{\mathbf{G}_m^{(1)} \mathbf{G}_m^{(1)\dagger}\} = P_m^{(1)}(\tau) + P_m^{(1)}(\omega_d) + 2P_m^{(1)}(\tau, \omega_d), \quad (\text{A.1})$$

where

$$\begin{aligned} P_m^{(1)}(\tau) &= \frac{1}{w_{m,1}} \sum_{q=1}^Q \frac{\partial f_q(\boldsymbol{\alpha}_m)}{\partial \tau_m^{(1)}} \frac{\partial f_q^*(\boldsymbol{\alpha}_m)}{\partial \tau_m^{(1)}} = \frac{4}{3} \frac{1}{w_{m,1}} \Delta\omega^2 |A_m^{(1)}|^2 Q; \\ P_m^{(1)}(\omega_d) &= \frac{1}{w_{m,2}} \sum_{q=1}^Q \frac{\partial f_q(\boldsymbol{\alpha}_m)}{\partial \omega_{d_m}^{(1)}} \frac{\partial f_q^*(\boldsymbol{\alpha}_m)}{\partial \omega_{d_m}^{(1)}} = \frac{1}{3} \frac{1}{w_{m,2}} T_s^2 D^2 |A_m^{(1)}|^2 Q; \\ P_m^{(1)}(\tau, \omega_d) &= \frac{1}{\sqrt{w_{m,1} w_{m,2}}} \sum_{q=1}^Q \frac{\partial f_q(\boldsymbol{\alpha}_m)}{\partial \tau_m^{(1)}} \frac{\partial f_q^*(\boldsymbol{\alpha}_m)}{\partial \omega_{d_m}^{(1)}} = \frac{1}{\sqrt{w_{m,1} w_{m,2}}} \Delta\omega D T_s |A_m^{(1)}|^2 Q; \end{aligned} \quad (\text{A.2})$$

with  $w_{m,1}$  and  $w_{m,2}$  being the weighting coefficients.

#### A.1.1. THE FP AND THE LD COST FUNCTIONS FOR AN FMCW RADAR NETWORK

The measurement model for the radar network is given by (2.1). The parameter vector is the target state vector that contains two different modalities: target position and velocity. Thus, we define  $\tilde{\boldsymbol{\alpha}}_m = [\sqrt{w_{1,m}} \boldsymbol{\alpha}_{m,1}, \sqrt{w_{2,m}} \boldsymbol{\alpha}_{m,2}]^T$ , where  $\boldsymbol{\alpha}_{m,1} = [x_m, y_m, z_m]^T$  and  $\boldsymbol{\alpha}_{m,2} = [v_{x_m}, v_{y_m}, v_{z_m}]^T$  with  $K_1 = 3$  and  $K_2 = 3$  components, respectively. The weighted linear system matrix  $\tilde{\mathbf{G}}_m^{(\mathcal{N})} \in \mathbb{R}^{NQ \times (K_1 + K_2)}$  consists of two submatrices  $\mathbf{G}_{m,1}^{(\mathcal{N})}$  and  $\mathbf{G}_{m,2}^{(\mathcal{N})}$ , which are defined as

$$[\mathbf{G}_{m,1}^{(\mathcal{N})}]_{(n-1)Q+q,d} = \frac{\partial f_{(n-1)Q+q}(\tilde{\boldsymbol{\alpha}}_m)}{\partial \beta_{m,1}} \frac{\partial \beta_{m,1}}{\partial [\boldsymbol{\alpha}_{m,1}]_d} \frac{1}{\sqrt{w_{m,1}}} + \frac{\partial f_{(n-1)Q+q}(\tilde{\boldsymbol{\alpha}}_m)}{\partial \beta_{m,2}} \frac{\partial \beta_{m,2}}{\partial [\boldsymbol{\alpha}_{m,1}]_d} \frac{1}{\sqrt{w_{m,2}}};$$

$$[\mathbf{G}_{m,2}^{(\mathcal{N})}]_{(n-1)Q+q,b} = \frac{\partial f_{(n-1)Q+q}(\tilde{\boldsymbol{\alpha}}_m)}{\partial \beta_{m,2}} \frac{\partial \beta_{m,2}}{\partial [\boldsymbol{\alpha}_{m,2}]_b} \frac{1}{\sqrt{w_{m,2}}};$$

with  $d = 1, \dots, K_1$  and  $b = 1, \dots, K_2$ .

The LD and the FP for the FMCW radar network can then be evaluated as

$$\text{LD}(\mathcal{L}) = \sum_{m=1}^M p_m \left( \log \det \left( \sum_{i \in \mathcal{L}} \mathbf{T}_m^{(i)} + \epsilon \mathbf{I}_K \right)^{-1} + K \log \epsilon \right), \quad (\text{A.3})$$

$$\text{FP}(\mathcal{L}) = \sum_{m=1}^M p_m \sum_{i,j \in \mathcal{L}} \mathbf{s}_m^{(i,j)}, \quad (\text{A.4})$$

where  $\mathbf{T}_m^{(i)} = \tilde{\mathbf{G}}_m^{(i)\dagger} \tilde{\mathbf{G}}_m^{(i)}$ ,  $\mathbf{s}_m^{(i,j)} = \sum_{n=1, l=1}^K [\mathbf{T}_m^{(i)}]_{n,l} [\mathbf{T}_m^{(j)}]_{n,l}$ . The closed-form expressions for the entries of the matrix  $\mathbf{T}_m^{(i)}$  are provided in the following section.

## A.2. THE EVALUATION OF THE FP AND LD IN (A.4) AND (A.3)

The matrix  $\mathbf{T}_m^{(i)} = \tilde{\mathbf{G}}_m^{(i)\dagger} \tilde{\mathbf{G}}_m^{(i)}$  with  $\tilde{\mathbf{G}}_m^{(i)} = \left[ \frac{1}{\sqrt{w_{m,1}}} \mathbf{G}_{m,1}^{(i)}, \frac{1}{\sqrt{w_{m,2}}} \mathbf{G}_{m,2}^{(i)} \right]$  is the weighted linear system matrix in the scenario of (multi-modal) target state vector estimation. The matrices  $\mathbf{G}_{m,1}^{(i)} \in \mathbb{R}^{Q \times K_1}$  and  $\mathbf{G}_{m,2}^{(i)} \in \mathbb{R}^{Q \times K_2}$  are defined as  $[\mathbf{G}_{m,1}^{(i)}]_{q,d} = \frac{\partial f_q(\tilde{\boldsymbol{\alpha}}_m)}{\partial \beta_{m,1}} \frac{\partial \beta_{m,1}}{\partial [\boldsymbol{\alpha}_{m,1}]_d} \frac{1}{\sqrt{w_{m,1}}} + \frac{\partial f_q(\tilde{\boldsymbol{\alpha}}_m)}{\partial \beta_{m,2}} \frac{\partial \beta_{m,2}}{\partial [\boldsymbol{\alpha}_{m,1}]_d} \frac{1}{\sqrt{w_{m,2}}}$  and  $[\mathbf{G}_{m,2}^{(i)}]_{q,b} = \frac{\partial f_q(\tilde{\boldsymbol{\alpha}}_m)}{\partial \beta_{m,2}} \frac{\partial \beta_{m,2}}{\partial [\boldsymbol{\alpha}_{m,2}]_b} \frac{1}{\sqrt{w_{m,2}}}$  with  $d = 1, \dots, K_1$  and  $b = 1, \dots, K_2$ . The parameter vector is  $\tilde{\boldsymbol{\alpha}}_m = \left[ \sqrt{w_{m,1}} \boldsymbol{\alpha}_{m,1}, \sqrt{w_{m,2}} \boldsymbol{\alpha}_{m,2} \right]^T$  with  $\boldsymbol{\alpha}_{m,1} = [x_m, y_m, z_m]^T$  and  $\boldsymbol{\alpha}_{m,2} = [v_{x_m}, v_{y_m}, v_{z_m}]^T$ .

The matrix  $\mathbf{T}_m^{(i)}$  can be then evaluated as

$$[\mathbf{T}_m^{(i)}]_{11} = P_m^{(i)}(\tau) \left( \frac{\partial \tau_m^{(i)}}{\partial x_m} \right)^2 + P_m^{(i)}(\omega_d) \left( \frac{\partial \omega_{d_m}^{(i)}}{\partial x_m} \right)^2 + 2P_m^{(i)}(\tau, \omega_d) \frac{\partial \tau_m^{(i)}}{\partial x_m} \frac{\partial \omega_{d_m}^{(i)}}{\partial x_m};$$

$$\begin{aligned} [\mathbf{T}_m^{(i)}]_{12} = [\mathbf{T}_m^{(i)}]_{21} &= P_m^{(i)}(\tau) \frac{\partial \tau_m^{(i)}}{\partial x_m} \frac{\partial \tau_m^{(i)}}{\partial y_m} + P_m^{(i)}(\tau, \omega_d) \frac{\partial \tau_m^{(i)}}{\partial x_m} \frac{\partial \omega_{d_m}^{(i)}}{\partial y_m} \\ &+ P_m^{(i)}(\tau, \omega_d) \frac{\partial \tau_m^{(i)}}{\partial y_m} \frac{\partial \omega_{d_m}^{(i)}}{\partial x_m} + P_m^{(i)}(\omega_d) \frac{\partial \omega_{d_m}^{(i)}}{\partial x_m} \frac{\partial \omega_{d_m}^{(i)}}{\partial y_m}; \end{aligned}$$

$$\begin{aligned} [\mathbf{T}_m^{(i)}]_{13} = [\mathbf{T}_m^{(i)}]_{31} &= P_m^{(i)}(\tau) \frac{\partial \tau_m^{(i)}}{\partial x_m} \frac{\partial \tau_m^{(i)}}{\partial z_m} + P_m^{(i)}(\tau, \omega_d) \frac{\partial \tau_m^{(i)}}{\partial x_m} \frac{\partial \omega_{d_m}^{(i)}}{\partial z_m} \\ &+ P_m^{(i)}(\tau, \omega_d) \frac{\partial \tau_m^{(i)}}{\partial z_m} \frac{\partial \omega_{d_m}^{(i)}}{\partial x_m} + P_m^{(i)}(\omega_d) \frac{\partial \omega_{d_m}^{(i)}}{\partial x_m} \frac{\partial \omega_{d_m}^{(i)}}{\partial z_m}; \end{aligned}$$

$$[\mathbf{T}_m^{(i)}]_{14} = [\mathbf{T}_m^{(i)}]_{41} = P_m^{(i)}(\tau, \omega_d) \frac{\partial \tau_m^{(i)}}{\partial x_m} \frac{\partial \omega_{d_m}^{(i)}}{\partial v_{x_m}} + P_m^{(i)}(\omega_d) \frac{\partial \omega_{d_m}^{(i)}}{\partial x_m} \frac{\partial \omega_{d_m}^{(i)}}{\partial v_{x_m}};$$

A

$$[\mathbf{T}_m^{(i)}]_{15} = [\mathbf{T}_m^{(i)}]_{51} = P_m^{(i)}(\tau, \omega_d) \frac{\partial \tau_m^{(i)}}{\partial x_m} \frac{\partial \omega_{d_m}^{(i)}}{\partial v_{y_m}} + P_m^{(i)}(\omega_d) \frac{\partial \omega_{d_m}^{(i)}}{\partial x_m} \frac{\partial \omega_{d_m}^{(i)}}{\partial v_{y_m}};$$

$$[\mathbf{T}_m^{(i)}]_{16} = [\mathbf{T}_m^{(i)}]_{61} = P_m^{(i)}(\tau, \omega_d) \frac{\partial \tau_m^{(i)}}{\partial x_m} \frac{\partial \omega_{d_m}^{(i)}}{\partial v_{z_m}} + P_m^{(i)}(\omega_d) \frac{\partial \omega_{d_m}^{(i)}}{\partial x_m} \frac{\partial \omega_{d_m}^{(i)}}{\partial v_{z_m}};$$

$$[\mathbf{T}_m^{(i)}]_{22} = P_m^{(i)}(\tau) \left( \frac{\partial \tau_m^{(i)}}{\partial y_m} \right)^2 + 2P_m^{(i)}(\tau, \omega_d) \frac{\partial \tau_m^{(i)}}{\partial y_m} \frac{\partial \omega_{d_m}^{(i)}}{\partial y_m} + P_m^{(i)}(\omega_d) \left( \frac{\partial \omega_{d_m}^{(i)}}{\partial y_m} \right)^2;$$

$$\begin{aligned} [\mathbf{T}_m^{(i)}]_{23} = [\mathbf{T}_m^{(i)}]_{32} &= P_m^{(i)}(\tau) \frac{\partial \tau_m^{(i)}}{\partial y_m} \frac{\partial \tau_m^{(i)}}{\partial z_m} + P_m^{(i)}(\tau, \omega_d) \frac{\partial \tau_m^{(i)}}{\partial y_m} \frac{\partial \omega_{d_m}^{(i)}}{\partial z_m} \\ &+ P_m^{(i)}(\tau, \omega_d) \frac{\partial \tau_m^{(i)}}{\partial z_m} \frac{\partial \omega_{d_m}^{(i)}}{\partial y_m} + P_m^{(i)}(\omega_d) \frac{\partial \omega_{d_m}^{(i)}}{\partial y_m} \frac{\partial \omega_{d_m}^{(i)}}{\partial z_m}; \end{aligned}$$

$$[\mathbf{T}_m^{(i)}]_{24} = [\mathbf{T}_m^{(i)}]_{42} = P_m^{(i)}(\tau, \omega_d) \frac{\partial \tau_m^{(i)}}{\partial y_m} \frac{\partial \omega_{d_m}^{(i)}}{\partial v_{x_m}} + P_m^{(i)}(\omega_d) \frac{\partial \omega_{d_m}^{(i)}}{\partial y_m} \frac{\partial \omega_{d_m}^{(i)}}{\partial v_{x_m}};$$

$$[\mathbf{T}_m^{(i)}]_{25} = [\mathbf{T}_m^{(i)}]_{52} = P_m^{(i)}(\tau, \omega_d) \frac{\partial \tau_m^{(i)}}{\partial y_m} \frac{\partial \omega_{d_m}^{(i)}}{\partial v_{y_m}} + P_m^{(i)}(\omega_d) \frac{\partial \omega_{d_m}^{(i)}}{\partial y_m} \frac{\partial \omega_{d_m}^{(i)}}{\partial v_{y_m}};$$

$$[\mathbf{T}_m^{(i)}]_{26} = [\mathbf{T}_m^{(i)}]_{62} = P_m^{(i)}(\tau, \omega_d) \frac{\partial \tau_m^{(i)}}{\partial y_m} \frac{\partial \omega_{d_m}^{(i)}}{\partial v_{z_m}} + P_m^{(i)}(\omega_d) \frac{\partial \omega_{d_m}^{(i)}}{\partial y_m} \frac{\partial \omega_{d_m}^{(i)}}{\partial v_{z_m}};$$

$$[\mathbf{T}_m^{(i)}]_{33} = P_m^{(i)}(\tau) \left( \frac{\partial \tau_m^{(i)}}{\partial z_m} \right)^2 + 2P_m^{(i)}(\tau, \omega_d) \frac{\partial \tau_m^{(i)}}{\partial z_m} \frac{\partial \omega_{d_m}^{(i)}}{\partial z_m} + P_m^{(i)}(\omega_d) \left( \frac{\partial \omega_{d_m}^{(i)}}{\partial z_m} \right)^2;$$

$$[\mathbf{T}_m^{(i)}]_{34} = [\mathbf{T}_m^{(i)}]_{43} = P_m^{(i)}(\tau, \omega_d) \frac{\partial \tau_m^{(i)}}{\partial z_m} \frac{\partial \omega_{d_m}^{(i)}}{\partial v_{x_m}} + P_m^{(i)}(\omega_d) \frac{\partial \omega_{d_m}^{(i)}}{\partial z_m} \frac{\partial \omega_{d_m}^{(i)}}{\partial v_{x_m}};$$

$$[\mathbf{T}_m^{(i)}]_{35} = [\mathbf{T}_m^{(i)}]_{53} = P_m^{(i)}(\tau, \omega_d) \frac{\partial \tau_m^{(i)}}{\partial z_m} \frac{\partial \omega_{d_m}^{(i)}}{\partial v_{y_m}} + P_m^{(i)}(\omega_d) \frac{\partial \omega_{d_m}^{(i)}}{\partial z_m} \frac{\partial \omega_{d_m}^{(i)}}{\partial v_{y_m}};$$

$$[\mathbf{T}_m^{(i)}]_{36} = [\mathbf{T}_m^{(i)}]_{63} = P_m^{(i)}(\tau, \omega_d) \frac{\partial \tau_m^{(i)}}{\partial z_m} \frac{\partial \omega_{d_m}^{(i)}}{\partial v_{z_m}} + P_m^{(i)}(\omega_d) \frac{\partial \omega_{d_m}^{(i)}}{\partial z_m} \frac{\partial \omega_{d_m}^{(i)}}{\partial v_{z_m}};$$

$$[\mathbf{T}_m^{(i)}]_{44} = P_m^{(i)}(\omega_d) \left( \frac{\partial \omega_{d_m}^{(i)}}{\partial v_{x_m}} \right)^2;$$

$$[\mathbf{T}_m^{(i)}]_{45} = [\mathbf{T}_m^{(i)}]_{54} = P_m^{(i)}(\omega_d) \frac{\partial \omega_{d_m}^{(i)}}{\partial v_{x_m}} \frac{\partial \omega_{d_m}^{(i)}}{\partial v_{y_m}};$$

$$[\mathbf{T}_m^{(i)}]_{46} = [\mathbf{T}_m^{(i)}]_{64} = P_m^{(i)}(\omega_d) \frac{\partial \omega_{d_m}^{(i)}}{\partial v_{x_m}} \frac{\partial \omega_{d_m}^{(i)}}{\partial v_{z_m}};$$

$$[\mathbf{T}_m^{(i)}]_{55} = P_m^{(i)}(\omega_d) \left( \frac{\partial \omega_{d_m}^{(i)}}{\partial v_{y_m}} \right)^2;$$

$$[\mathbf{T}_m^{(i)}]_{56} = [\mathbf{T}_m^{(i)}]_{65} = P_m^{(i)}(\omega_d) \frac{\partial \omega_{d_m}^{(i)}}{\partial v_{y_m}} \frac{\partial \omega_{d_m}^{(i)}}{\partial v_{z_m}};$$

$$[\mathbf{T}_m^{(i)}]_{66} = P_m^{(i)}(\omega_d) \left( \frac{\partial \omega_{d_m}^{(i)}}{\partial v_{z_m}} \right)^2.$$

The derivatives of the time delay and the Doppler frequency with respect to target coordinate and velocity vectors are given in (2.51) and (2.52). The matrix  $\mathbf{T}_m^{(i)}$  can be easily truncated for the scenarios, where only target position or velocity is estimated. For example, for 3D target localization based on trilateration technique, the parameter vector is  $\boldsymbol{\alpha}_m = [x_m, y_m, z_m]^T$ . The entries of the measurement matrix  $\mathbf{G}_{m,1}^{(i)} \in \mathbb{R}^{Q \times K_1}$  are then given by  $[\mathbf{G}_{m,1}^{(i)}]_{q,d} = \frac{\partial f_q(\boldsymbol{\alpha}_m)}{\partial \beta_{m,1}} \frac{\partial \beta_{m,1}}{\partial \alpha_{m,d}}$ . The matrix  $\mathbf{T}_m^{(i)} \in \mathbb{R}^{K_1 \times K_1}$  can be evaluated at  $w_{m,2} = 0$ .



# B

## THE OFF-GRID RADAR SELECTION

*Conventional topology optimization approaches are based on gridding of the areas of potential radar positions. This affects the quality of the solution, as it allows the radar nodes to be placed only on the points of the available set. In order to mitigate the effect of gridding, we use the first-order Taylor series approximation of the cost function around the radar grid points. It results in a representation of the radar area as a set of bins allowing one radar position per bin to be selected. This appendix presents an extension of the off-grid sensor selection technique to the 2D radar topology selection problem that is represented with a non-linear measurement model. Numerical results that prove the efficiency of this technique are presented thereafter. The conclusion section outlines this appendix.*

## B.1. INTRODUCTION

A common feature of most of the allocation techniques is the representation of the areas of potential radar locations with the set of grid points  $\mathcal{N}$ . Consequently, the optimality of the solution depends on how properly the set of potential radar positions  $\mathcal{N}$  is defined. As was demonstrated in [2], a fine gridding does not lead to an optimal solution in terms of spatial diversity, as it aims to select all sensor locations from one informative bin. Moreover, the computational complexity of the optimization algorithms is mainly determined by the total number of radars  $N$  ( $N = |\mathcal{N}|$  with  $|\mathcal{N}|$  being cardinality of the set  $\mathcal{N}$ ).

In this chapter, we present an extension to the continuous sensor placement (CSP) approach presented in [2] to the radar network non-linear measurement model, where optimal radar topology has to be selected in a 2D space. In order to mitigate the effect of gridding, we use the first-order Taylor series approximation of the parameter function. The CSP approach does not require fine gridding, but allows for off-grid radar selection leading to an improved solution in terms of the mean squared error.

### B.1.1. GENERAL FRAMEWORK

For the non-linear measurement model (2.1), the MSE of the least-squares estimate is equal to the Cramér-Rao lower bound and is given by

$$\text{MSE}(\boldsymbol{\alpha}_m) = \text{tr} \left\{ \left( \sum_{n=1}^N \frac{1}{(\sigma^{(n)})^2} \frac{\partial f^{(n)}}{\partial \boldsymbol{\alpha}_m} \left( \frac{\partial f^{(n)}}{\partial \boldsymbol{\alpha}_m} \right)^\dagger \right)^{-1} \right\}, \quad (\text{B.1})$$

where  $\text{tr}(\cdot)$  is the trace operator.

Using the first-order Taylor series expansion, we linearize terms  $(\partial f^{(n)} / \partial \boldsymbol{\alpha}_m)$  around every point  $(x^{(n)}, y^{(n)})$  from the set of potential radar nodes locations

$$f'_{\boldsymbol{\alpha}_m}{}^{(n)} \approx f'_{\boldsymbol{\alpha}_m}{}^{(n)} + \Delta x^{(n)} f'_{\boldsymbol{\alpha}_m x^{(n)}}{}^{(n)} + \Delta y^{(n)} f'_{\boldsymbol{\alpha}_m y^{(n)}}{}^{(n)}, \quad (\text{B.2})$$

where  $f'_{\boldsymbol{\alpha}_m}{}^{(n)} = \frac{\partial f^{(n)}}{\partial \boldsymbol{\alpha}_m}$ ,  $f'_{\boldsymbol{\alpha}_m x^{(n)}}{}^{(n)} = \frac{\partial}{\partial x^{(n)}} \left( \frac{\partial f^{(n)}}{\partial \boldsymbol{\alpha}_m} \right)$ , and  $f'_{\boldsymbol{\alpha}_m y^{(n)}}{}^{(n)} = \frac{\partial}{\partial y^{(n)}} \left( \frac{\partial f^{(n)}}{\partial \boldsymbol{\alpha}_m} \right)$ . With the interpolation the local shifts of the function  $f(\boldsymbol{\alpha})$  can be represented. This results in a representation of the areas of potential radar locations with bins instead of grid points. The second-order interpolation (polar) can be used as an alternative technique [2], [3].

Then the MSE from (B.1) will be:

$$\begin{aligned}
\text{MSE}(\boldsymbol{\alpha}_m) &= \text{tr} \left\{ \left( \sum_{n=1}^N \frac{1}{(\sigma^{(n)})^2} \left[ f'_{\alpha_m}{}^{(n)} + \Delta x^{(n)} f'_{\alpha_m x^{(n)}}{}^{(n)} + \Delta y^{(n)} f'_{\alpha_m y^{(n)}}{}^{(n)} \right] \right. \right. \\
&\quad \left. \left. \times \left[ f'_{\alpha_m}{}^{(n)} + \Delta x^{(n)} f'_{\alpha_m x^{(n)}}{}^{(n)} + \Delta y^{(n)} f'_{\alpha_m y^{(n)}}{}^{(n)} \right]^\dagger \right)^{-1} \right\} \\
&= \text{tr} \left\{ \left( \sum_{n=1}^N \frac{1}{(\sigma^{(n)})^2} \left( f'_{\alpha_m}{}^{(n)} (f'_{\alpha_m}{}^{(n)})^\dagger + \Delta x^{(n)} \left[ f'_{\alpha_m}{}^{(n)} (f'_{\alpha_m x^{(n)}}{}^{(n)})^\dagger + (f'_{\alpha_m}{}^{(n)})^\dagger f'_{\alpha_m x^{(n)}}{}^{(n)} \right] \right. \right. \right. \\
&\quad \left. \left. \left. + \Delta y^{(n)} \left[ f'_{\alpha_m}{}^{(n)} (f'_{\alpha_m y^{(n)}}{}^{(n)})^\dagger + (f'_{\alpha_m}{}^{(n)})^\dagger f'_{\alpha_m y^{(n)}}{}^{(n)} \right] + (\Delta x^{(n)})^2 \left[ (f'_{\alpha_m x^{(n)}}{}^{(n)})^\dagger f'_{\alpha_m x^{(n)}}{}^{(n)} \right] \right. \right. \right. \\
&\quad \left. \left. \left. + (\Delta y^{(n)})^2 \left[ (f'_{\alpha_m y^{(n)}}{}^{(n)})^\dagger f'_{\alpha_m y^{(n)}}{}^{(n)} \right] \right. \right. \right. \\
&\quad \left. \left. \left. + \Delta x^{(n)} \Delta y^{(n)} \left[ f'_{\alpha_m x^{(n)}}{}^{(n)} (f'_{\alpha_m y^{(n)}}{}^{(n)})^\dagger + f'_{\alpha_m y^{(n)}}{}^{(n)} (f'_{\alpha_m x^{(n)}}{}^{(n)})^\dagger \right] \right) \right) \right)^{-1} \right\}, \tag{B.3}
\end{aligned}$$

where the derivatives  $f'_{\alpha_m}{}^{(n)}$ ,  $f'_{\alpha_m x^{(n)}}{}^{(n)}$ , and  $f'_{\alpha_m y^{(n)}}{}^{(n)}$  are given by

$$f'_{x_m}{}^{(n)} = \frac{2}{c} \frac{x_m - x^{(n)}}{R_m^{(n)}}; \tag{B.4}$$

$$f'_{y_m}{}^{(n)} = \frac{2}{c} \frac{y_m - y^{(n)}}{R_m^{(n)}}; \tag{B.5}$$

$$f'_{x_m x^{(n)}}{}^{(n)} = \frac{2}{c} \frac{1}{(R_m^{(n)})^3} \left( (x_m - x^{(n)})^2 - (R_m^{(n)})^2 \right); \tag{B.6}$$

$$f'_{y_m y^{(n)}}{}^{(n)} = \frac{2}{c} \frac{1}{(R_m^{(n)})^3} \left( (y_m - y^{(n)})^2 - (R_m^{(n)})^2 \right); \tag{B.7}$$

$$f'_{y_m x^{(n)}}{}^{(n)} = \frac{2}{c} \frac{1}{(R_m^{(n)})^3} (x_m - x^{(n)}) (y_m - y^{(n)}); \tag{B.8}$$

$$f'_{x_m y^{(n)}}{}^{(n)} = \frac{2}{c} \frac{1}{(R_m^{(n)})^3} (x_m - x^{(n)}) (y_m - y^{(n)}). \tag{B.9}$$

Such an approximation is used in order to eliminate the effect of gridding and allow for off-grid radar selection within the bin size  $\Delta x^{(n)} \times \Delta y^{(n)}$ .

Introducing the optimization variables:  $\mathbf{w}$ ,  $\mathbf{v}_x$ ,  $\mathbf{v}_y$ ,  $\mathbf{u}_x$ ,  $\mathbf{u}_y$ , and  $\mathbf{g}$ , the performance function will be given by

$$\begin{aligned}
f_p(\mathbf{w}) &= \text{tr} \left\{ \left( \sum_{n=1}^N \frac{1}{(\sigma^{(n)})^2} \left( w^{(n)} f'_{\alpha_m}{}^{(n)} (f'_{\alpha_m}{}^{(n)})^\dagger \right. \right. \right. \\
&\quad \left. \left. + v_x^{(n)} \left[ f'_{\alpha_m}{}^{(n)} (f'_{\alpha_m x^{(n)}}{}^{(n)})^\dagger + (f'_{\alpha_m}{}^{(n)})^\dagger f'_{\alpha_m x^{(n)}}{}^{(n)} \right] \right. \right. \\
&\quad \left. \left. + v_y^{(n)} \left[ f'_{\alpha_m}{}^{(n)} (f'_{\alpha_m y^{(n)}}{}^{(n)})^\dagger + (f'_{\alpha_m}{}^{(n)})^\dagger f'_{\alpha_m y^{(n)}}{}^{(n)} \right] \right. \right. \\
&\quad \left. \left. + u_x^{(n)} \left[ (f'_{\alpha_m x^{(n)}}{}^{(n)})^\dagger f'_{\alpha_m x^{(n)}}{}^{(n)} \right] + u_y^{(n)} \left[ (f'_{\alpha_m y^{(n)}}{}^{(n)})^\dagger f'_{\alpha_m y^{(n)}}{}^{(n)} \right] \right) \right) \right\} \tag{B.10}
\end{aligned}$$

$$+ \mathbf{g}^{(n)} \left[ f'_{\alpha_m x^{(n)}} \left( f'_{\alpha_m y^{(n)}} \right)^\dagger + f'_{\alpha_m y^{(n)}} \left( f'_{\alpha_m x^{(n)}} \right)^\dagger \right]^{-1} \},$$

where  $\mathbf{w} = [w^{(1)}, \dots, w^{(N)}]^T \in \{0, 1\}^N$  is a Boolean selection vector that has to be designed;  $\mathbf{v}_x = [v_x^{(1)}, \dots, v_x^{(N)}]^T$  with  $v_x^{(n)} = w^{(n)} \Delta x^{(n)}$ ;  $\mathbf{v}_y = [v_y^{(1)}, \dots, v_y^{(N)}]^T$  with  $v_y^{(n)} = w^{(n)} \Delta y^{(n)}$ ;  $\mathbf{u}_x = [u_x^{(1)}, \dots, u_x^{(N)}]^T$  with  $u_x^{(n)} = w^{(n)} (\Delta x^{(n)})^2$ ;  $\mathbf{u}_y = [u_y^{(1)}, \dots, u_y^{(N)}]^T$  with  $u_y^{(n)} = w^{(n)} (\Delta y^{(n)})^2$ ; and  $\mathbf{g} = [g^{(1)}, \dots, g^{(N)}]^T$  with  $g^{(n)} = w^{(n)} \Delta x^{(n)} \Delta y^{(n)}$ .

Following [2], the continuous sensor placement problem in a 2D space can be formulated as minimization of  $l_2/l_1$ -norm of the matrix  $\mathbf{Z} = [\mathbf{w}, \mathbf{v}_x, \mathbf{v}_y, \mathbf{u}_x, \mathbf{u}_y, \mathbf{g}] \in \mathbb{R}^{N \times 6}$ :

$$\begin{aligned}
 & \min_{\mathbf{Z}, \mathbf{u}_x, \mathbf{u}_y} \|\mathbf{Z}\|_{2,1} \\
 & \text{s.t. } f_p(\mathbf{w}, \mathbf{v}_x, \mathbf{v}_y, \mathbf{u}_x, \mathbf{u}_y, \mathbf{g}) \leq \eta_{\max} \quad \forall \alpha_m \in \mathcal{M} \\
 & \mathbf{Z} = [\mathbf{w}, \mathbf{v}_x, \mathbf{v}_y, \mathbf{u}_x, \mathbf{u}_y, \mathbf{g}], \\
 & \begin{bmatrix} \mathbf{U}_x & \mathbf{v}_x \\ \mathbf{v}_x^T & \mathbf{1} \end{bmatrix} \succeq 0, \text{diag}(\mathbf{U}_x) = \mathbf{u}_x, \\
 & \begin{bmatrix} \mathbf{U}_y & \mathbf{v}_y \\ \mathbf{v}_y^T & \mathbf{1} \end{bmatrix} \succeq 0, \text{diag}(\mathbf{U}_y) = \mathbf{u}_y, \\
 & 0 \leq w^{(n)} \leq 1, n = 1, \dots, N, \\
 & -0.5\delta \leq v_x^{(m)} \leq 0.5\delta, n = 1, \dots, N, \\
 & -0.5\delta \leq v_y^{(m)} \leq 0.5\delta, n = 1, \dots, N, \\
 & 0 \leq u_x^{(m)} \leq 0.25\delta^2, n = 1, \dots, N, \\
 & 0 \leq u_y^{(m)} \leq 0.25\delta^2, n = 1, \dots, N, \\
 & -0.25\delta^2 \leq g^{(n)} \leq 0.25\delta^2, n = 1, \dots, N,
 \end{aligned} \tag{B.11}$$

where  $\delta$  is a bin size, which is assumed to be same for both  $x$  and  $y$  dimensions,  $\eta_{\max}$  is the threshold on the maximum value of the localization error, and  $l_2/l_1$ -norm is defined as

$$\|\mathbf{Z}\|_{2,1} = \sum_{n=1}^N \sqrt{(w^{(n)})^2 + (v_x^{(n)})^2 + (v_y^{(n)})^2 + (u_x^{(n)})^2 + (u_y^{(n)})^2 + (g^{(n)})^2}. \tag{B.12}$$

*Note* that the optimization problem (B.11) can be solved with one iteration or by using a re-weighted minimization algorithm similar to Algorithm 1, where the weighting vector  $\mathbf{u}$  is introduced in order to provide a sparse solution.

## B.2. NUMERICAL RESULTS

We apply the developed approach to a short-range FMCW radar network topology optimization. Each radar transmits a sequence of linear frequency modulated pulses that is given by:

$$x^{(n)}(t) = A_0 \exp\left(j t \left[ \omega_c + \text{frac}\left(\frac{t}{T_s}\right) \Delta \omega \right]\right), \tag{B.13}$$

where  $A_0 = |A_0| \exp(j\phi_0)$  is the transmit signal amplitude,  $\omega_c = 2\pi f_c$  with  $f_c$  the signal center frequency,  $\Delta \omega = 2\pi \Delta f$  with  $\Delta f$  the signal bandwidth,  $n = 1, \dots, N$ , and  $T_s$  is the

sweep time. The signal reflected from the moving target related to the  $m$ th grid point is shifted in time and frequency:

$$y_m^{(n)}(t) = A_m^{(n)} x^{(n)}(t - \tau_m^{(n)}) e^{-j(t-\tau)\omega_{d_m}^{(n)} + \xi(t)^{(n)}, \quad (\text{B.14})$$

where  $A_m^{(n)} = |A_m^{(n)}| e^{j\varphi_m^{(n)}}$  is the non-fluctuating amplitude of the received signal;  $\tau_m^{(n)}$  is the signal time delay;  $\omega_{d_m}^{(n)} = 2\pi f_{d_m}^{(n)}$  with  $f_{d_m}^{(n)}$  the Doppler frequency of the received signal;  $\xi(t)$  is a zero-mean i.i.d. Gaussian noise with variance  $\sigma^2$ . For the parameters of a single radar node the reader is referred to Chapter 5, Table 5.1.

Positions of the radar nodes are optimized in order to provide the required localization accuracy of the target within the surveillance area (shown with blue points in Figure B.1). We compare the results of two convex optimization algorithms, namely the sparsity-promoting algorithm for on-grid radar selection and the algorithm, presented in this chapter, for off-grid radar selection. The bin size for off-grid radar placement was selected to be the same for  $x$ - and  $y$ -coordinates and is  $\delta = 200$  m that allows for the selection of the radar nodes in the corridor with a width of 200 m. For the on-grid radar selection we set the threshold on the maximum value of the localization error as equal to 3 m, while the threshold on the maximum MSE was set to  $1 \text{ m}^2$ . This results in the selection of six radar positions. Figure B.1 shows topologies of two radar networks. The average errors of target localization over the area of target potential location  $\sigma_p \approx 1.10$  [m] and  $\sigma_p \approx 0.83$  [m] for on- and off-grid radar selection algorithms. The distribution of the target localization error in the areas enclosed by two selected radar topologies is shown in Figure B.2. As one can see, the shift of the radar units towards the target area results in lower localization errors in the second topology (Figure B.2b), as compared to the first one (Figure B.2a).

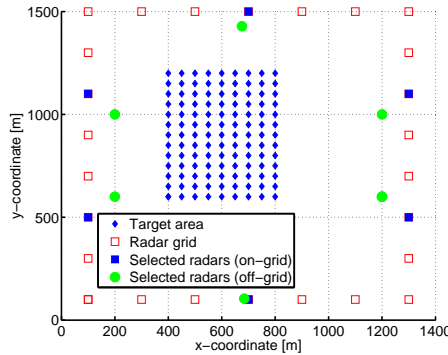
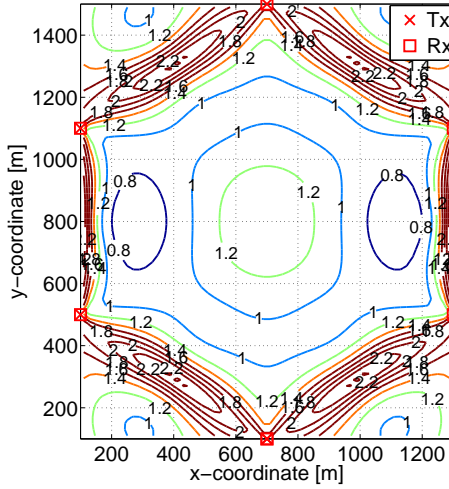


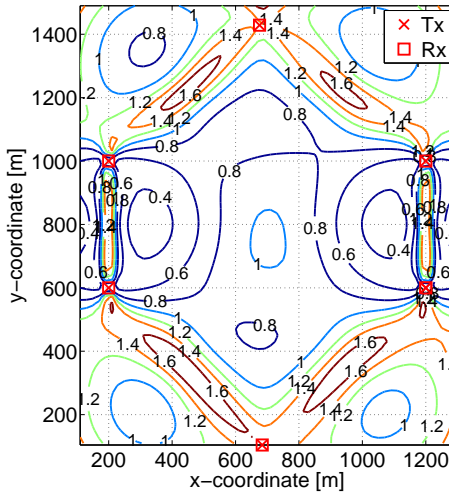
Figure B.1: The selected positions of the monostatic radars using discrete (on-grid) and continuous (off-grid) optimization approaches

### B.3. CONCLUSION

The radar network topology optimization algorithm that allows for continuous radar sensor placement was tackled in this chapter. The optimization algorithm that supports



(a) radar positions, selected from grid points of the radar grid



(b) radar positions, selected within bins that represent target area

Figure B.2: Contour plots of the target localization error ( $\sigma_p$ , m) in the network of six monostatic radars that explore the autonomous mode of signal transmission-reception

a general, non-linear measurement model, was presented. The mean squared error was used as performance measure of the radar network. The MSE has been linearized around radar positions, resulting in an optimal off-grid radar network topology selection. Numerical analysis has shown that such a selection provides lower MSE of target localization, compared to the radar geometry selected on-grid.

## REFERENCES

- [1] I. M. Ivashko and A. G. Yarovoy, *Off-grid radar node placement for target localization in radar networks*, in *2016 CIE International Conference on Radar (Radar 2016)* (2016) pp. 1–4.
- [2] S. P. Chepuri and G. Leus, *Continuous sensor placement*, *IEEE Signal Processing Letters* **22**, 544 (2015).
- [3] C. Ekanadham, D. Tranchina, and E. P. Simoncelli, *Recovery of sparse translation-invariant signals with continuous basis pursuit*, *IEEE Transactions on Signal Processing* **59**, 4735 (2011).



# C

## DATA ASSOCIATION ALGORITHM FOR MULTIPLE TARGETS LOCALIZATION IN THE NETWORKS OF MONOSTATIC RADARS

*This appendix addresses the data association problem in a monostatic radar network using the measurements from a single moment of time, e.g. without a priori knowledge of the target's state vector. It is assumed that the target position is estimated from the set of time delay measurements, done locally in each of the omnidirectional radars.*

### C.1. SYSTEM MODEL AND PROBLEM FORMULATION

THE network of  $N$  monostatic omnidirectional radars with coordinates  $(x^{(n)}, y^{(n)}, z^{(n)})$ , ( $n = 1, \dots, N$ ) is considered. It is assumed that target detection is performed locally in each of the radar nodes and corresponding time delay measurements, related to the targets' ranges, are forwarded to the central processing unit (CPU), where the target localization is performed. It is assumed that detection probability is equal to one  $P_d = 1$ . Therefore, the number of detections in each of the radars is the same as the number of targets in the scene and is equal to  $M$ . Targets are assumed to be point scatterers.

Following the general measurement model given in (2.1), the vector of accumulated measurements from  $m$ th target is  $y_m \in \mathbb{R}^N$ , where  $y_m^{(n)} = \tau_m^{(n)} c/2 + \xi_m^{(n)}$  ( $m = 1, \dots, M$  with  $M$  number of targets). For convenience, we introduce notation  $\tilde{R}_m^{(n)}$  for the measured target range.

In the noiseless measurement model with no signal attenuation, the accuracy of target range estimation is limited by the radar range resolution  $\Delta R^{(n)}$  [2]. Consequently, the true target range  $R_m^{(n)}$  will be within the interval

$$\tilde{R}_m^{(n)} - \frac{\Delta R^{(n)}}{2} \leq R_m^{(n)} \leq \tilde{R}_m^{(n)} + \frac{\Delta R^{(n)}}{2}. \tag{C.1}$$

When there is more than one target in the scene ( $M > 1$ ), the correct association of the set of the  $M$  measurements from  $N$  radars has to be made in order to form  $N$ -tuple of measurements that constitute each of  $m$ th target. In the noiseless measurement model, true target position corresponds to the point of the intersection of the ranging spheres with centres  $(x^{(n)}, y^{(n)}, z^{(n)})$  of the radar nodes locations. If the measurement accuracy is subject to the radar range resolution, the true target ranges will be bounded by

$$\left\{ \begin{array}{l} (\tilde{R}_m^{(1)} - \Delta R^2)^2 \leq (R_m^{(1)})^2 \leq (\tilde{R}_m^{(1)} + \Delta R^2)^2; \\ (\tilde{R}_m^{(2)} - \Delta R^2)^2 \leq (R_m^{(2)})^2 \leq (\tilde{R}_m^{(2)} + \Delta R^2)^2; \\ \vdots \\ (\tilde{R}_m^{(N)} - \Delta R^2)^2 \leq (R_m^{(N)})^2 \leq (\tilde{R}_m^{(N)} + \Delta R^2)^2; \end{array} \right. \tag{C.2}$$

In contrast, the ghost target position is the one that results in the intersection of ranging spheres from different targets (Fig.1.2).

The three-stage deghosting algorithm, which is aimed at mitigating incorrect data associations, is presented in the following sections. The first stage is the target localization via a trilateration algorithm, based on a direct calculation method. The second stage is the analysis of the localized targets by means of geometrical interpretation of their location with respect to radar nodes. The third stage is the analysis of  $\tilde{N}$ -tuples, which is a set of measurement indexes from each radar  $\{q_m^{(1)}, q_m^{(2)}, \dots, q_m^{(N)}\}$ , where  $q_m^{(n)} = 1, \dots, M$  is the measurement index in  $n$ th radar.

### C.2. STAGE 1 - TARGET LOCALIZATION

For the sake of simplicity, one  $N$ -tuple of measurements  $\{\tilde{R}^{(1)}, \tilde{R}^{(2)}, \tilde{R}^{(3)}, \tilde{R}^{(4)}\}$  and a radar network of four radars are considered. Assuming infinite radar resolution, inequalities

from (C.2) are reduced to

$$\begin{cases} (x - x^{(1)})^2 + (y - y^{(1)})^2 + (z - z^{(1)})^2 = (\tilde{R}^{(1)})^2; \\ (x - x^{(2)})^2 + (y - y^{(2)})^2 + (z - z^{(2)})^2 = (\tilde{R}^{(2)})^2; \\ (x - x^{(3)})^2 + (y - y^{(3)})^2 + (z - z^{(3)})^2 = (\tilde{R}^{(3)})^2; \\ (x - x^{(4)})^2 + (y - y^{(4)})^2 + (z - z^{(4)})^2 = (\tilde{R}^{(4)})^2; \end{cases} \quad (\text{C.3})$$

where  $(x, y, z)$  are target coordinates.

Subtracting the second equation from the first, the third equation from the first and leaving the third equation as it is, we get a system of three equations with three unknowns  $x, y$  and  $z$  (the fourth measurement  $\tilde{R}^{(4)}$  is not used here)

$$\begin{cases} (2x - x^{(1)} - x^{(2)})(x^{(2)} - x^{(1)}) + (2y - y^{(1)} - y^{(2)})(y^{(2)} - y^{(1)}) + \\ + (2z - z^{(1)} - z^{(2)})(z^{(2)} - z^{(1)}) = (\tilde{R}^{(1)})^2 - (\tilde{R}^{(2)})^2; \\ (2x - x^{(1)} - x^{(3)})(x^{(3)} - x^{(1)}) + (2y - y^{(1)} - y^{(3)})(y^{(3)} - y^{(1)}) + \\ + (2z - z^{(1)} - z^{(3)})(z^{(3)} - z^{(1)}) = (\tilde{R}^{(1)})^2 - (\tilde{R}^{(3)})^2; \\ (x - x^{(3)})^2 + (y - y^{(3)})^2 + (z - z^{(3)})^2 = (\tilde{R}^{(3)})^2; \end{cases} \quad (\text{C.4})$$

These equations (C.4) are reduced to quadratic form

$$\begin{cases} x = a_1 y + a_2 z + b_1; \\ y = a_3 z + b_2; \\ Az^2 + Bz + C = 0; \end{cases} \quad (\text{C.5})$$

with the following coefficients

$$A = (a_1 a_3 + a_2)^2 + a_3^2 + 1;$$

$$B = 2(a_1 a_3 + a_2)(a_1 b_2 + b_1) - 2x^{(3)}(a_1 a_3 + a_2) + a_3 b_2 - 2y^{(3)} a_3 - 2z^{(3)};$$

$$C = (a_1 b_2 + b_1)^2 - x^{(3)}(2a_1 b_2 + 2b_1 - x^{(3)}) + b_2^2 + y^{(3)}(y^{(3)} - 2b_2) + (z^{(3)})^2 - (R^{(3)})^2;$$

where

$$a_1 = -\frac{\Delta y^{(2,1)}}{\Delta x^{(2,1)}}; \quad a_2 = -\frac{\Delta z^{(2,1)}}{\Delta x^{(2,1)}}; \quad a_3 = -\frac{\Delta x^{(3,1)} a_2 + \Delta z^{(3,1)}}{\Delta x^{(3,1)} a_1 + \Delta y^{(3,1)}};$$

$$b_1 = \frac{\Delta y^{(2,1)} y^{(2,1)}}{2\Delta x^{(2,1)}} + \frac{\Delta z^{(2,1)} z^{(2,1)}}{2\Delta x^{(2,1)}} + \frac{(R^{(1)})^2 - (R^{(2)})^2}{2\Delta x^{(2,1)}} + \frac{x^{(2,1)}}{2};$$

$$b_2 = -\frac{1}{2(\Delta x^{(3,1)} a_1 + \Delta y^{(3,1)})} \quad (\text{C.6})$$

$$\times \left[ 2\Delta x^{(3,1)} b_1 - \Delta x^{(3,1)} x_{31} - y^{(3,1)} \Delta y^{(3,1)} - z^{(3,1)} \Delta z^{(3,1)} - (R^{(1)})^2 + (R^{(3)})^2 \right];$$

where  $\Delta x^{(n,m)} = x^{(n)} - x^{(m)}$ ,  $x^{(n,m)} = x^{(n)} + x^{(m)}$ ;  $\Delta y^{(n,m)} = y^{(n)} - y^{(m)}$ ,  $y^{(n,m)} = y^{(n)} + y^{(m)}$ ;  $\Delta z^{(n,m)} = z^{(n)} - z^{(m)}$ ,  $z^{(n,m)} = z^{(n)} + z^{(m)}$ . The quadratic equation (C.5) has one or two solutions  $\tilde{\mathbf{s}}_1 = (\tilde{x}_1, \tilde{y}_1, \tilde{z}_1)$  and/or  $\tilde{\mathbf{s}}_2 = (\tilde{x}_2, \tilde{y}_2, \tilde{z}_2)$ , which are potential locations of the true target. We evaluate ranges  $R_1^{(q)}$  and  $R_2^{(q)}$  from these locations to  $N - 3$  radar nodes ( $q = 1, \dots, N - 3$ ), measurements from which were not used for estimation of positions  $\tilde{\mathbf{s}}_1$  and  $\tilde{\mathbf{s}}_2$ . In the considered scenario, it is the fourth radar. In case of a true target, the evaluated ranges shall match the measured ones with a certain accuracy, which we define as  $\delta R$  (Algorithm 4). In the case of noiseless measurements, the threshold value can be selected as one that is equal to the radar range resolution  $\delta R = \Delta R$ , whereas for noisy measurements, the threshold  $\delta R$  shall be accurately selected in order to minimize the number of true targets that can be removed. For example, this value of threshold accuracy can be selected as  $\delta R = \Delta R + \sigma^{(n)}$ , where  $\sigma^{(n)}$  is the standard deviation of the measurement noise.

---

**Algorithm 4:** Target localization algorithm based on  $N$ -tuple of measurements, associated with one target

---

**input** :  $N$ -tuple of measurements  $\{\tilde{R}_m^{(1)}, \dots, \tilde{R}_m^{(N)}\}$   
**output**: Coordinate vector of (potentially) true target  
**for**  $i \leftarrow 1$  **to** number of combinations of three measurements  $C_3^N = N!/(3!(N-3)!)$   
**do**  
    **if**  $B^2 - 4AC \geq 0$  from (C.5) **then**  
        evaluate  
         $R_{m,1}^{(q)} = \sqrt{(\tilde{x}_1 - x^{(q)})^2 + (\tilde{y}_1 - y^{(q)})^2 + (\tilde{z}_1 - z^{(q)})^2}$ ;  
         $R_{m,2}^{(q)} = \sqrt{(\tilde{x}_2 - x^{(q)})^2 + (\tilde{y}_2 - y^{(q)})^2 + (\tilde{z}_2 - z^{(q)})^2}$ ;  
        **if**  $|R_{m,1}^{(q)} - \tilde{R}_m^{(q)}| \leq \delta R$  **or**  $|R_{m,2}^{(q)} - \tilde{R}_m^{(q)}| \leq \delta R$  **then**  
            analyzed  $N$ -tuple of measurements is associated with (potentially) true target position and will be further analyzed;  
        **else**  
            analyzed  $N$ -tuple is formed with the measurements from different targets and is classified as ghost  
        **end**  
    **end**  
**end**

---

### C.3. STAGE 2 - ANALYSIS OF THE TARGET-NETWORK GEOMETRY

This stage of deghosting is based on the analysis of  $C$  measurement combinations, used for target localization in the preceding stage. The basic idea of this procedure is to find out if the spheres from  $N$  radar nodes with radiuses  $\tilde{R}^{(1)}, \dots, \tilde{R}^{(N)}$  intersect

or not. If they do intersect, then the intersection point corresponds to the true target position. If not, then this combination of measurements defines the ghost target. Not all of the range measurements that form the combination  $\tilde{R}^{(1)}, \tilde{R}^{(2)}, \tilde{R}^{(2)}, \dots, \tilde{R}^{(N)}$  are analyzed simultaneously. This set is randomly divided into the combinations of three measurements and each of them is analyzed separately.

Without loss of generality, we consider the 2D spatial model of the target and three radars. In the noiseless measurement model, there will be one point of intersection of three circles  $O$  that corresponds to the target position (in 3D model - two points). Within the following algorithm we check whenever the range circles from three radars marked with points  $A, C, F$  intersect (Fig. C.1). Points  $B$  and  $D$  are the intersection points of target ranges from radars located at  $A$  and  $C$ ,  $O$  is the point of intersection of the range circle from radar  $F$  with the line  $BD$ . In case of the intersection of three range circles,  $O$  has to be on the line  $BD$ .

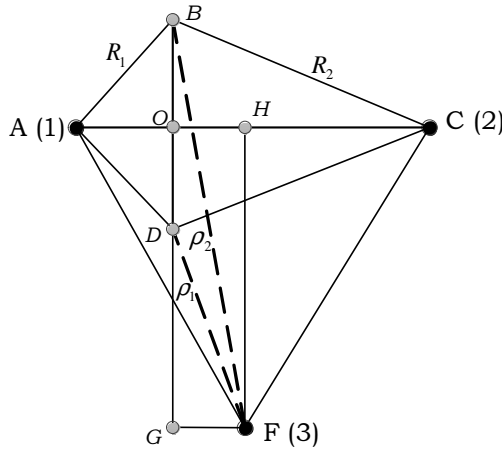


Figure C.1: Schematic illustration of the target localization

First, the distances  $r_D = FD$  and  $r_B = FB$  from radar  $F$  to the points of intersection of two range circles of radars  $A$  and  $C$  are evaluated.

*Solution:*

$BO = OD$ ;  $AB = R^{(1)}$ ;  $BC = R^{(2)}$ ;  $R^{(1)}$  and  $R^{(2)}$  are distances from the target to the first and the second radars respectively;

$AC = d_{12}$ ;  $AF = d_{13}$ ;  $FC = d_{23}$  are distances between the radars;

$\frac{1}{2}BO \cdot d_{12} = S_{ABC}$ ,

where  $S_{ABC}$  is the area of the triangle  $\Delta ABC$ , evaluated from Heron's formula

$$S_{ABC} = \frac{1}{4} \sqrt{4(R^{(1)})^2(R^{(2)})^2 - ((R^{(1)})^2 + (R^{(2)})^2 - d_{12}^2)^2}.$$

Consequently,  $BO = \frac{2S_{ABC}}{d_{12}}$ .

Similarly,  $FH = GO = \frac{2S_{AFC}}{d_{12}}$ , where  $S_{AFC}$  is the area of the triangle  $\Delta AFC$ .

From the Pythagorean theorem  $CH^2 = FC^2 - FH^2 = d_{23}^2 - FH^2$ ;

$$OC^2 = BC^2 - BO^2 = (R^{(2)})^2 - BO^2;$$

Then,  $OH = OC - CH$  ( $CH$  - from triangle  $\Delta FCH$ , where  $FC$  is known,  $FH$  has been found); and  $GF = OH$ .

Similarly  $GD = GO - OD = FH - BO$ .

Then we get  $r_D^2 = FD^2 = GF^2 + GD^2$ ; and  $r_B^2 = FB^2 = GF^2 + (FH + BO)^2$ .

The distances  $r_D$  and  $r_B$  depend on the measured ranges  $\tilde{R}^{(1)}$  and  $\tilde{R}^{(2)}$ :  $r_D = f(\tilde{R}^{(1)}, \tilde{R}^{(2)}, d_{12}, d_{13}, d_{23})$ ;  $r_B = f(\tilde{R}^{(1)}, \tilde{R}^{(2)}, d_{12}, d_{13}, d_{23})$ . In the noiseless measurement model, the measured values  $\tilde{R}^{(1)}$  and  $\tilde{R}^{(2)}$  depend on the radar resolution  $\Delta R$  and can take values from intervals  $[R^{(1)} - \Delta R/2, R^{(1)} + \Delta R/2]$  and  $[R^{(2)} - \Delta R/2, R^{(2)} + \Delta R/2]$ , respectively. Taking this into account, the distances  $r_D$  and  $r_B$  can take values

$$\begin{aligned} \boldsymbol{\rho}_1 &= \begin{bmatrix} \rho_{11} \\ \rho_{12} \\ \rho_{13} \\ \rho_{14} \end{bmatrix} = \begin{bmatrix} f(R^{(1)} + \frac{\Delta R}{2}, R^{(2)} + \frac{\Delta R}{2}, d_{12}, d_{13}, d_{23}) \\ f(R^{(1)} - \frac{\Delta R}{2}, R^{(2)} - \frac{\Delta R}{2}, d_{12}, d_{13}, d_{23}) \\ f(R^{(1)} + \frac{\Delta R}{2}, R^{(2)} - \frac{\Delta R}{2}, d_{12}, d_{13}, d_{23}) \\ f(R^{(1)} - \frac{\Delta R}{2}, R^{(2)} + \frac{\Delta R}{2}, d_{12}, d_{13}, d_{23}) \end{bmatrix}; \\ \boldsymbol{\rho}_2 &= \begin{bmatrix} \rho_{21} \\ \rho_{22} \\ \rho_{23} \\ \rho_{24} \end{bmatrix} = \begin{bmatrix} f(R^{(1)} + \frac{\Delta R}{2}, R^{(2)} + \frac{\Delta R}{2}, d_{12}, d_{13}, d_{23}) \\ f(R^{(1)} - \frac{\Delta R}{2}, R^{(2)} - \frac{\Delta R}{2}, d_{12}, d_{13}, d_{23}) \\ f(R^{(1)} + \frac{\Delta R}{2}, R^{(2)} - \frac{\Delta R}{2}, d_{12}, d_{13}, d_{23}) \\ f(R^{(1)} - \frac{\Delta R}{2}, R^{(2)} + \frac{\Delta R}{2}, d_{12}, d_{13}, d_{23}) \end{bmatrix}; \end{aligned} \quad (C.7)$$

According to (C.1), the measured noiseless target range from the third radar is bounded by the interval of values  $[R^{(3)} - \Delta R/2, R^{(3)} + \Delta R/2]$ . If the true target is located in close proximity to point  $D$  or  $B$ , then at least one of the following inequalities has to be satisfied

$$\min(\boldsymbol{\rho}_1) < \tilde{R}^{(3)} + \frac{\Delta R}{2} < \max(\boldsymbol{\rho}_1) \quad (C.8)$$

$$\min(\boldsymbol{\rho}_1) < \tilde{R}^{(3)} - \frac{\Delta R}{2} < \max(\boldsymbol{\rho}_1) \quad (C.9)$$

$$\min(\boldsymbol{\rho}_2) < \tilde{R}^{(3)} + \frac{\Delta R}{2} < \max(\boldsymbol{\rho}_2) \quad (C.10)$$

$$\min(\boldsymbol{\rho}_2) < \tilde{R}^{(3)} - \frac{\Delta R}{2} < \max(\boldsymbol{\rho}_2), \quad (C.11)$$

where  $\tilde{R}^{(3)}$  is the measured target range from the third radar  $F$  to the target. A graphical representation of this condition is shown in Fig. C.2, where the true target is located in close proximity to point  $D$ .

If the set of measurements determines true target position, at least one of the conditions from (C.11) has to be satisfied for each  $C_3^N = \frac{N!}{3!(N-3)!}$  possible combination of three measurements.

For example, in case of four radars and the measurement combination  $\{\tilde{R}^{(1)}, \tilde{R}^{(2)}, \tilde{R}^{(3)}, \tilde{R}^{(4)}\}$  at least one of the following combinations of three measurements has to satisfy at least one of the constraints from (C.11)

$$\begin{aligned} &\tilde{R}^{(1)}, \tilde{R}^{(2)}, \tilde{R}^{(3)}; \\ &\tilde{R}^{(1)}, \tilde{R}^{(3)}, \tilde{R}^{(4)}; \\ &\tilde{R}^{(2)}, \tilde{R}^{(3)}, \tilde{R}^{(4)}; \\ &\tilde{R}^{(1)}, \tilde{R}^{(2)}, \tilde{R}^{(4)}. \end{aligned} \quad (C.12)$$

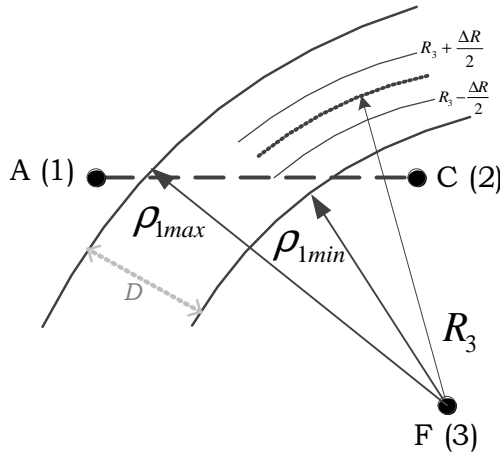


Figure C.2: Schematic illustration of condition (C.11)

C

## C.4. STAGE 3 - DEGHOSTING, BASED ON THE MEASUREMENT TUPLE ANALYSIS

According to the model considered with  $P_d = 1$  and  $P_{fa} = 0$ , the number of measurements in the  $n$ th radar form  $M$ -tuple, an ordered list of  $M$  measurements. Consequently, each target is represented by measurement  $N$ -tuple, where each observation belongs to a different radar. Another type of tuple,  $\tilde{N}$ -tuple, is introduced, where the measurement sequence of each radar that constitutes the target is stored. Intuitively,  $\tilde{N}$ -tuples that define  $M$  true targets can not be identical, i.e.  $(q_m^{(1)}, q_m^{(2)}, \dots, q_m^{(N)}) \neq (q_l^{(1)}, q_l^{(2)}, \dots, q_l^{(N)})$  ( $l \neq m, l = 1, \dots, M$ ). We refer to the entries of  $\tilde{N}$ -tuple as *radar marks* as well.

Each combination of range measurements that constitutes the target is described with  $\tilde{N}$ -tuple. For example, for the  $\tilde{N}$ -tuple measurement indexes  $\{3_m^{(1)}, 1_m^{(2)}, 5_m^{(3)}, 10_m^{(4)}\}$ , it means that the third, the first, the fifth, and the tenth measurements were used from the first, the second, the third, and the fourth radars to estimate position of the  $m$ th target. With analysis of  $\tilde{N}$ -tuples of measurement indexes, we count repetition value  $r_m$  of the measurement index from the  $n$ th radar for each target. If the repetition value is higher than one, the decision is made to estimate target position based on the range measurements that belong to different targets (Algorithm 5).

Table C.1 shows a scenario, in which first elements in two tuples from the the third and the ninth targets are the same. For the rest of the targets, there is no repetition in the elements from  $\tilde{N}$ -tuple. Therefore, these targets are identified as the true targets. Then the second entries of the tuples that constitute the 3rd and the 9th targets are analysed.

As one can see, the second entry in the tuple that constitutes the ninth target has already been used for localization in the fourth target, which was previously defined as the true one. At the same time, the second element from the measurement tuple of the third radar is not repeated in any of the considered measurement tuples. Based on this,

---

**Algorithm 5:** Ananalysis of the measurement tuples

---

**input** :  $N$ -tuples of measurement indexes for all potential targets locations.  
**output:**  $N$ -tuples that correspond to ghost targets  
**for**  $n \leftarrow 1$  **to**  $N$  **do**  
    **if**  $r_m > 2$  **then**  
        |  $m$ th  $N$ -tuple constitute ghost target  
    **else**  
        |  $m$ th  $N$ -tuple constitute true target  
    **end**  
**end**

---

we conclude that the third target is the true target and the ninth target is the ghost and should be eliminated (Table C.2).

An example, in which the analysis of the measurement tuples cannot assure ghost mitigation is shown in Table C.3. The fourth element from the first unresolved measurement combination has been used for localization of the true target. Therefore, this measurement combination is referred to as one that corresponds to the ghost target. The sixth and the eight elements from the measurement tuple of the first radar have not been used for constitution of the true targets. Consequently, corresponding measurement combinations have to be further analyzed. The analysis of the measurements tuples from the succeeding radars does not allow one to discriminate between the true and the ghost targets.

Radar No.	1	2	3	4	Real/False
Radar marks No.	1	3	3	3	R
	2	2	2	2	R
	3	1	2	4	?
	2	2	1	2	R
	4	4	4	1	R
	5	6	5	6	R
	6	7	7	5	R
	7	5	6	7	R
	3	4	1	5	?

Table C.1: Analysis of the measurements from the first radar

### C.5. CASE STUDY

In this section, the proposed three-stage deghosting algorithm is applied for 3D localization of multiple targets from the set of range measurements in the radar network. The radar network consists of four omnidirectional monostatic radar nodes with the following coordinates:  $I_1 = [-1000, 1000, 5]$ ,  $I_1 = [1000, 1000, 30]$ ,  $I_1 = [1000, -1000, 10]$ ,  $I_1 = [-1000, -1000, 15]$ .

Radar No.	1	2	3	4	Real/False
Radar marks No.	1	3	3	3	R
	2	2	2	2	R
	3	1	2	4	R
	2	2	1	2	R
	4	4	4	1	R
	5	6	5	6	R
	6	7	7	5	R
	7	5	6	7	R
3	4	1	5	F	

Table C.2: Analysis of the measurements from the second radar

Radar No.	1	2	3	4	Real/False
Radar marks No.	1	1	1	1	R
	2	2	2	2	R
	3	3	3	3	R
	4	4	4	4	R
	5	5	5	5	R
	7	7	7	7	R
	4	7	8	3	?
	6	6	6	6	?
	6	8	8	8	?
	8	6	6	6	?
	8	8	8	8	?

Table C.3: Additional filtration of potential ghosts

Figure C.3 presents the results of the deghosting algorithm depending on the radar range resolution  $\Delta R$  for different numbers of targets on the scene  $M$ . The radar range resolution  $\Delta R$  is assumed to be the same for all radars in the network. Targets' positions were generated randomly within the volume  $1000\text{ m} \times 1000\text{ m} \times 1000\text{ m}$ . The results of the deghosting algorithm were averaged for  $10^3$  Monte Carlo runs. As apparent from the results, the number of ghost targets increases with decreasing radar range resolution. Two times worse resolution leads to approximately two times more ghost targets. Moreover, a larger number of targets results in a larger number of ghosts due to the increase in the number of measurement combinations. It can be clearly observed that for  $M > 6$  targets, the number of ghosts increases drastically. The effect of each step of the deghosting procedure for  $M = 10$  targets is shown in Fig. C.4a. As one can see, each of the steps of the deghosting procedure leads to a subsequent decrease in the number ghosts.

Improved performance of the deghosting algorithm is observed for a scenario with target area dimensions of  $1000\text{ m} \times 1000\text{ m} \times 100\text{ m}$  (Fig.C.4b). In the previous scenario

(Fig.C.4b), the radars' altitudes were significantly smaller than those of the targets (around 1000 m). That resulted in less spatial diversity, and thus worse performance of the ghost target elimination. For a scenario with target altitudes of about 100 m, the vertical diversity of the radar nodes and targets is higher and leads to more efficient ghost mitigation.

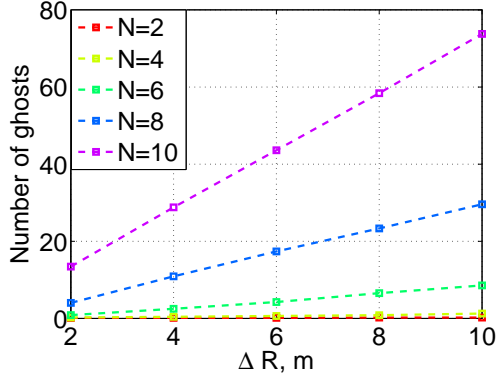
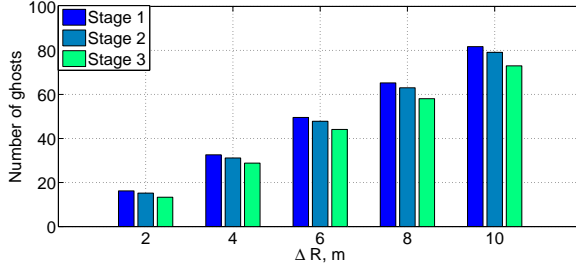
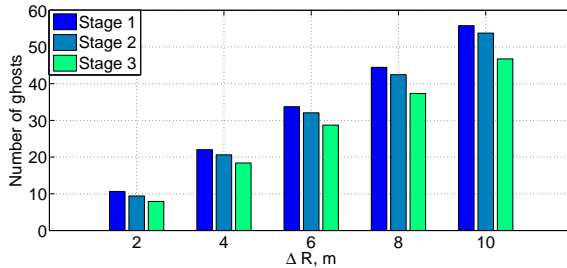


Figure C.3: Number of ghost targets depending on the radar range resolution for noiseless measurement model (target is located within the volume 1000 m × 1000 m × 1000 m).



(a) 1000 m × 1000 m × 1000 m



(b) 1000 m × 1000 m × 100 m

Figure C.4: Number of ghosts target depending on the radar range resolution  $\Delta R$  for  $M = 10$  targets

Figure C.5 reports the results of the deghosting algorithm for the noisy measurement model. The noise is modelled as a normally distributed random value with zero-mean and variance  $(\sigma^{(n)})^2$ ,  $\mathcal{N}(0, (\sigma^{(n)})^2)$ . Rayleigh or Rician distributions can be used to represent a multipath signal propagation model. Meanwhile, it is assumed that noisy measurements do not affect target detection performance. The results demonstrate a substantial increase of the number of ghost targets with increase of the noise variance value, both for high and low radar range resolution.

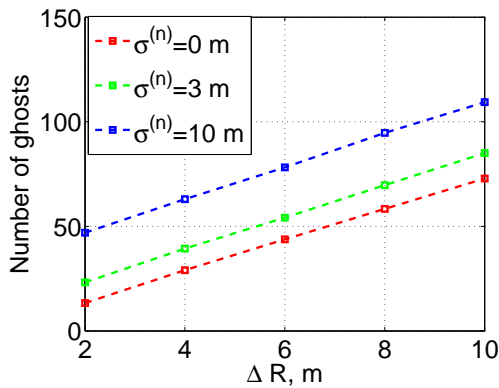


Figure C.5: Number of ghosts for different noise variances  $(\sigma^{(n)})^2$  (number of targets  $M = 10$ ; target is located within the volume  $1000\text{ m} \times 1000\text{ m} \times 1000\text{ m}$ )

## C.6. CONCLUSION

The three-stage deghosting algorithm for multiple target localization in a distributed radar network with omnidirectional antennas has been developed. It has been shown that efficiency of the deghosting procedure itself depends on the number of targets, their constellation in the scene, radar range resolution and noise variance. The more targets have to be resolved in the scene, the higher the radar range resolution required to minimize the ghosts number. In particular, for 3D localization of  $M = 10$  targets with  $N = 4$  radars, two times fewer ghosts are observed at the range resolution  $\Delta R = 2\text{ m}$  than at the range resolution  $\Delta R = 10\text{ m}$ .

## REFERENCES

- [1] A. Samokhin, I. Ivashko, and A. Yarovoy, *Algorithm for multiple targets localization and data association in distributed radar networks*, in *Radar Symposium (IRS), 2014 15th International* (2014) pp. 1–6.
- [2] M. Richards, J. Scheer, and W. Holm, *Principles of Modern Radar: Basic Principles*, Principles of Modern Radar (SciTech Pub., 2010).



# SUMMARY

The ultimate goal of any sensing system is to build situation awareness. Existing solutions for a single radar node that have to assure extended areas of coverage with high resolution measurements (in range, cross-range, and Doppler) are physically cumbersome (large antenna size) and typically require large operational resources (high transmit power, wide bandwidth and long integration time).

Combining data from multiple spatially separated nodes located at several locations offers a possibility to use radars with low-cost omnidirectional antennas to cover wide areas and overcome operational limitations such as sector blockage due to landscape or high-rise buildings. Thus, performance of the complete system becomes dependent not only on the parameters of a single radar node, but on the number of nodes and their location (system topology) as well. A proper selection of both node-related (transmit power, operational frequency and bandwidth, integration time, etc.) and system-related (node location, node cooperation) resources is an important design task, which forms the major focus of this thesis.

The first part of this dissertation is dedicated to the development of the radar network performance assessment tool, while the second part provides the framework for radar network topology optimization. The potential accuracy of the target parameters estimation has been used for radar network performance assessment. The developed tool incorporates parameters of a single radar node as well as system parameters (positions of the nodes and their cooperation), evaluated using Cramér-Rao lower bound. Using the tools developed, performance of different types of radar networks have been studied and compared in this thesis. For the radar network topology optimization several convex and greedy algorithms have been used, making the optimization approach versatile. Validation and performance comparison of the optimization algorithms have been performed in this thesis.

The results obtained in this research can be used to evaluate the potential performance of radar networks for different applications and provide a solution to key problems of their topology design.



# SAMENVATTING

Het einddoel van elk waarneming systeem is om bij te dragen aan de totstandkoming van een beter inzicht. Bestaande oplossingen voor een enkele radar node om een uitgebreid dekkingsgebied met hoge resolutiemetingen te garanderen (in bereik, cross-range, en Doppler), zijn fysiek omslachtig (grote antenne afmetingen) en vergen doorgaans grote operationele middelen (hoog zendvermogen, grote bandbreedte en lange integratie tijd).

Het combineren van data van meerdere ruimtelijk gescheiden nodes op verschillende locaties, biedt de mogelijkheid, om radars met goedkope omnidirectionele antennes om grote gebieden te bestrijken en operationele beperkingen zoals sector blokkade vanwege landscape of hoogbouw, te overwinnen. De prestaties van het gehele systeem wordt niet alleen afhankelijk van de parameters van een radar node, maar het aantal nodes en hun locatie (systeemtopologie). Een juiste selectie van zowel node-gerelateerde (zendvermogen, operationele frequentie en bandbreedte, integratie tijd, enz.) en systeem gerelateerde (node locatie, node samenwerking) middelen, is een belangrijke ontwerpogave, welke de belangrijkste focus van dit proefschrift vormt.

Het eerste deel van dit proefschrift is gewijd aan de ontwikkeling van de radar netwerk prestatiebeoordelingsinstrument, terwijl het tweede deel het kader voor radar netwerktopologie optimalisatie vormt. De mogelijke nauwkeurigheid van de doelparameters schatting is gebruikt voor radar netwerk prestatiebeoordeling. Het ontwikkelde instrument integreert parameters van een enkele radar node alsmede systeemparameters (posities van de nodes en hun samenwerking), bepaald met behulp van de Cramér-Rao ondergrens. Gebruikmakend van de ontwikkelde instrumenten zijn de prestaties van de verschillende typen radar netwerken bestudeerd en vergeleken in dit proefschrift. Voor de radar netwerk topologieoptimalisatie zijn verscheidene convex en greedy algoritmen gebruikt, waardoor de optimalisatiebenadering veelzijdig is geworden. Validatie en prestatievergelijking van de optimalisatie algoritmen zijn uitgevoerd in dit proefschrift.

De verkregen resultaten in dit onderzoek kunnen worden gebruikt om de haalbare prestatie van radar netwerken voor verschillende toepassingen te evalueren en bieden een oplossing voor hoofdproblemen van hun topologie ontwerp.



# LIST OF PUBLICATIONS

8. **I.M. Ivashko, G. Leus and A.G. Yarovoy**, *Radar network topology optimization for joint target position and velocity estimation*, Elsevier Signal Processing **130**, 279-288 (2016).
7. **I.M. Ivashko, O. A. Krasnov and A.G. Yarovoy**, *Sparsity-based Optimization of the Sensors Positions in Radar Networks with Separated Transmit and Receive Nodes*, Int. J. Distrib. Sen. Netw. **2016**, 26 (2016).
6. **I.M. Ivashko and A.G. Yarovoy**, *Off-grid radar node placement for target localization in radar networks*, 2016 CIE International Conference on Radar (Radar 2016), 1-4 (2016).
5. **I.M. Ivashko, O. A. Krasnov and A.G. Yarovoy**, *Some aspects of the multistatic radar network topology optimization*, 2016 17th International Radar Symposium (IRS), May, 1-5 (2016).
4. **I.M. Ivashko, O. A. Krasnov and A.G. Yarovoy**, *Topology optimization of monostatic radar networks with wide-beam antennas*, European Radar Conference (EuRAD), pp. 133-136 (2015).
3. **I.M. Ivashko, O. A. Krasnov and A.G. Yarovoy**, *Receivers topology optimization of the combined active and WiFi-based passive radar network*, 11th European Radar Conference (EuRAD), Rome, pp. 517-520 (2014).
2. **A. Samokhin, I. Ivashko, and A. Yarovoy**, *Algorithm for multiple targets localization and data association in distributed radar networks*, 15th International Radar Symposium (IRS), Gdansk, 1-6 (2014).
1. **I.M. Ivashko, O. A. Krasnov and A.G. Yarovoy**, *Performance Analysis of Multisite Radar Systems*, 10th European Radar Conference (EuRAD), Nuremberg, pp. 459-462 (2013).



# ACKNOWLEDGMENTS

First, I would like to thank my promoter A. G. Yarovoy, for giving me opportunity to conduct this PhD research. I am thankful for his encouragement, patience, and guidance on how to be a better scientist. I also would like to thank my daily supervisor Dr. O. A. Krasnov for his openness and numerous discussions that we had on my research.

I am grateful to Dr. Jonathan Bosse for sharing his experience in the field of signal processing, constructive feedback on my research, and friendly attitude. I enjoyed collaboration with Prof. G.Leus. His insightful questions and discussions that we had, inspired me a lot. I also thank to Dr. Sundeep Chepuri for our discussions on sparse sensing.

I would like to convey my thanks to colleagues and friends from MS3 group: Xiaohua Lian, Galina Babur, Yuan He, Nadia Haider, Alexey Narykov, Dario Petri, Albert Oude Nijhuis, Dimitriy Penkin, Nikita Petrov, Sharef Neemat, Shilong Sun, Fred van der Zwan, and Etienne Goossens. Special thanks to Minke van der Put for her openness, cordial concern, and help with administrative issues.

I would also like to mention my dear friends that I have met in The Netherlands so far and that made my staying here enjoyable: Alexandra and Vladimir, Dimitriy and Oxana, Angelina and Oleg, Elena and Yuli, Daria and others. Dear Afsane and Behrooz, thank you for everything! You have been like a family to us! I would like to thank my dear friends from Ukraine: Denis, Alexandra, Valentina and Victor, Anna and Vasiliy. Thank you for your support over distances and for always keeping in touch!

I am very thankful to my parents, Galyna and Mykola, for their unconditional love and support, no matter what I was doing. I am indebted to my husband Artem for his love, understanding, and inspiration to move on. My dear son Ivan, thank you for being in this world and for giving me time to work on my thesis!